IMPROVEMENTS TO THE DIRECT-SUN OZONE OBSERVATIONS TAKEN WITH THE BREWER SPECTROPHOTOMETER

Vladimir Savastiouk

A thesis submitted to the Faculty of Graduate Studies
in partial fulfillment of the requirements
for the degree of

Doctor of Philosophy

Graduate Programme in Physics and Astronomy
York University
Toronto, Ontario

March 2006

Abstract

The Brewer spectrophotometer has been used for ozone, sulphur dioxide and UV radiation measurements for 20 years. Now, in more than 40 countries around the world, some 160 instruments regularly collect data using direct-sun and zenith-sky, near-UV radiation. In the research presented here it is shown that using these data it is possible to extract information on aerosol optical depth and the effective temperature of the ozone layer, and to compensate the ozone results for the varying temperature of the stratosphere. This was made possible by the development of new, more detailed analysis software and by the introduction of more comprehensive laboratory testing of each Brewer spectrophotometer. The results of implementation of these advancements have been compared with other data sources. The comparisons show a very good agreement both for the temperature of the ozone layer and the aerosol optical depth.

A modification of the MKII type of Brewer spectrophotometer allows measurements to be made in the visible part of the solar spectrum. These visible ozone measurements are taken at large solar zenith angles, which valuably extend the period of ground-based ozone measurements at high-latitude sites. For stations near the Arctic Circle, for example, the time accessible to ground-based direct-sun measurements is extended by about two months each year.

A significant aspect of this work is that the analysis software is backward compatible and allows extraction of aerosol optical depth and the effective temperature of the ozone layer from archived measurements. A second significant result is that ozone column amounts from the visible measurements provide an opportunity for better understanding the ozone behavior in the Arctic and Antarc-

tic by extending the time when ground-based direct-sun ozone measurements are available. These developments are especially significant in the light of increasing interest from the community in providing high-quality, world-wide ground-based reference data for comparison to satellite-based measurements.

Acknowledgements

"In science the credit goes to the man who convinces the world, not the man to whom the idea first occurs."   — Sir Francis Darwin

"The most exciting phrase to hear in science, the one that heralds the most discoveries, is not "Eureka!", but "That's funny..." " — Isaac Asimov

Table of contents

List of figures

List of tables

1 Introduction

A measurement is only as good as the data analyst's understanding of how the instrument works. In other words, one must understand the physics and chemistry that is occurring, refraction, reflection, conversion of photons into electrical signals and so on. Thus, a detailed analysis of the processes inside the instrument and the use of this information to process the data can significantly improve the quality of the final measurement. In addition, measurements by instruments for which the signal may be a convolution of several processes, such as scattering and absorption, require particular attention to the interpretation of the data. Ozone measurements definitely fall into this category.

The importance of ozone measurements was highlighted by the discovery of the Ozone Hole over Antarctica in 1985, but many instruments for measuring ozone had been collecting data for decades before that. Even today, researchers continue to investigate how well these instruments actually measure ozone and try to improve the quality of the measurements. The improvement can be achieved by introducing new, more sophisticated hardware, or by implementing better processing algorithms, or both.

The dramatic increase in computational power of computers in recent years has provided the opportunity to include more complex calculations in data analysis. This has provided the ability to extract more information from the same set of data than ever before. In addition, new types of measurements, which would have been too difficult to interpret without the help of fast computers, have emerged.

The Brewer spectrophotometer is a good example of an evolving system for measuring atmospheric constituents. The Brewer spectrophotometer, a Canadian

invention, was developed in the late 1970s as an automated instrument to monitor total ozone and sulphur dioxide columns. Being automated, the Brewer spectrophotometer has been a valuable addition to the world ozone network as it can collect data at remote stations without permanent, highly-trained personnel present. Over the years, both the hardware and the software of the Brewer spectrophotometer have been improved to achieve better precision and accuracy of the measurements. In addition, the instrument has become a tool to measure the UV radiation and ozone vertical profile in addition to total columns. This thesis further advances the applications of the Brewer spectrophotometer as well as fine-tunes some of the existing measurements.

1.1 The aim

This thesis is about adding new, and improving existing, direct-sun measurements made with the Brewer spectrophotometer. Particularly, this work is focussed on the following three goals:

1) Improving ozone and SO_2 calculations from the Brewer direct-sun measurements to increase the accuracy of the calculated values and to reduce their dependence on the presence of aerosol. The incorporation of more instrument-specific information into the calculations accomplishes this. Currently, the algorithm for the retrieval of ozone and sulphur dioxide for all Brewer instruments utilizes coefficients derived from solving the radiation transfer equations for a single reference instrument with a particular set of optical and mechanical characteristics. However, each Brewer spectrophotometer is unique with a slightly different set of operating wavelengths and these differences are not fully reflected

in the algorithm. Also, the neutral density filters used to attenuate solar radiation have different optical depths at different operating wavelengths and this is not taken into account in the existing calculations. This study shows that solving the radiation transfer equations for each instrument individually along with including information about the transmission of the neutral density filters improves the accuracy of the ozone and sulphur dioxide retrievals, which, in turn, increases the number of measurements of acceptable quality. Also, the solution produces an estimate of the aerosol optical depth, which is not currently a routine calculation.

2) Creating a solution algorithm that properly accounts for the effective temperature of the ozone layer so as to produce temperature-independent ozone values and to make comparisons of ozone values at different locations more meaningful. This is achieved by solving the radiation transfer equation with temperature-dependent ozone absorption coefficients. In the current algorithm, a fixed temperature of the ozone layer (-45ºC) is assumed for all locations and all times. In reality, the temperature of the ozone layer has a seasonal variation, which is different depending on location. This study provides an algorithm for calculating ozone and sulphur dioxide columns without any assumptions about the temperature of the ozone layer. Instead, the ozone-weighted mean, or effective, temperature is estimated directly from the direct-sun measurements.

3) Introducing visible light measurements of ozone in the atmosphere to increase the number of measurements at large solar zenith angles, which is critical for high-latitude locations. The Brewer spectrophotometer was designed to measure the total column ozone in the atmosphere using near-UV solar radiation. A minor modification of the MKII model Brewer spectrophotometer allows the detection of the visible part of the solar spectrum between 550 nm and 620 nm. This modification is usually referred to as the MKV Brewer spectrophotometer.

This study presents an algorithm for collecting and analysing these data in order to deduce the total column ozone.

The most common method of measuring ozone uses the ultra-violet region of the spectrum. However, this method is not very accurate at solar zenith angles greater than about 70º. As the sun sinks toward the horizon, the path that light has to travel through the atmosphere becomes very large. This produces a large attenuation of light at shorter wavelengths by Rayleigh scattering and ozone absorption. At some point, almost no light at these wavelengths reaches the ground. This, in combination with the stray light at shorter wavelengths inside the instrument, makes it very difficult to make precise measurements. An alternative for low-sun measurements is to use the visible part of the spectrum where ozone absorption and Rayleigh scattering are much smaller and the measurements can continue up to near sunset and start just after sunrise. The modification in the Brewer spectrophotometer necessary for such measurements does not affect the ability of the Brewer spectrophotometer to take the standard measurements in the near-UV spectrum.

The advantage of taking direct-sun rather than zenith-sky measurements, equally in UV and in the visible, is that the airmass enhancement factors for zenith-sky measurements strongly depend on the vertical distribution of ozone in the atmosphere, which changes and is not usually known in advance. The dependence of the retrieved column ozone on ozone vertical distribution is much smaller from direct-sun measurements made even at very large solar zenith angles.

1.2 What was done

In order to conduct this study, two MKII Brewer spectrophotometers were modified by adding a filter wheel assembly with the appropriate order filters to allow the selection of measurements in the near-UV or visible parts of the solar spectrum. Tuning and optical alignment were done for both instruments to ensure good performance. Tuning of the Brewer spectrophotometer, among other things, involves setting the high voltage of the photomultiplier to the optimal value, adjusting the level of the photon-counter discriminator and establishing the proper time delay for the slit mask motor.

After both instruments were made operational, each of them was carefully characterized in the laboratory. Measurements were made of the slit and dispersion functions, spectral characteristics and the wavelength-dependent attenuation of the neutral density filters. A test was conducted to determine the dependence of the instruments′ response to changes in their internal temperature. The electronic parts of the instruments were thoroughly tested to establish the dead time of the system and to ensure that a rapidly changing signal is measured just as accurately as a constant signal. The azimuth and the zenith drives as well as the motor that rotates the dispersing grating were tested. All of the information obtained during these tests is used either to make the measurement or at the data analysis stage.

The next step was the calibration of the instruments by operating them beside a calibrated standard instrument. During this phase, the only changes that were made were in the constants used for ozone and sulphur dioxide calculations. At the same time software was developed to allow the instruments to collect the data in the visible part of the spectrum.

Definitely, the real test for any instrument is taking it into the field. The two instruments were taken to different locations in Canada. One of the locations was the Meteorological Service of Canada′s (MSC′s) headquarters in Toronto, which is the calibration centre for the Global Brewer Ozone network. The other locations where the data were collected included Canadian Forces Station (CFS) Alert, which is the most northern point in Canada, MSC′s station at Eureka, Nunavut and at Vanscoy, Saskatchewan. Travelling to all these places with the instruments was a truly memorable experience.

While the instruments were coping with an ambient temperature range from -50° C to +40° C, the theoretical basis for the data analysis was prepared. Two separate tasks were completed. First, the standard algorithm for analysing Brewer data was improved by solving the radiation transfer equation for each instrument individually and by calculating the aerosol optical depth and the effective temperature of the ozone layer from the same measurements. Second, an algorithm for analysing spectral data from the visible part of the solar spectrum was developed.

All data collected were processed and then compared, where possible, with the results from other instruments. Satellite and ground-based ozonometers provided good independent comparison data for ozone. Ozone and temperature profiles obtained with lidars and ozonesondes helped in analysing the quality of the ozone temperature retrieval. These comparisons demonstrated that the improved algorithm for ozone and sulphur dioxide calculations increases the quality of the direct-sun measurements and provides a good estimate of the effective ozone temperature. The comparison of the aerosol optical depth calculated from the Brewer data with satellite measurements of aerosol showed good agreement. Since all Brewer spectrophotometers' raw data (photon counts) from direct-sun

16

measurements are recorded in computer files, recalculations using this new algorithm can be performed on past measurements. This will improve the accuracy of all ozone and sulphur dioxide results, obtain the corresponding aerosol optical depths and calculate the effective temperature of the ozone layer. Software has already been developed as part of this study to process raw photon count data using the new algorithm.

A comparison of ozone values derived from visible spectral measurements with those from the near-UV was also conducted. The MKV Brewer spectrophotometer can measure ozone, switching between the visible and the near-UV light, for a few hours a day provided that the solar zenith angle spans at least the range 70° to 86° at the location. These data were collected by the two instruments modified for this study and two other instruments built to the same standards for Eureka, Canada and Oslo, Norway. The results demonstrated that ozone measurements using visible light are a valuable compliment to existing near-UV measurements. These measurements increase the number of observation days during the year at high latitudes, where there are times when the Sun is above the horizon but does not reach 70° zenith angle. Of course, the solar zenith angle ranges mentioned here were estimated for a mean ozone column. The actual cut-off is determined by the slant ozone column, which should be at least 1.3 cm.

1.3   Outline of Dissertation

This dissertation consists of six chapters. Chapter two reviews the background information about the composition and vertical structure of the Earth's atmosphere and how these relate to the scattering and absorption of solar radiation.

This includes a discussion of the formation and destruction of the ozone in the atmosphere and how the dynamics of the atmosphere affects the ozone distribution around the globe. An overview of different instruments used for measuring ozone in the atmosphere is given in Chapter 3.

Chapter four deals specifically with the Brewer spectrophotometer. A description of the main components of the Brewer spectrophotometer is presented as well as method used to prepare the instrument for making measurements. Also, the methods of collecting and analyzing data are described. The new ozone measurement using the visible part of the solar spectrum is introduced. The retrievals of the aerosol optical depth and the effective temperature of the ozone layer are described. A discussion of known uncertainties is also included.

The results of the application of the improved calculations to previously collected data and the comparison with the standard algorithm are given in Chapter five. The results of the newly developed visible measurements are also provided.

Finally, in Chapter six, conclusions are presented about the different types of calculations discussed in the dissertation. Also included are recommendations on the implementation of the findings of this study. In addition, a number of areas for possible future improvements and enhancements of the use of the Brewer spectrophotometer are identified.

2 The Earth′s atmosphere

In this Chapter, we present the context for the importance and the challenge of making accurate ozone measurements. For this purpose, it is sufficient to limit the discussion to altitudes below 100 km. While there is no firm boundary marking the end of the terrestrial atmosphere, virtually all of the atmospheric mass, over 99.99%, is found below 100 km of altitude.

2.1 Composition of the atmosphere

Just three gaseous elements together account for nearly 99.9% of the 'dry' component of the Earth′s atmosphere [Wayne, 1991]. These gases are nitrogen (N_2), oxygen (O_2) and argon (A). The proportion of the three basic gases in the atmosphere by volume, 78% of nitrogen, 21% of oxygen and 0.9% of argon, is almost constant up to altitudes above 100 km.

The gases that account for the remaining 0.1% of the atmosphere, because they exist only in small amounts, are called the trace gases. These include carbon dioxide, ozone, methane, oxides of nitrogen, neon, helium, chlorofluorocarbons (CFC′s) and many others. Although these gases comprise only 0.1% of the atmosphere, they are still a very important part of the atmosphere. Ozone, for example, blocks harmful solar UV radiation; water vapour and carbon dioxide, along with ozone, play an important role in the atmospheric radiation balance; and chlorofluorocarbons are the main chemicals, CFCs, that caused the ozone hole.

The vertical distribution of trace gases varies from gas to gas reflecting sources and sinks. For ozone, the number density increases rapidly from about 10 km to its maximum between 20 and 25 km depending on latitude (see Figure 2.1).

Aside from gaseous components in the atmosphere, there exist solid and liquid particles, from nanometres to millimetres in size, called aerosols. Examples of naturally formed aerosols are sea salt, dust and emissions from volcanic eruptions. In addition, there are aerosols that are the by-product of human activities. These include smoke from fires of different origin and droplets of sulphuric acid formed by sulphur dioxide released from power plants.

One class of aerosols in the stratosphere plays a very important role in ozone chemistry. They are called Polar Stratospheric Clouds, or PSCs, and are clouds of ice particles formed at very cold temperatures. Two types of PSCs are distinguished, PSC I and PSC II. PSC II contains water ice crystals formed at temperatures below -85ºC (188 K). The composition of PSC I is not fully understood, although some researchers [e.g. Mehrtens, 1999] believe that they contain a combination of nitric acid, sulphuric acid, HCl and water. PSC I appear to be created at temperatures below -78°C (195 K).

2.2 Vertical structure

The temperature vertical profile is a good starting point for illustrating the basic atmospheric vertical structure.
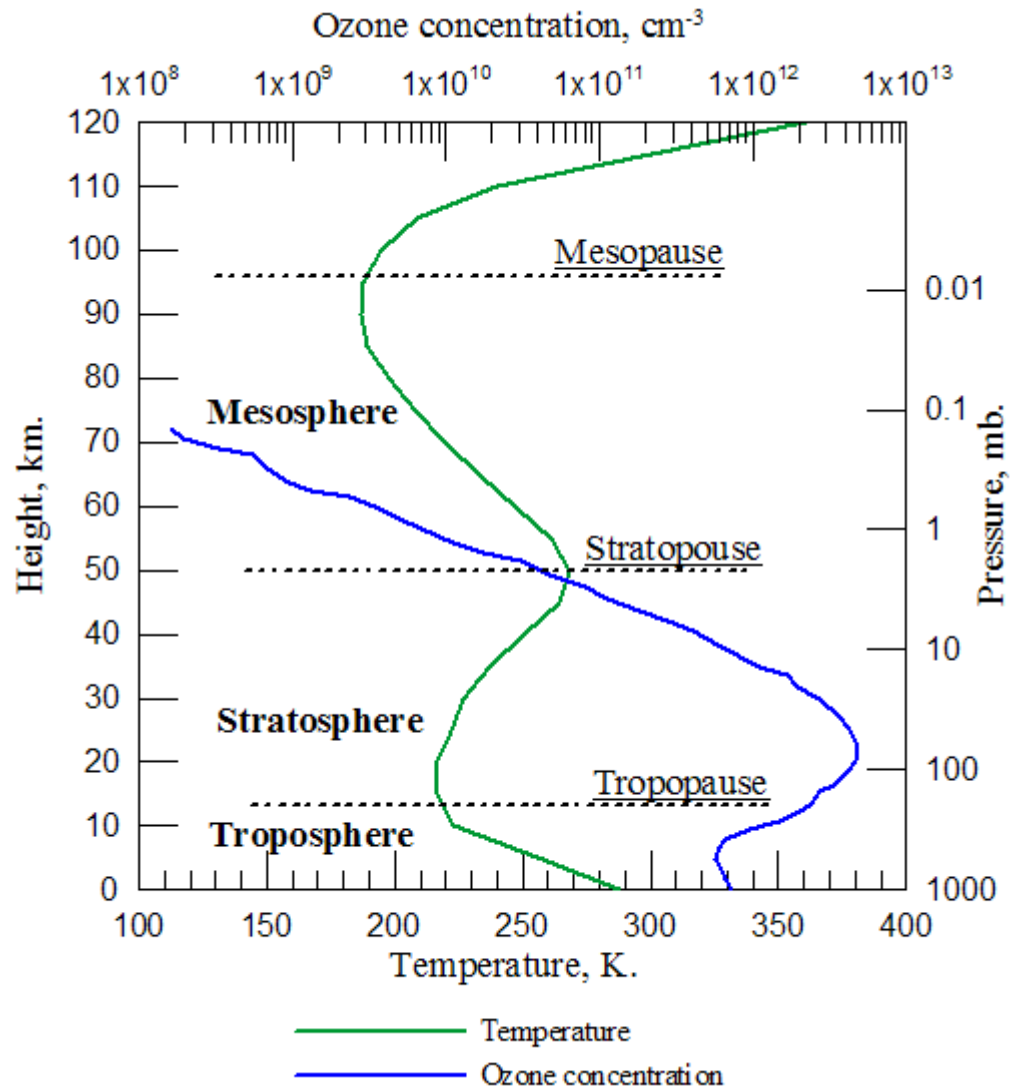
Figure 2.1 Vertical structure of the atmosphere.

The rate of change of temperature with height is different at different altitudes. Figure 2.1 shows average vertical temperature and ozone profiles in the Earth's atmosphere.

Note that in the lowest part of the atmosphere, called the troposphere, temperature decreases with height up to altitude of about 10 km depending on latitude.

In the next region, called the stratosphere, temperature increases with height up to 55 km, after which it starts decreasing again in the mesosphere. The boundary between the troposphere and the stratosphere is called the tropopause. It is found at higher altitudes in the equatorial region than in the Polar Regions. The boundary between the stratosphere and the mesosphere is called the stratopause.

Because of the different temperature lapse rate, the rate at which temperature changes with height, the troposphere and the stratosphere have very different dynamics. While in the troposphere vertical motion of air is common, there is almost no vertical motion in the stratosphere. The reason for that lies in the stability of stratospheric air.

If a parcel of air is displaced upwards, it expands due to lower pressure and therefore cools. If the temperature of the surrounding air decreases more rapidly with height, the parcel will keep rising until equilibrium is found, i.e. the temperature of the parcel becomes equal to the temperature of the air surrounding it. This process occurs in the troposphere and results in a variety of weather phenomena. In the stratosphere, on the other hand, temperature rises with height and the displaced parcel will be colder than the surrounding air, so it will sink back downwards. Similarly, a parcel displaced downwards will rise back. Such situation is called stable stratification, thus the name - the stratosphere. Strictly speaking, it is not enough to have the temperature rise with height for air stability; the rate of temperature increase must be above the adiabatic lapse rate.

The three main atmospheric parameters relate to each other through the ideal gas law:

$$P = \rho R T \tag{2.1}$$

where P is atmospheric pressure, T is atmospheric temperature, ρ is the mass density of the gas and R is the ideal gas constant (for dry atmospheric air R=287 J/kg/K). Both pressure and density decrease with height in the terrestrial atmosphere, while temperature has a more complex behaviour. The barometric law gives pressure at a particular height z in isothermal atmosphere:

$$P(z) = P(0)\exp(-\int_{0}^{z}\frac{dz}{H})$$ (2.2)

where H=RT/g, g being the acceleration due to gravity. The relation between p and z is given usually, for a mean temperature profile, by the scales in Figure 2.1.

2.3 Solar radiation and Earth atmosphere

The sun emits energy over a wide spectrum of wavelengths. For our purposes, a good approximation of the solar spectrum is that of a black body radiator at 5777 K. The flux of the radiation from the surface of a black body radiator at any given wavelength depends on the temperature of the surface. The relationship between the radiance M_λ, at wavelength λ, and temperature T, for a black body is given by Planck's law:

$$M_\lambda = \frac{c_1}{\lambda^5}\frac{1}{e^{c_2/\lambda T}-1}$$ (2.3)

where c_1 and c_2 are the first and second radiation constants with values $c_1=2\pi hc^2=3.74\ 10^8\ Wm^{-2}\mu m^4$ and $c_2 = hc/k = 1.44\ 10^4\ \mu mK$; h is Planck's con-

23

stant and k is Boltzmann's constant. Figure 2.2 compares the extraterrestrial solar spectrum to a spectrum of a black body at 5777 K that was scaled.
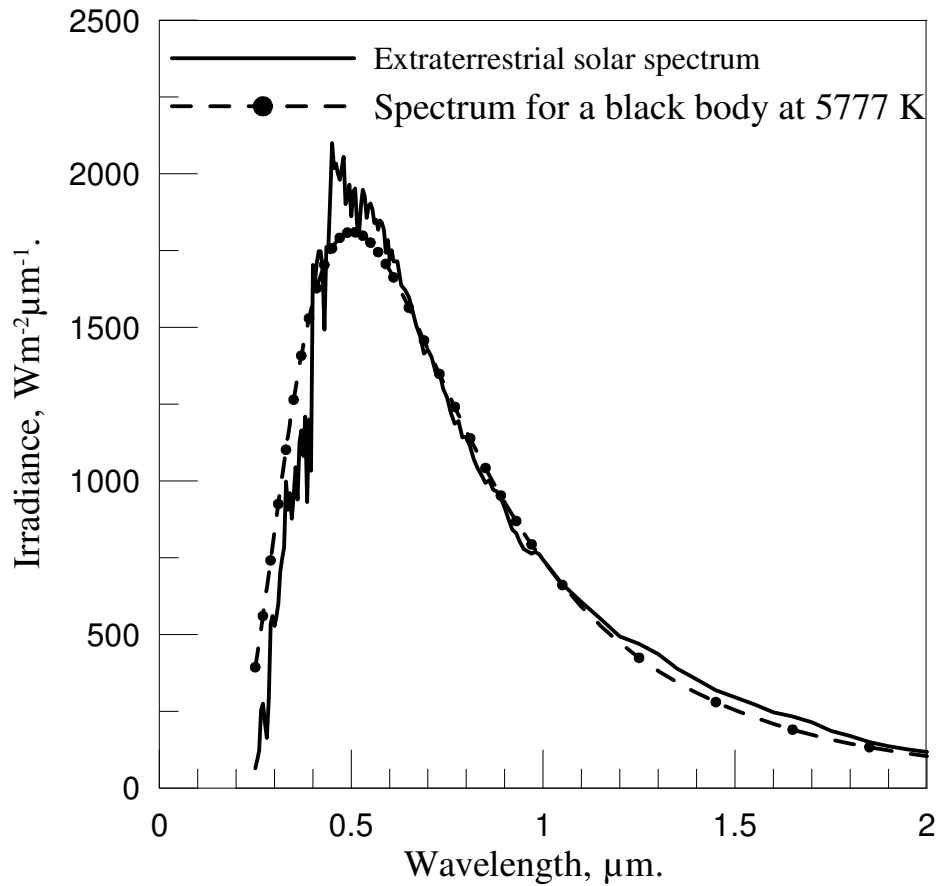
Figure 2.2 Extraterrestrial solar spectrum.

Note that the intensity of the solar radiation decreases rapidly with decreasing wavelength for wavelengths shorter than 0.5 μm. This means the intensity in the 0.2-μm region, essential in ozone production, is very small by comparison.

The surface of the Earth absorbs some of the visible light coming from the sun and is warmed by this radiation, the surface then re-emits this energy in the form

of infrared (thermal) radiation. On average, the spectrum of radiation emitted by the Earth is similar to that of a black body radiator at 253 K. Gases like water vapour and carbon dioxide absorb this thermal energy, re-emitting some of it back into the surroundings.
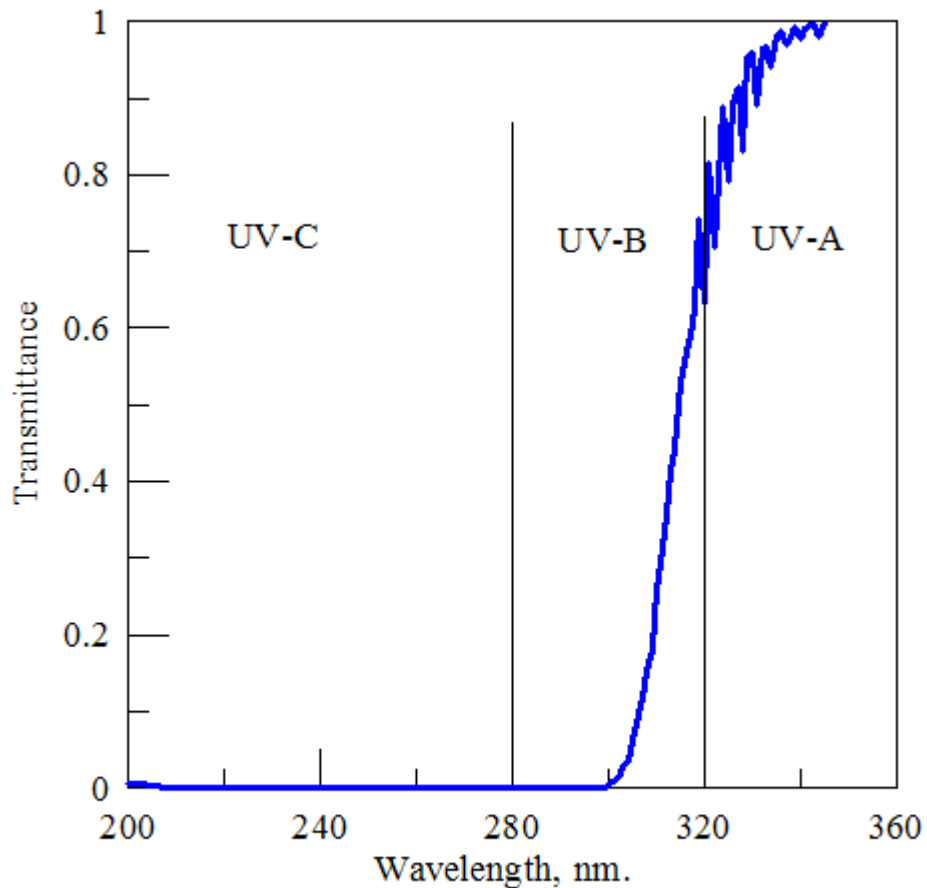
Typical atmosphere with ozone column of 300 DU, solar zenith angle 60 degrees.

Figure 2.3 Transmittance of the ozone layer.

Ozone column of 300 DU, solar zenith angle of 60°.

Heating in the stratosphere, on the other hand, is due to the strong absorption of solar UV radiation by ozone as seen in Figure 2.3, which also shows how UV radiation is often split into three regions: UV-A, UV-B and UV-C. In fact, ozone absorbs the UV-C part (200-280 nm) entirely. Approximately 90% of all atmospheric ozone is in the stratosphere at altitudes between 10 and 50 km (see Figure 2.1). As solar UV radiation travels through this ozone layer, its intensity decreases due to the absorption. Since the temperature in the stratosphere depends on how much solar UV radiation is absorbed per unit mass of air, temperature decreases with decreasing altitude in the stratosphere.

The temperature varies with latitude (Figure 2.4) and with season (Figure 2.5). Sun elevation and atmospheric dynamics play a role in these variations. The temperature at the altitude of maximum ozone absorption can vary by 10 K throughout the year at middle latitudes. To put this temperature variation in perspective, the sensitivity of the standard Brewer algorithm of calculating ozone to the change in ozone temperature is approximately 1% per 10K change. It is even larger, about 3%, for the Dobson spectrophotometer. Taking into account the possibility of bigger variations of effective temperature of the ozone layer due to the seasonal vertical profile changes and an occasional dramatic change in temperature after volcanic eruptions [Fussen, 1999], the final effect on ozone is noticeably greater than 1%, which for some scientific applications is significant. Also, in order to compare the ozone values obtained from sites at different latitudes, i.e. different stratospheric temperatures, it is important to reduce the influence of the temperature on calculated ozone values.
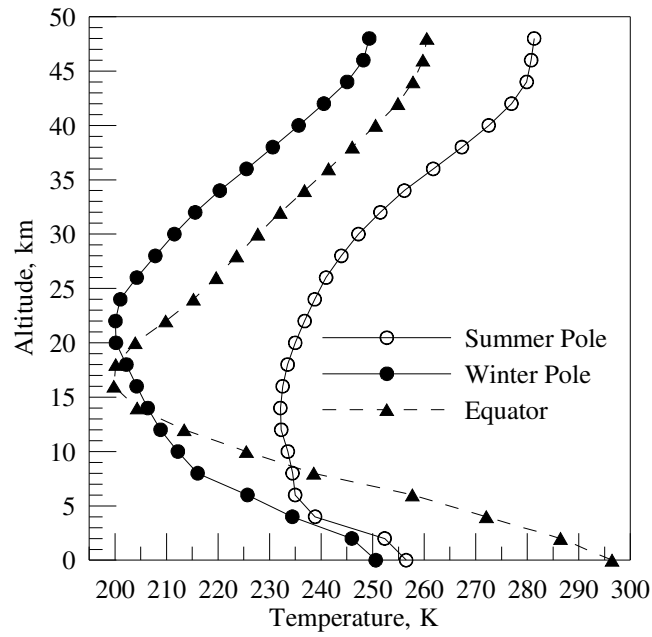
Figure 2.4 Variations in the temperature profile with latitude.
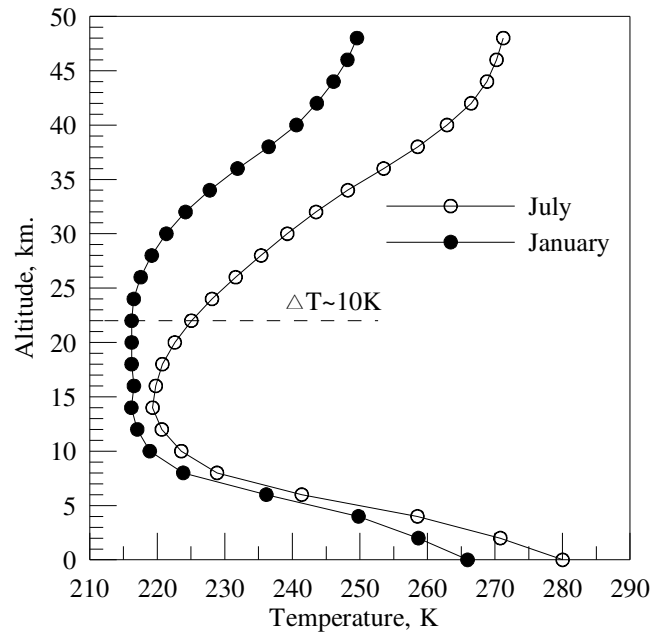
Figure 2.5 Seasonal change in the temperature profile at 50ºN.

27

2.4 Ozone formation and destruction

Many important trace gases, unlike the three major gases, do not have constant mixing ratios in the atmosphere. Not only do they comprise a different fraction of the air at different altitudes and different parts of the globe, but also this proportion changes with time, sometimes very quickly. Ozone is such a trace gas.

The reason the mixing ratio of ozone changes with place and time lies in two temporally changing elements in the atmosphere: chemical reactions and dynamical processes [Salby, 1996]. While dynamical processes usually transport all atmospheric components, which include ozone, in the region, chemical reactions do not necessarily involve ozone. Since ozone is the focus of this study, only those chemical processes that relate to ozone will be discussed.

The understanding of ozone photochemistry started in the early 1930s when Chapman [Chapman, 1930] suggested a cycle of photochemical reactions that create and destroy ozone. This cycle is now known as the Chapman cycle.

The Chapman cycle

In the Chapman cycle, ozone production starts when a high-energy, ultraviolet photon (with wavelength shorter than 242 nm) splits an oxygen molecule into atomic oxygen:

$$O_2 + h\nu \rightarrow O + O \tag{2.4}$$

where $h\nu$ represents a photon with wavelength c/ν while c is the speed of light and h is Planck′s constant. The rate of this reaction depends on the number of avail-

28

able high-energy photons, which decreases rapidly as sunlight penetrates deeper into the atmosphere.

Oxygen atoms are very reactive and they react quickly, within about 5 milliseconds at 30 km [Chartrand et al., 1999], with oxygen molecules forming ozone:

$$O_2 + O + M \rightarrow O_3 + M \qquad (2.5)$$

Here and in all equations in this chapter, M represents any other molecule (usually N_2 or O_2) needed for energy and momentum balance.

Ozone strongly absorbs UV radiation. Figure 2.3 shows the stratospheric ozone layer transmittance in the UV at the surface. By absorbing UV radiation, the ozone molecule is dissociated quite quickly (minutes to an hour) to form an oxygen atom and an oxygen molecule. Depending on the wavelength (i.e. energy) of the photon, the dissociation will produce atomic and molecular oxygen in either the ground state (first reaction) or an excited state (second reaction, $\lambda<310$ nm):

$$\begin{aligned} O_3 + h\nu &\rightarrow O(^3P) + O_2(^3\Sigma) \\ &\rightarrow O(^1D) + O_2(^1\Delta) \end{aligned} \qquad (2.6)$$
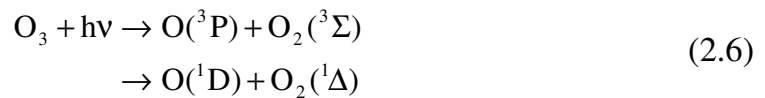
The excited $O(^1D)$ and $O_2(^1\Delta)$ are quickly converted to the ground state in collisions with other molecules, releasing the excess energy in the form of kinetic, vibrational and rotational energy. As before, the newly formed oxygen atom in the ground state almost immediately reacts with O_2 to form ozone, preserving the ozone amount and converting the energy of the UV photons into thermal energy. It is some of this energy that is carried away by molecule M in reaction (2.5).

The net result of these three reactions is the production of ozone and the conversion of UV radiation into heat. The rate of this process at any given part of the atmosphere will depend on the number of oxygen molecules and the number of high-energy UV photons. Since molecular oxygen is uniformly distributed around the globe, it is the differences in solar UV radiation that results in the ozone production differences. These differences are largely due to solar zenith angle, which in turn depends on latitude and longitude. Since in the tropical and equatorial regions the Sun is nearly overhead at local noon every day of the year, it is these regions, in the middle stratosphere, where most ozone is produced. At the same time, the destruction of ozone in the middle atmosphere is also rapid.

In the Chapman cycle ozone reacts with oxygen atoms to form two oxygen molecules:

$$O_3 + O \rightarrow O_2 + O_2 \qquad (2.7)$$

and this reaction alone balances the ozone production. However, ozone measurements that became available soon after the Chapman cycle was introduced showed ozone concentrations in the tropics much smaller than the reactions in the Chapman cycle predicted. There are two reasons that explain this disagreement. First, meridional circulation carries ozone away from the tropical region to the poles, which is described in the next section. Second, there are other reactions that destroy ozone, the most significant of which are catalytic cycles. Such cycles are called catalytic because they involve a catalyst, a substance causing chemical reactions in which it is not consumed. Each catalyst molecule, therefore, can participate in a catalytic cycle many times before it is transformed to a non reac-

tive form by some other reaction. Hence, even small amounts of catalytic molecules can cause serious ozone destruction.

The most important catalytic cycles for ozone are the HO_X cycle, the NO_X cycle, the Cl_X cycle and the Br_X cycle. Since production of ozone generally requires atomic oxygen, reactions other then creation of ozone but consuming oxygen atoms also reduce ozone amount. Some of the catalytic cycles involve such reactions.

In the HO_X cycle, odd oxygen, a name for the sum of ozone and atomic oxygen, is destroyed by reactions with reactive hydrogen species, hydroxyl radical (HO) and hydroperoxyl (HO_2). In the stratosphere these species are produced by O^1D reacting with methane and H_2O, carried there from its tropospheric origins, including coal mining, crop residue burning and industrial activity.

Reactive nitrogen species, NO_X, in the stratosphere are created from N_2O by reaction with atomic oxygen in the exited state, $O(^1D)$. N_2O originates in the troposphere and is brought into the stratosphere by the same dynamic process that brings water and methane. Sources of N_2O in the troposphere include fertilizers, oceans and soil.

The catalytic cycles involving reactive forms of chlorine (Cl and ClO) became an important issue in stratospheric chemistry during last two decades. It is the increase in chlorine that led to the creation of the Antarctic ozone hole. There are natural and artificial sources of chlorine in the stratosphere. About 0.6 ppbv of chlorine is considered as natural. However, the majority of chlorine atoms come into the stratosphere in the form of artificial compounds, chlorofluorocarbons (CFCs) or hydrochlorofluorocarbons (HCFCs).

The bromine catalytic cycles are another very efficient ozone destroyer and, like chlorine, bromine is carried into the stratosphere from the troposphere.

Sources of bromine include methyl bromide (CH_3Br), the product of biological processes in oceans and an agricultural activity on the land, and two synthetic compounds called Halon-1211 ($CBrClF_2$) and Halon-1301 ($CBrF_3$), which are used as fire suppressants. The two artificial compounds have long enough lifetimes they and can be transported into the stratosphere. In the upper stratosphere, they are split by high-energy UV photons and release the bromine into more chemically active forms. Br and BrO are the reactive forms of bromine, while HOBr and $BrONO_2$ are relatively unreactive. However, photolysis of non-reactive forms of bromine can occur even with visible low-energy light. Therefore, bromine in the stratosphere exists mostly in reactive forms. This and the fact that most bromine catalytic cycles do not require atomic oxygen makes bromine very efficient in ozone destruction.

In the upper stratosphere, where atomic oxygen is readily available, the following reactions take place. X in these reactions can be HO, Cl, Br or NO.

$$
\begin{aligned}
X + O_3 &\rightarrow XO + O_2 \\
\underline{XO + O \rightarrow X + O_2} \\
net: O_3 + O &\rightarrow 2O_2
\end{aligned}
\tag{2.8}
$$

The above reactions are limited by the availability of atomic oxygen.

The next two catalytic cycles that destroy odd oxygen in the lower stratosphere are more complex. The first involves bromine and chlorine:

$$BrO + ClO \xrightarrow{h\nu} Br + ClO_2$$
$$ClO_2 + M \rightarrow Cl + O_2 + M$$
$$Cl + O_3 \rightarrow ClO + O_2 \qquad (2.9)$$
$$Br + O_3 \rightarrow BrO + O_2$$
$$\overline{net: 2O_3 \rightarrow 3O_2}$$
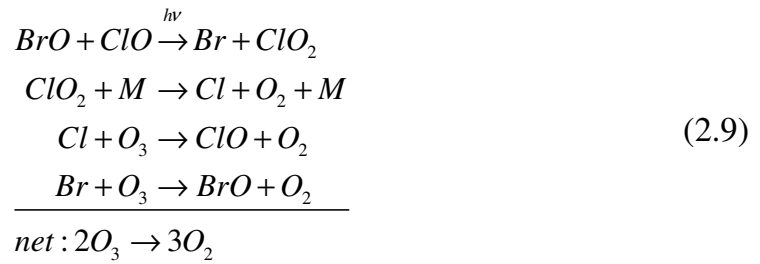
and the other involves self-reaction of ClO:

$$ClO + ClO + M \rightarrow Cl_2O_2 + M$$
$$Cl_2O_2 + h\nu \rightarrow 2Cl + O_2$$
$$2(Cl + O_3 \rightarrow ClO + O_2) \qquad (2.10)$$
$$\overline{net: 2O_3 \rightarrow 3O_2}$$
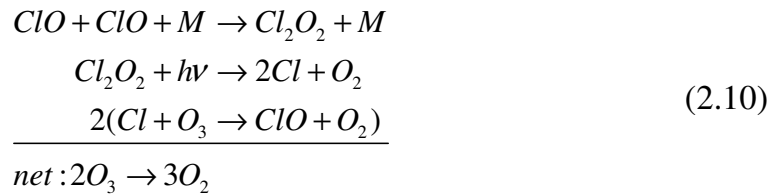
These two cycles destroy odd oxygen very efficiently, without being limited by the availability of atomic oxygen. However, the presence of polar stratospheric clouds is required to release reactive forms of chlorine from non-reactive HCl and $ClONO_2$.

The following heterogeneous reactions only occur efficiently on the surface of a particle (ice particles in case of PSCs):

$$HCl + ClONO_2 \rightarrow HNO_3 + Cl_2$$
$$ClONO_2 + H_2O \rightarrow HNO_3 + HOCl$$
$$HCl + HOCl \rightarrow H_2O + Cl_2 \qquad (2.11)$$
$$N_2O_5 + HCl \rightarrow HNO_3 + ClONO$$
$$N_2O_5 + H_2O \rightarrow 2HNO_3$$
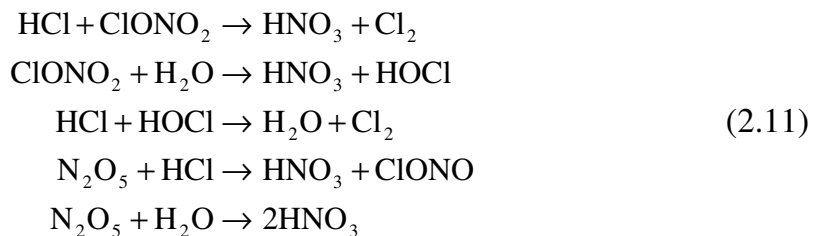
Cl_2 and HOCl, formed by the above reactions can be easily photolyzed by UV and visible light. Since without PSCs the above reactions cannot occur, the existence

33

of the ozone hole is limited to early spring, when the stratosphere is cold enough to form PSCs, yet some sunlight, necessary for photolysis, is present.

Besides freeing reactive forms of chlorine, the above reactions lock nitrogen in the non-reactive form of nitric acid (HNO_3) preventing the reaction between ClO and NO_2 to form non-reactive $ClONO_2$ under normal conditions. This dramatically increases the amount of ClO, resulting in Cl_X catalytic ozone loss.

The only way to interrupt the catalytic cycles is by converting the catalyst into relatively non-reactive species (also called reservoir species) by some other reaction. For HO_X such non-reactive species are H_2O, HNO_3 or HNO_4. They can be created in reactions such as:

$$OH + HO_2 \rightarrow H_2O + O_2$$
$$OH + NO_2 + M \rightarrow HNO_3 + M \qquad (2.12)$$
$$HO_2 + NO_2 + M \rightarrow HNO_4 + M$$
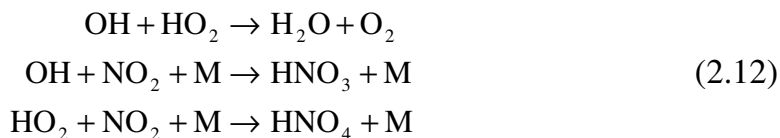
As with HO_X, there are reactions that transform NO_X into relatively non-reactive forms, e.g.

$$NO_2 + OH + M \rightarrow HNO_3 + M$$
$$NO_2 + HO_2 + M \rightarrow HNO_4 + M \qquad (2.13)$$
$$NO_3 + NO_2 + M \rightarrow N_2O_5 + M$$
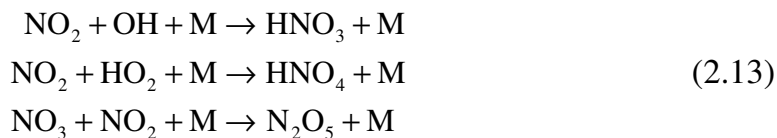
As for other catalysts, there are reactions that convert reactive chlorine into reservoir forms:

$$Cl + CH_4 \rightarrow HCl + CH_3$$
$$ClO + HO_2 \rightarrow HOCl + O_2 \qquad (2.14)$$
$$ClO + NO_2 + M \rightarrow ClONO_2 + M$$

34
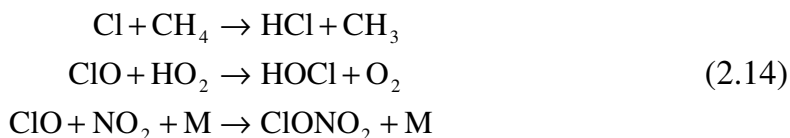
Ozone chemistry and its dynamics affect the global ozone distribution. The next section discusses the dynamical processes in the atmosphere including the meridional circulation.

2.5   Atmospheric dynamics

Air motions affect the distribution of ozone both in the troposphere and in the stratosphere [Holton, 1992]. Moreover, tropospheric dynamics affects the stratosphere. However, the dynamical patterns in these two regions are quite different. The negative temperature lapse rate in the troposphere allows convective (vertical) air motions, while in the stratosphere such motions are more constrained.

A number of factors influence air motion in the atmosphere. These include differences in pressure and temperature, the rotation of the Earth, and mountains. Differences in pressure act to move air from regions with high pressure to regions with low pressure. Warmer, less dense air in the troposphere rises, while colder, denser air sinks. The rotation of the Earth affects air movement through the Coriolis force. Mountains create orographic gravity waves [Goody, 1972].

The unequal heating of the Earth's surface results in some regions with warmer air and some with colder air. As warmer air rises, a low-pressure system can develop. Similarly, sinking colder air can create a high-pressure system. If it were not for the Coriolis force, air would move directly from regions with high pressure to regions with low pressure.

2.5.1 The Coriolis force

The Coriolis force exists due to the different linear velocities of the surface of the Earth at different latitudes [Goody, 1972]. Since the Earth is a solid body (for our purposes), the angular velocity is the same at all latitudes. However, since the distance from the surface to the axis of rotation changes from zero at the poles to its maximum value at the equator, the linear velocity, proportional to this distance, also changes from zero at the poles to its maximum value at the equator. Therefore, any body (including an air parcel) that is affected by the Earth's gravity moving in any direction other than along an east-west line will change its radius of rotation and thus its velocity relative to the surface of the Earth. Moving towards the pole will result in deflection to the east (the same direction as rotation of the Earth) and moving from pole to the equator will result in deflection to the west. In other words, in the Northern hemisphere any moving body will turn to the right of its direction of motion, while in the Southern hemisphere it will turn to the left.

2.5.2 Cyclones and anticyclones

Now back to high and low pressure systems. Air leaving a high-pressure region in the Northern hemisphere will deflect to the right, resulting in clockwise motion around the region (anticyclone), while deflection of the air coming toward a low-pressure region will result in counterclockwise motion (cyclone). Such systems can be quite persistent and last for several days. As they move, they transport tropospheric air from place to place.

The motion associated with cyclones and anticyclones also plays a major role in short-term changes in tropopause height leading to redistribution of ozone in the stratosphere and large, up to 10%, short-term fluctuations in ozone.

2.5.3 The jet stream

Although cyclones and anticyclones can exist for several days, their spatial effect is local, rarely more than a thousand kilometres. There is a dynamic phenomenon in the atmosphere with much larger spatial dimensions. This phenomenon is called the jet stream.
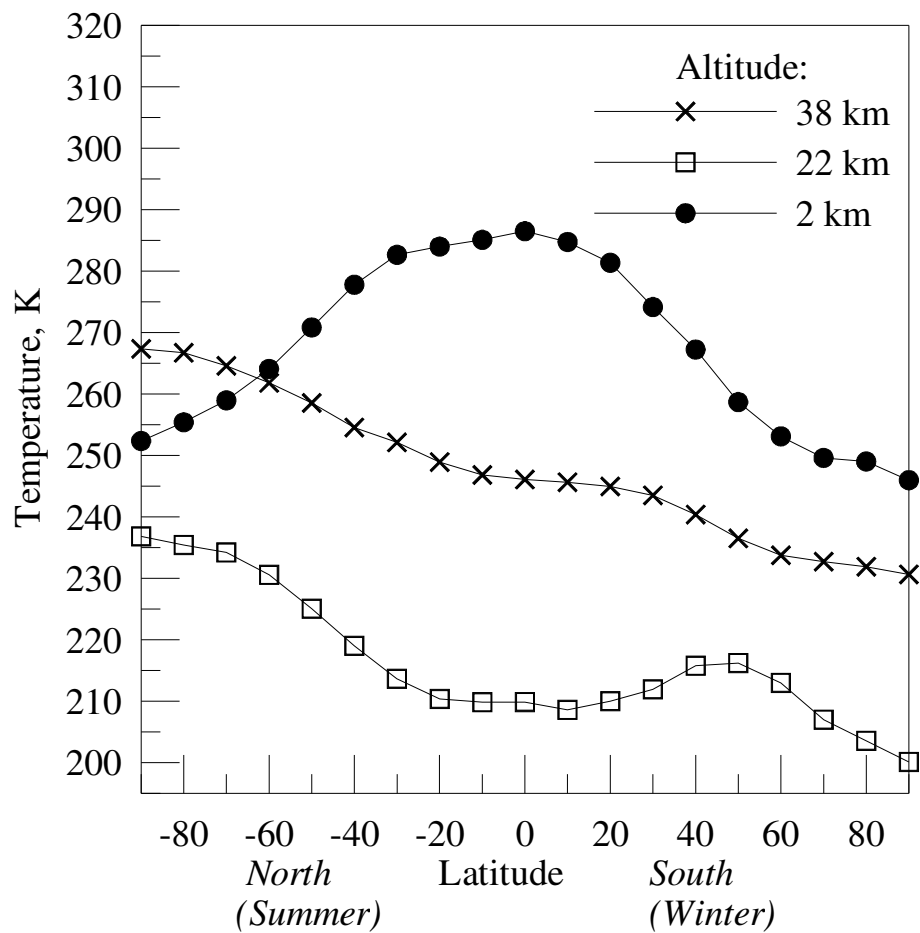
Figure 2.6 Meridional variation of temperature.

From the data on the TOMS/EP web site.

On a global scale, the troposphere at the equator is always warmer than at the poles (see Figure 2.6) due to unequal heating of the ground from the sun. This temperature gradient sets up a very strong westerly (from west to east) wind, or jet stream, in the upper troposphere around the poles. It is most pronounced where the temperature gradient is the greatest. The mean location of the jet stream is marked in Figure 2.7 with a 'J'. The jet stream exists in the upper troposphere and, although very little ozone is present there, it can affect the distribution of ozone by moving the tropopause or by affecting the tropospheric ozone amount. A similar jet stream in the stratosphere, called the polar vortex, however, has a much greater effect on ozone distribution.

2.5.4 The polar vortex

As noted earlier, the temperature in the stratosphere depends on how much solar UV radiation is absorbed by ozone. Therefore, during the polar night (winter) when there is no solar radiation to absorb, temperatures in the stratosphere over the winter pole cool to 180K or less if there is no atmospheric wave activity transporting mid-latitude heat to polar regions.

In contrast, temperatures in the stratosphere over the summer pole, with 24-hour sunlight, rise to 270K or higher. Therefore, unlike the troposphere, a meridional temperature gradient in the stratosphere above 25 km exists from pole to pole, not from the equator to the poles (Figure 2.7). Consequently, a strong (up to 50 m/s) westerly jet in the stratosphere exists only in the winter hemisphere. In the summer hemisphere, stratospheric winds are mostly easterly and not as strong (about 20 m/s). Much like the tropospheric jet stream, the stratospheric jet stream is mostly pronounced where the temperature gradient is the greatest. The air polewards of the stratospheric jet is named the polar vortex and once the vortex

establishes, this air becomes isolated from the stratospheric air on the other side of the jet. It is inside the polar vortex that polar stratospheric clouds can form and these may catalyze ozone destruction. As the sun rises in the spring, the stratosphere warms and the polar vortex weakens.
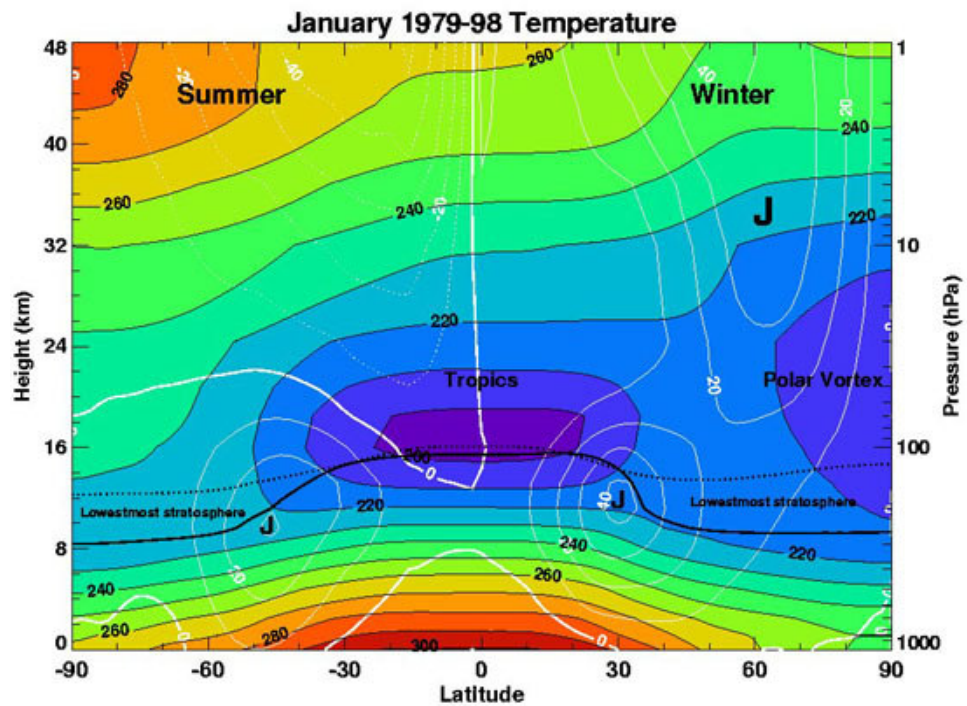
Figure 2.7 Polar vortex in the winter hemisphere.

Adopted from http://see.gsfc.nasa.gov/edu/SEES/strat/class/S_class.htm .

2.5.5 The Brewer-Dobson circulation

Based on measurements of H_2O and Helium in the stratosphere, Brewer [1949] and Dobson [1956] suggested a meridional circulation existed from the upper troposphere to the lower stratosphere at equatorial latitudes. This circulation transports tropical tropospheric air upwards into the stratosphere, then polewards and finally downwards in the middle and polar latitudes.

Rossby waves play an important role in the Brewer-Dobson circulation [Charney, 1961]. These waves are created by the latitudinal gradient of the Coriolis force. Combined with large mountains or the ocean-land temperature gradient, this gradient sets up Rossby waves of extremely large wavelengths of about 10,000 km. Such waves are either standing waves or waves that slowly move westward. Rossby waves originate in the troposphere and can propagate into the stratosphere delivering easterly momentum depending on the stratospheric winds, which can act as a filter. This easterly momentum decelerates the westerly stratospheric jet stream and can even displace it, resulting in a displacement of the polar vortex. The displacement of the polar vortex allows warmer middle latitude stratospheric air to enter the polar region, creating a thermodynamic imbalance. This warmer air cools quickly and sinks. It is this sinking that initiates the meridional Brewer-Dobson circulation.

To understand the mechanism of this circulation, imagine a large circular pot of water with a cube of ice floating in the centre. Water near the ice is cooling and becomes heavier, so it sinks. To replace sinking water, a radial (towards the ice) flow on the surface begins, in turn establishing a bottom-to-surface flow on the sides of the pot. To close the loop, a centre-to-side flow on the bottom of the pot is created. Similarly, sinking cold air in the polar stratosphere establishes a meridional stratospheric flow from tropics to the pole and upwards flow in the tropics.

40

The Brewer-Dobson circulation transports trace gases from the troposphere into the stratosphere near the tropics and carries them polewards. For example, it transports CFCs from the tropical troposphere to the polar stratosphere. It also redistributes ozone from its production in the equatorial tropical stratosphere to the poles.

The downward flow in the Brewer-Dobson circulation starts at the middle latitudes where it penetrates the tropopause. In the Polar Regions, on the other hand, the downward flow only reaches the lower stratosphere.

The Brewer-Dobson circulation together with a longer ozone lifetime in the lower stratosphere explains the accumulation of ozone in the Polar Regions.

The Brewer-Dobson circulation is much weaker in the Southern hemisphere than in the Northern hemisphere because of the lack of large-scale topographical features or large ocean-land temperature gradient needed to create Rossby waves. As a result, the Antarctic polar vortex is much more isolated from the rest of the stratosphere and, with absence of warmer middle latitude air, it is much colder than Arctic polar vortex. Colder temperatures inside the Antarctic polar vortex allow polar stratospheric clouds to form more often than inside the Arctic vortex, resulting in more ozone destruction near the South Pole than near the North Pole.

2.6   Ozone distribution and trends

Ozone measurements contribute greatly to understanding atmospheric processes. Changes in ozone concentrations are tightly tied to other changes in the atmosphere and have been the focal point of remote sounding community for decades. During this time various estimates have been calculated about trends in

ozone concentrations. To make a valid statement about ozone trends one needs a very accurate, stable standard for ozone measurements. This is why it is important to improve the quality of the ozone measurements with the Brewer spectrophotometer, which is becoming the ground-based standard for measuring ozone and studying ozone trends.

2.6.1   Ozone variations
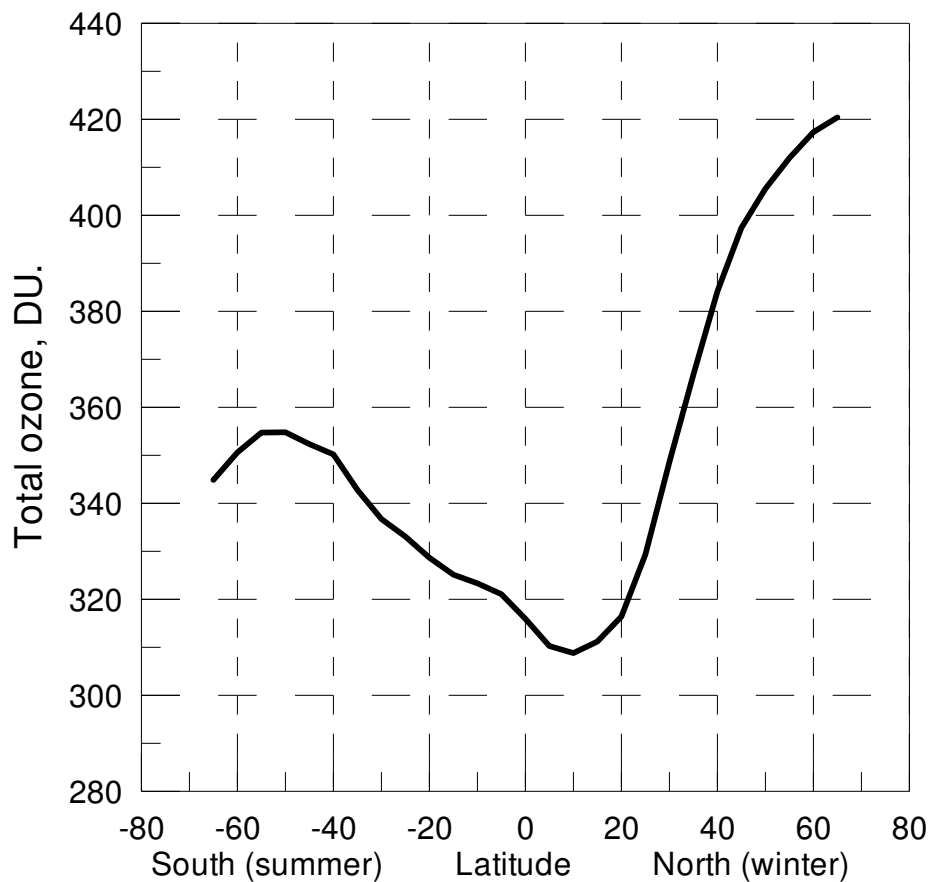
Figure 2.8 Column ozone variation with latitude.

Deduced from TOMS data.

Ozone varies both spatially and temporally. These variations are due to chemical and dynamical processes in the atmosphere. Away from the Polar Regions, variations in column ozone on a daily basis are primarily due to dynamical processes in the atmosphere rather than to ozone formation and destruction processes. Variations in solar flux, on a variety of time scales, from the 11-year solar cycle, to the 27-day solar rotation period can affect ozone generation in the stratosphere. Dynamical processes redistribute the ozone. Factors such as temperature and pollution of the stratosphere affect ozone destruction processes.

Most ozone is produced in the equatorial stratosphere, since the sun remains in the tropics all year round. Production of ozone in the middle latitude stratosphere, increases in the summer and decreases in the winter. Of course, everywhere in the stratosphere and lower mesosphere more ozone is produced during the day than during the night.

Processes such as the quasi-biennial oscillation in the tropical wind direction affect the strength of the Brewer-Dobson circulation. On a smaller scale, synoptic scale weather systems can transport ozone in the troposphere from place to place and change the height of the tropopause, all of which are used in statistical methods for forecasting ozone column.

2.6.2 The ozone hole

Human activity has affected the balance that previously existed between ozone production and destruction. The discovery of the ozone hole in 1985 [Farman et al., 1985], underlined the importance of taking ground-based ozone measurements. As it turned out, the satellite ozonometer, which could have been the first to detect the ozone hole, effectively flagged all total ozone measurements below a certain level as climatologically impossible (which was true before the

43

hole was known) and set them aside. It was the Dobson spectrophotometer at the British Antarctic Survey site that first detected a dramatic ozone loss over the Antarctic.

Because the absorption of UV radiation by ozone is a major source of heat in the stratosphere, ozone depletion changes the thermal balance in the atmosphere. The World Meteorological Organization has addressed these changes in the Scientific Assessment of Ozone Depletion [2002].

2.7   Equations governing radiation transfer in the atmosphere

There are some assumptions that need to be introduced before the following discussion of radiation transfer in the atmosphere begins. For the purpose of the direct-sun measurements, a spherically homogeneous atmosphere is considered with corrections for visible solar zenith angle values due to refraction.

2.7.1   Beer-Lambert law

As solar radiation propagates through the Earth's atmosphere, its intensity[1] (power per unit area per unit wavelength per unit solid angle) is attenuated by atmospheric constituents [Lenoble, 1985]. The attenuation, called extinction, occurs via two mechanisms: absorption and scattering. *Absorption of radiation* is a process whereby a photon is absorbed during interaction with a molecule. As a result of absorption, the absorbing molecule can increase its internal energy or split into two component molecules or atoms. *Scattering of radiation* is a process

---

1 also called *radiance* in the remote sensing community.

of redirecting energy from photons. The probability of a collision between a photon and a molecule or a particle depends on the nature of the molecules or particles and on the wavelength of the photon. An effective cross-section, σ, of such collisions can be determined for each photochemical species.
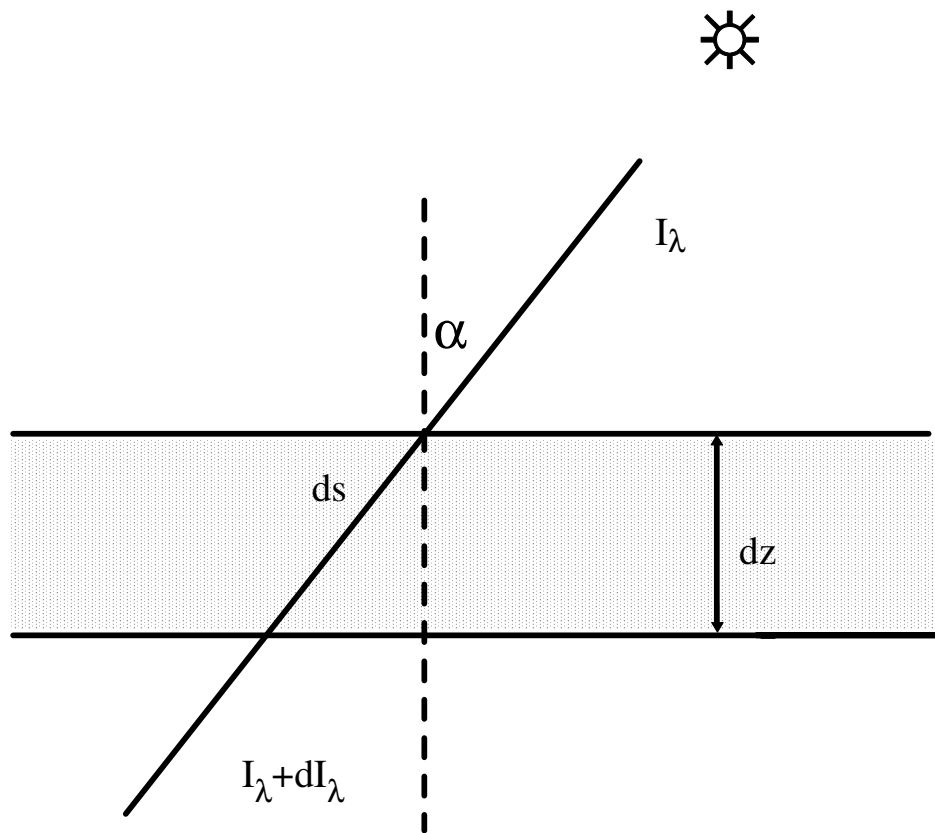
Figure 2.9 A thin layer of an absorber illuminated by solar radiation.

The Beer-Lambert law describes the attenuation of a ray of incident irradiance passing through an infinitesimally thin layer with scattering not considered. In

Figure 2.9 a layer with vertical thickness dz is illuminated by a ray of irradiance I_λ with wavelength λ and incident angle α. The change of the irradiance across the layer, dI_λ, is given by

$$dI_\lambda = -k_\lambda I_\lambda ds \qquad (2.15)$$

where k_λ is the extinction coefficient (units cm^{-1} or m^{-1}). This coefficient is the product of the concentration N of the particles (expressed in particles per unit volume) and the extinction cross-section σ (expressed in units of area per molecule):

$$k_\lambda = N\sigma_\lambda \qquad (2.16)$$

Substituting (2.16) into (2.15) and integrating (2.15) along the path, s, of the ray gives the relation between the irradiance at the beginning of the path, I^0_λ, and I_λ

$$I_\lambda = I^0_\lambda \exp(-\int_s \sigma_\lambda N(s) ds) \qquad (2.17)$$

The optical depth τ over the path is defined as

$$\tau(\lambda, s) = \int_s \sigma_\lambda N(s) ds \qquad (2.18)$$

For a mixture of different species, the total optical depth is the sum of the optical depths for each of the species, i.e.

$$\tau = \tau_1 + \tau_2 + \dots \tag{2.19}$$

If the extinction cross-section does not change along the path, the optical depth can be expressed as

$$\tau(\lambda, s) = \sigma_\lambda \int_s N(s) ds \tag{2.20}$$

Assuming horizontal homogeneity of the atmosphere, the integral can be transformed into integration over the vertical coordinate z as:

$$\tau(\lambda, s) = \sigma_\lambda \int_z N(z) \frac{ds}{dz} dz \tag{2.21}$$

The ratio ds/dz in (2.21) is called the air mass factor, often denoted as m or μ.

2.7.2 Calculation of the air mass factor

Usually most of the attenuation due to a specific species (ozone, sulphur dioxide) occurs in a thin layer, thus the ratio ds/dz can be treated as constant in (2.21). To derive the analytical formula for the air mass factor, consider a thin layer at an altitude h over the surface of the Earth (Figure 2.10). The radius of the Earth is denoted as R_E. For an apparent solar zenith angle θ the sine law is

$$\frac{\sin \theta}{R_E + h} = \frac{\sin \alpha}{R_E} \tag{2.22}$$

Because the layer under consideration is relatively thin, the shaded triangle in Figure 2.10 is a right angle triangle. Then

$$dz = \cos(\alpha) \, ds$$

$$\text{or} \tag{2.23}$$

$$\frac{ds}{dz} = \sec(\alpha)$$
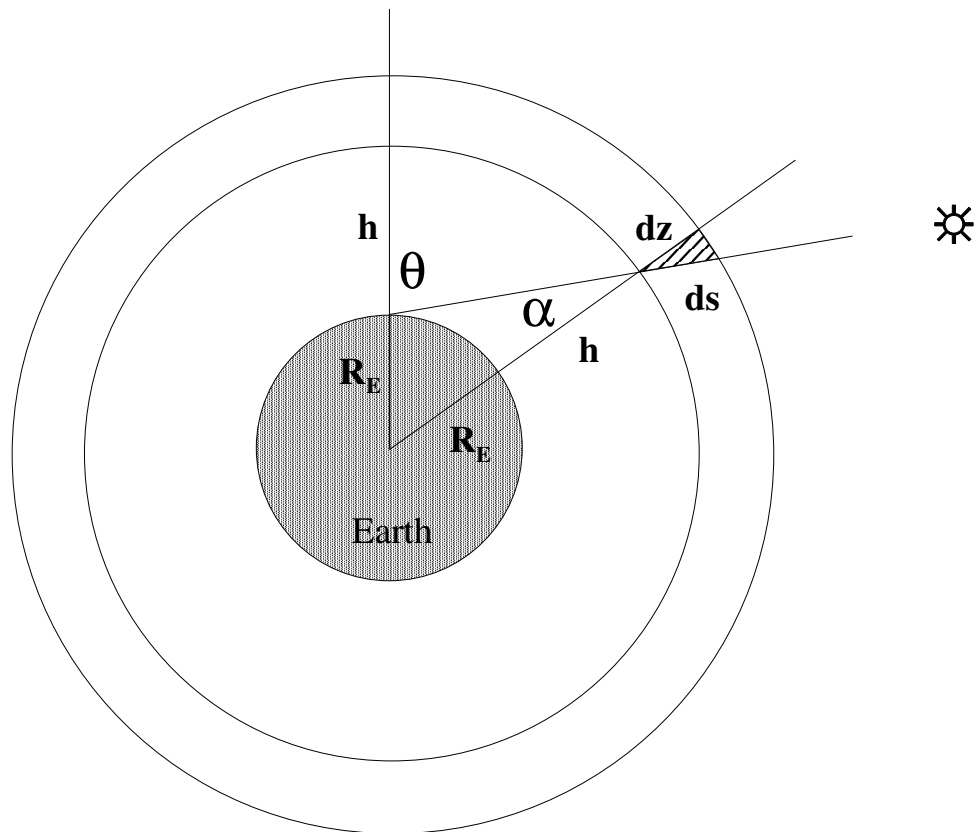
Figure 2.10 Derivation of the air mass factor.

Expressing sec(α) from equation (2.22) then

$$\sec(\alpha) = \dfrac{1}{\sqrt{1 - \left(\dfrac{R_E \sin\theta}{R_E + h}\right)^2}} \qquad (2.24)$$

Now using m for the air mass factor, equation (2.21) for the optical depth can be written as

$$\tau(\lambda, s) = \sigma_\lambda m \int_z N(z)dz \qquad (2.25)$$

Usually, for direct-sun measurements the actual vertical distribution N(z) is not important and only the integral is.

2.7.3 Total column amount and the Dobson Unit

The total column amount for species in the atmosphere is defined as a depth of the layer that a species would form if the layer were at the standard pressure and temperature. The ambient concentration of gaseous species at standard pressure, 1013.25 mb, and temperature, 273.15 K, is given by Loschmidt's number $N_0 = 2.687 \cdot 10^{19}$ cm^{-3}. Then the total column amount X can be expressed through

$$N_0 X = \int_z N(z)dz \qquad (2.26)$$

The total column amount has units of length. For example, the global average for the total column amount of ozone is about 3 mm. For ozone and sulphur dioxide, the Dobson Unit (DU) is often used to express the total column amounts. By

definition 100 DU = 1 mm column amount and the global ozone average is then 300 DU. The expression for the optical depth (2.25) now becomes

$$\tau(\lambda, s) = \sigma_\lambda N_0 m X \qquad (2.27)$$

The cross-section σ_λ on the right hand side of the expression (2.27) is the only term that has not yet been addressed yet.

2.7.4   Absorption by ozone and sulphur dioxide

The absorption coefficients for different species are measured in the laboratory by analysing radiation passing through a vessel containing a known amount of the gas in question. Conducting such measurements at different temperatures allows tabulation of the temperature dependency of the absorption coefficients [e.g. Brion et al., 1997].

In the UV operating region of the Brewer spectrophotometer two gases absorb strongly. These are ozone and sulphur dioxide. Ozone absorption depends significantly on temperature, while the temperature dependence of sulphur dioxide absorption is very small and can be neglected [Hearn and Joens, 1991]. In the case of temperature-dependant cross-sections, expression (2.27) will have σ_λ at the effective temperature of the ozone layer.

In this study, ozone absorption cross-sections for the UV region measured by Brion et al. [1997] are used. This group measured ozone absorption at five different temperatures (K): 218, 228, 243, 273 and 295 (see Figure 2.11). Because about 90% of the ozone in the atmosphere is found in the stratosphere, where temperatures are close to 228 K, ozone cross-sections at 218, 228, 243 and 273 K were used to interpolate temperature dependence at each wavelength with a parabola fitted to the four measured values (Figure 2.12).
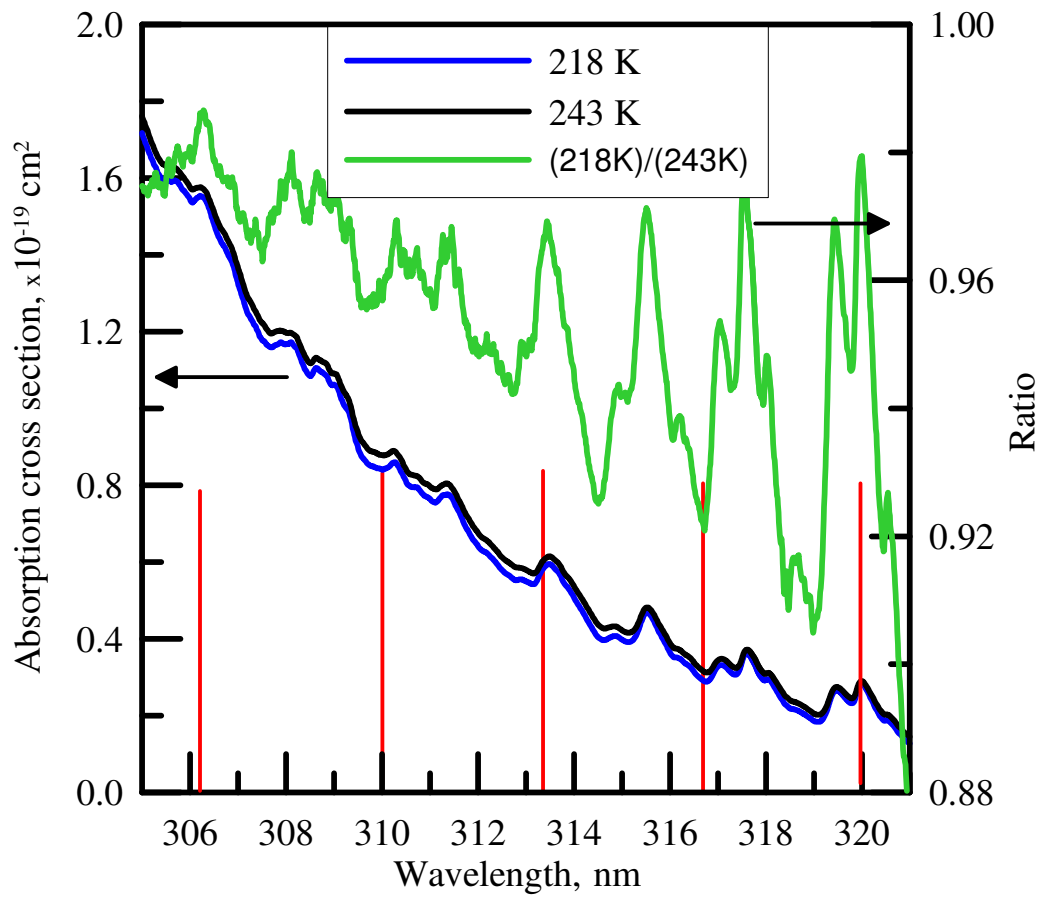
Figure 2.11 Ozone cross-sections in the UV at two temperatures.
Also shown is the ratio of the cross-sections at those temperatures.
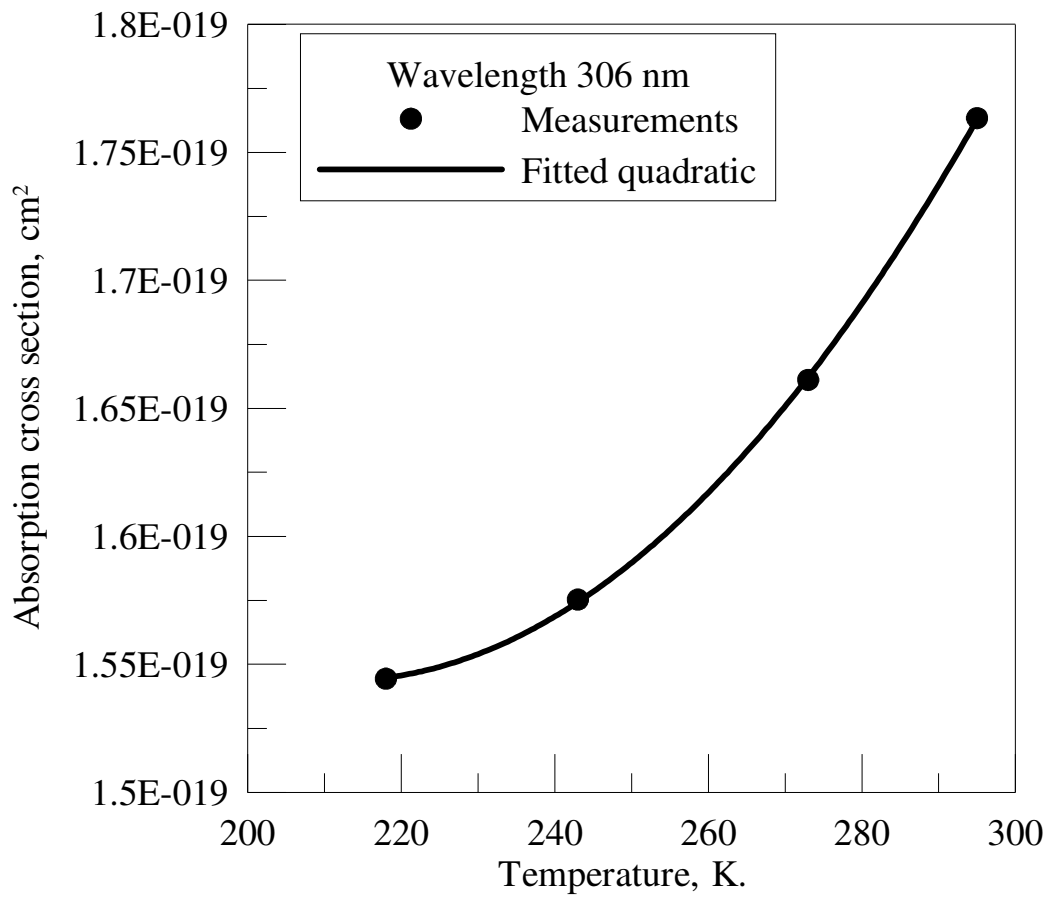
Figure 2.12 Interpolation of the ozone cross-sections with a quadratic.

The ozone absorption cross-section at any given temperature T is then

$$\sigma(\lambda, T) = A(\lambda) + B(\lambda)T + C(\lambda)T^2 \tag{2.28}$$

Absorption cross-sections for sulphur dioxide from Hearn and Joens [1991] were adopted (Figure 2.13). Those are the same data that are used in the standard Brewer algorithm.
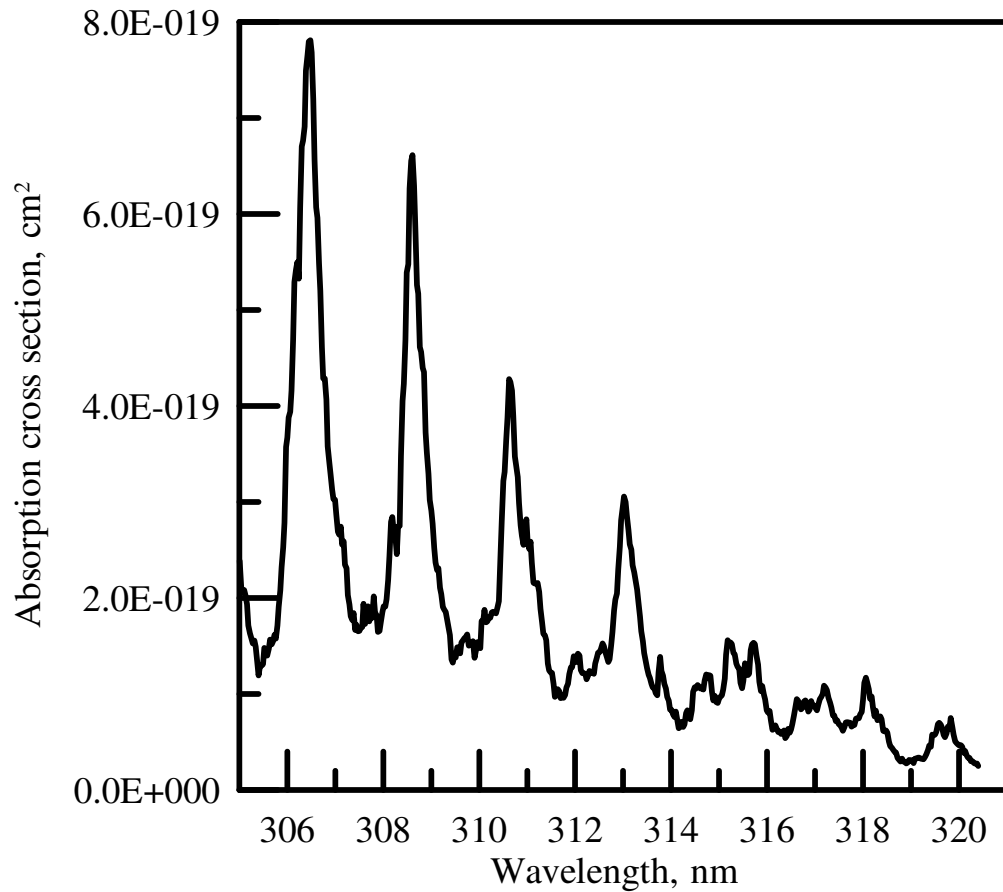
Figure 2.13 Sulphur dioxide cross-sections.

For the visible part of the spectrum, the absorption cross-sections measured by the Global Ozone Monitoring Experiment (GOME) group [Burrows, 1999] are

used (Figure 2.14). In the Brewer operating region (550 - 620 nm) ozone is the only strong absorber (weak BrO, HCHO, NO_2, H_2O, O_4). The temperature dependence of the ozone cross-section in the visible part is very small and can be neglected.
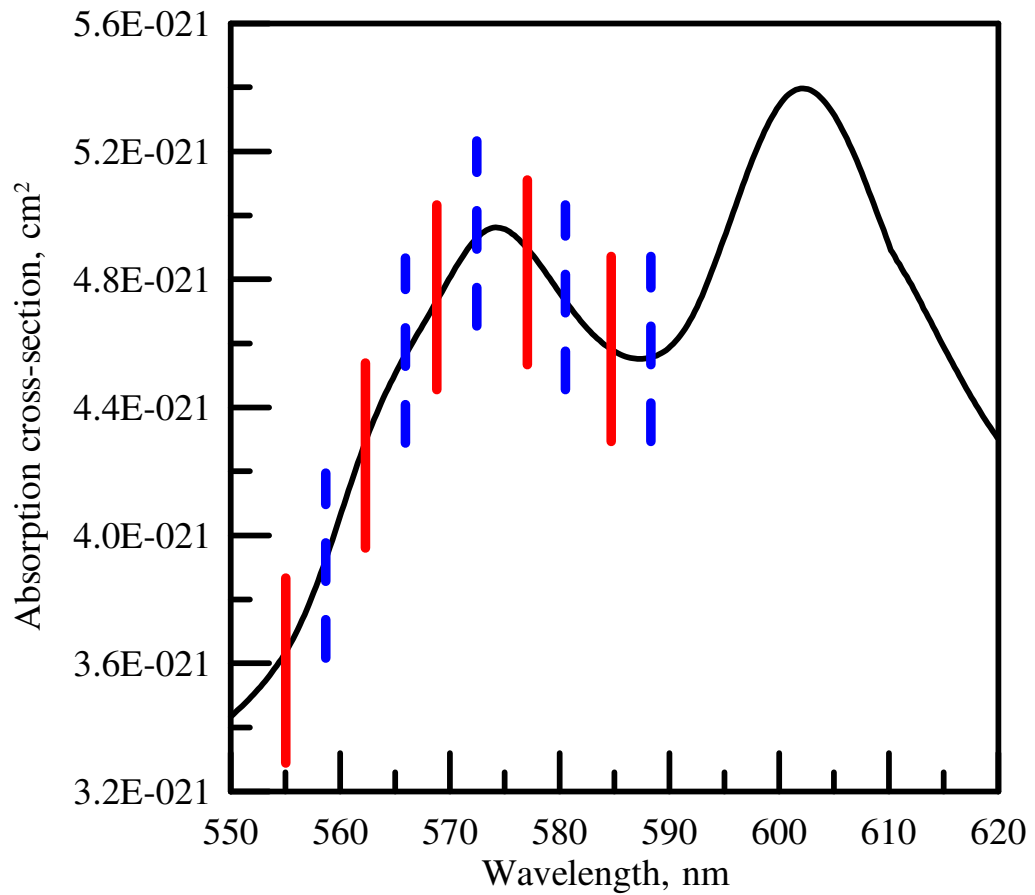
Figure 2.14 Ozone cross-sections in the visible region.

2.7.5 Scattering by air molecules and aerosols

The atmospheric particles responsible for scattering vary in size from gas molecules (~10^{-8} cm) to large raindrops and hail particles (~1 cm). The relative intensity of the scattered light depends strongly on the ratio of the particle size to the wavelength of the incident radiation. If this ratio is small, the scattered light is distributed equally into the forward and backward directions. Such scattering is called Rayleigh scattering and is applicable to scattering by air molecules. For large particles, a larger fraction of the light is scattered in the forward direction. This type of scattering is called Mie scattering (applicable to spherical particles).

Rayleigh scattering theory is well defined [see, for example, Penndorf 1957, Elterman 1968, and Bates 1984]. In the theory, the scattering cross-section at wavelength λ for anisotropic molecules with concentration N is given by

$$\sigma_\lambda = \frac{24\pi^2 (n^2-1)^2}{\lambda^4 N^2 (n^2+2)^2}\left(\frac{6+3\rho}{6-7\rho}\right) \tag{2.29}$$

where n is the refractive index and ρ is the depolarization factor. Both n and ρ vary with wavelength. The molecular scattering optical depth for a unit air mass ($m = 1$) is then

$$\tau(\lambda) = \int \sigma_\lambda N(z) dz \tag{2.30}$$

An approximate expression for the Rayleigh optical depth at the standard ground pressure from Bucholtz [1995] was used in the form

$$\tau^s_{Rayleigh}(\lambda) = \beta^s_\lambda = 8.66 \bullet 10^{-3}\, \lambda^{-(3.6772+0.000389\lambda+94.26/\lambda)} \tag{2.31}$$

55

where the wavelength λ is in nm. This approximation is good to 0.2% for wavelengths in the 250-500 nm range. The above formula can be modified for arbitrary ground pressure by

$$\beta_\lambda = \beta_\lambda^s \frac{P}{P^s} \qquad (2.32)$$

where P^s is the standard and P is any ground pressure.

The scattering by a spherical atmospheric aerosol is governed by Mie theory. Without the knowledge of the nature of aerosol, the exact calculations of aerosol optical properties are very difficult, if not impossible, and usually, formulas are used that approximate the spectral behaviour. In this study the Ångstrom approximation for unit air mass is used [see, for example, Iqbal 1983]

$$\tau_{\text{Aerosol}}(\lambda) = \delta_\lambda = a\left(\frac{1}{\lambda}\right)^b \qquad (2.33)$$

where wavelength λ is in nm, *a* is Angstrom turbidity coefficient which represents the amount of aerosol in the atmosphere and b is the wavelength exponent with typical values from 0.5 to 1.3. In this study, the wavelength exponent with the value of -1 was used, the same assumption as for the standard Brewer algorithm. This assumption is based on the fact that over a short wavelength range (300 nm to 320 nm) the exponential function in Eq. 2.26 can be accurately approximated by a linear function. The main differences between the algorithms come from the different sets of the operating wavelengths for each Brewer instrument.

3 Overview of the methods used for ozone measurements

There are many ways to measure ozone in the atmosphere [see, for example, Grant, 1989]. Ozone concentrations can be measured directly by taking a sample of air and chemically analysing it for ozone. Such measurements are called *in-situ* because the measurements are done at the same place where the air to be measured is. Another approach is to measure ozone concentrations remotely. In this approach, the ability of ozone to absorb or emit electromagnetic radiation is exploited. So-called passive remote sounding uses natural sources of radiation like the sun or the moon to probe the atmosphere. Thermal emission of radiation from the atmosphere itself is also used. Active remote sounding uses artificial light sources such as lasers. Ozone measuring instruments also differ by their "work place". Some instruments are ground-based, some are mounted on airplanes or satellites and some fly on weather balloons.

This chapter provides a brief description of some widely used methods for measuring ozone and gives examples of instruments that realize these methods.

3.1 In-situ measurements

As mentioned above, *in-situ* measurements provide information about the ozone concentrations at the place of the measurement. The concentrations can be measured chemically, as in ozonesondes, or optically, as in some gas-analyzers (Dasibi for example). *In-situ* instruments can be used on board of a weather

balloon or an airplane to measure the vertical structure of the ozone layer [Brewer, 1960]. The obvious advantage of using *in-situ* technique is the actual measurement of the ozone concentration at a particular spot. This has provided the scientific community a long record of ground ozone measurements and ozone profiles in the troposphere and part of the stratosphere. The limitation of *in-situ* measurements is in the difficulty to obtain the ozone profile in the entire stratosphere due to height limitations of the weather balloons and the lack of reliability of the *in-situ* instruments at low pressure and temperature [Davies, 2000].

3.2   Remote sensing

It is not always possible or practical to do in-situ measurements and remote sensing is used instead. This technique, as mentioned above, involves detecting and analysing electromagnetic radiation that carries information about the atmosphere [Deepak, 1977,1980]. There are two major types of remote sensing: passive and active. Instruments using passive remote sensing techniques for studying the atmosphere take advantage of radiation emitted or reflected by natural sources like the sun or the moon. Active remote sensing relies on artificial sources of radiation, such as radar or lidar.

Remote sensing techniques are used both for column type measurements where only the total amount of atmospheric constituents in the path is measured, and for retrieving the profiles where information about the vertical distribution of the constituents is recovered.

3.2.1 Ground-based passive sounding

The most widely known ground-based ozonometers are the Dobson spectro-photometer (the Dobson) and the Brewer spectrophotometer (the Brewer). These are used world-wide to measure the total ozone column as well as the vertical ozone profile.

The Dobson was developed around 1927 [Dobson 1931, 1957, 1968] and the Brewer was built in the late 1960s. Both the Dobsons and the Brewers make the ozone measurements by registering the absorption due to ozone in the Huggins bands (near UV), but this thesis will present a working algorithm for the Brewer spectrophotometer to measure ozone in the Chappuis bands (red). The direct-sun measurements are considered more accurate with these instruments because of simple ray geometry. The zenith-sky measurements are done mostly during cloudy periods when the direct-sun measurements fail. Zenith-sky measurements at sunset and sunrise are used to estimate the ozone vertical profile.

The Dobsons have a double monochromator for increased spectral purity. The Brewers have several modifications, one of which, the MKIII modification, has a double and the rest have a single monochromator.

The presence of aerosols and sulphur dioxide in the atmosphere affects the measurements from Dobson spectrophotometers [Komhyr, 1980; Evans, 1981; Dobson, 1968]. The algorithm realized in the Brewer spectrophotometers was meant to account for sulphur dioxide and aerosol, however it was not fully achieved until we introduced the improved algorithm presented in this thesis.

Most Dobsons are not automatic and require a human operator to perform measurements and all Brewers are fully automatic, which allows each Brewer to perform series of tests routinely and record all measurements in computer files. In

addition, the Brewer spectrophotometer as an automatic instrument can be installed at sites where trained personnel are not constantly present.

The benefit of having a wide, well-established ground based ozone network, aside from the quality data that is the centre of this thesis, is the existence of a reliable reference for ozone measurements. This is especially important in our age of satellite measurements. The global coverage is impossible with ground-based network and this is where satellites have a huge role, but they need a solid reference for comparison.

3.2.2 Satellite-based remote sounding

As mentioned above, satellite-based instruments are able to provide global coverage and most do so daily.

Satellite-based remote sounding is done by detecting radiation either from nadir or from the limb of the atmosphere. The latter include the occultation technique and the measurements of radiation emitted by the atmosphere.

The Total Ozone Mapping Spectrometer (TOMS) is an example of the nadir measurements. It has been taking measurements since 1978 on board of three satellites [Bhartia et al, 1983, 1984, 1988; McPeters, 1996]. In addition to providing daily global ozone maps, TOMS data is analyzed to deduce aerosol optical depth.

Limb

Stratospheric Aerosol and Gas Experiment (SAGE)

The SAGE II instrument is a seven-channel sun photometer [http://www-sage2.larc.nasa.gov, Yue et al., 1995]. A holographic grating dis-

perses the incoming radiation into spectral regions centred at the 1020, 940, 600, 525, 453, 448, and 385 nm wavelengths. The instrument uses the solar occultation technique measure attenuated solar radiation through the Earth's limb in the seven channels. During each sunset and sunrise event the extraterrestrial solar irradiance is also measured for use as a reference. The "onion-peeling" approach is used to obtain 1-km vertical resolution profiles of aerosol extinction, ozone, nitrogen dioxide, and water vapour. While the focus of the measurements is on the lower and middle stratosphere, resulting aerosol, ozone and water vapour profiles often extend well into the troposphere under cloud-free conditions.

Launched on October 5, 1984, the instrument was planned to be operational for two years. It has marked its 17 years on orbit in 2001 and still generates data. The next generation of the instrument, SAGE III, is now in orbit. It will enhance the existing measurements and introduce new features. One important addition will be the ability to detect clouds present at altitudes between 6 km and 30 km which includes the Polar Stratospheric Clouds that play such an important role in ozone photochemistry.

HALogen Occultation Experiment (HALOE)

HALOE is another instrument aboard UARS spacecraft. Using solar occultation it measures O_3, HCl, HF, CH_4, H_2O, NO, NO_2, aerosol extinction, and temperature versus pressure. At the Earth's limb the instrument's field of view is 1.6 km and over a one-year period the latitudinal coverage is from 80° S to 80° N and includes extensive observations of the Antarctic region during spring. The vertical profiles are retrieved for the altitude range of 15 km to 60-130 km depending on channel. The ozone vertical profiles are of very good accuracy in clear conditions (~5% above 250 mb). The aerosol situation affects the results greatly and can reduce the accuracy to only 50% under post-volcanic conditions. The

61

HALOE team maintains an excellent web site at haloedata.larc.nasa.gov with quality and validation results as well as data archives and coverage maps.

Emission

Microwave Limb Sounder (MLS)

MLS is a three-mirror antenna system receiving thermal radiation from the atmospheric limb [http://mls.jpl.nasa.gov]. Launched on September 12, 1991 on NASA's Upper Atmosphere Research Satellite (UARS) [Barath et al., 1993], MLS within days started providing valuable information about stratospheric SO_2 injected by volcano Pinatubo erupted on June 15 of that year.

The signal from the atmosphere is separated and delivered to 3 radiometers: the 63 GHz radiometer for temperature and pressure measurements, the 183 GHz radiometer for water vapour and ozone in the stratosphere and mesosphere, and the 205 GHz radiometer for stratospheric ClO and ozone, as well as stratospheric sulphur dioxide, lower stratospheric nitric acid, and upper tropospheric water vapour. The instrument has an on-board calibration.

Scans of the limb are, under normal operation, performed continuously day and night with the integration time of about 2 seconds.

The main MLS products are stratospheric profiles of ozone, ClO, water vapour and temperature. MLS was the first satellite instrument to confirm earlier conclusions from ground-based and aircraft instruments that Antarctic vortex was filled with ClO in the regions where ozone was depleted. MLS observations have been used in studies of high latitude dynamics, namely polar vortices. It also provides global coverage for stratospheric ozone and in combination with TOMS total ozone column data ultimately can contribute to better understanding the tropospheric ozone changes.

Although some technical problems led to limiting the scientific agenda, MLS continues providing important information about the Earth's atmosphere. The MLS team does a wonderful job on the Internet of keeping public informed about the status of the mission as well as publishing the data.

3.2.3   Active sounding technique

DIfferential Absorption Lidar (DIAL)

The differential absorption lidar (DIAL) technique has been used since 1966. In this technique, two laser wavelengths are transmitted into the atmosphere and a receiver detects radiation backscattered from molecules and aerosols. One wavelength is used as a reference and has to be relatively unaffected by ozone while the other wavelength is tuned to an absorption feature of ozone. In order to optimize the DIAL signal at different altitudes, a pair of shorter wavelengths (usually 285 and 299 nm) is used for lower altitudes and a pair of longer wavelengths (usually 308 and 351 nm) is used for higher altitudes.

The receiver in the DIAL system is a telescope with a filter to reject out-of-band radiation. An aperture is used to limit the field-of-view to further reduce background radiation from the sky.

Since the signal scattered at different altitudes reaches the receiver at different times, the DIAL instrument directly measures the vertical profile of ozone. The profile can be integrated to obtain the column ozone amounts.

The accuracy of the DIAL instrument is limited by interference from other molecular species that absorb in the same spectral region (for example SO_2) and by the uncertainty in the values of the ozone absorption cross-sections. There is also a limitation on precision coming from photon noise. When utilising only two wavelengths, the effect from aerosols cannot be removed. Generally, the meas-

urement precision is about 5% for altitudes lower than 25 km, decreasing to 20% at 47 km, with an average vertical resolution of about 1 km. The precision can be improved by reducing the vertical resolution.

A number of ground-based lidar systems have been measuring ozone in the stratosphere including the high Arctic station at Eureka, Nunavut [Donovan 1996, 1997, 1998]. The obvious advantage of the DIAL system is that the vertical distribution of ozone can be measured from the ground. The disadvantages are the high cost of construction and operation and the system immobility. Although some DIAL systems are capable of measuring ozone during the day, most are limited to night-time measurement only. As with many complex systems, a well-trained person must be present in order to conduct measurements.

4 The Brewer Ozone Spectrophotometer

Section 3.2.1 provided a brief description of the Brewer spectrophotometer. This chapter is devoted to a more detailed look at the hardware, software and the data processing algorithms of the Brewer spectrophotometer.

4.1 Main components of the Brewer spectrophotometer

The Brewer spectrophotometer consists of fore-optics, monochromator, photomultiplier, electronics, and power supply (see Figure 4.1). To be fully flexible in azimuth direction the Brewer spectrophotometer needs to be mounted on an azimuth tracker.

The first element of the *fore-optics* of the Brewer spectrophotometer is a reflecting prism (ZP1). The prism can be rotated around the optical axis of the fore-optics with a stepper motor. The rotation of the prism allows the instrument to change the zenith angle of the observation. During operation, the instrument can be pointed at a number of light sources; often the sun, but the moon, the zenith sky or the internal calibration lamps also serve as light sources.

There are three filter wheels controlled by stepper motors in the instrument. The first filter wheel (FW1) is used to switch between an open aperture, a ground quartz plate, polarizer 1 (perpendicular to entrance slit), polarizer 2 (parallel to entrance slit) and a blocker. The ground quartz is used as a diffuser for direct-sun and lamp measurements; one of the polarizers is used during all zenith-sky meas-

urements and the other is only used for research purposes; the blocker is used for dark count tests and the open aperture is in use for moon and UV measurements.
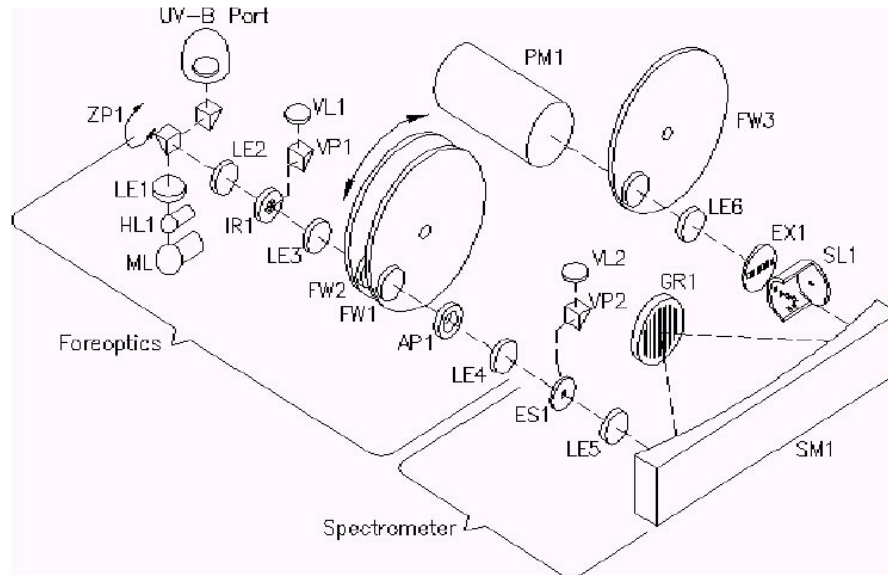
Figure 4.1 Optical elements of the Brewer spectrophotometer.
Adapted from Brewer Spectrophotometer Operator's Manual by Kipp&Zonen.

The second filter wheel (FW2) has an open aperture and a set of 5 neutral density filters to attenuate incoming radiation to a level that can be measured by a single UV-sensitive photomultiplier (PM1) used in the photon counting mode. To select a particular order in the spectrum produced by the diffracting grating (GR1) the third filter wheel (FW3) is used. In the standard configuration of a MKII Brewer, there is no FW3 since such instruments only work in the UV and the order

filter is mounted in the photomultiplier lens mount. As part of this study, one MKII Brewer (#029) was modified and fitted with FW3 to allow the selection of the visible spectrum in addition to the UV. The diffracting grating is an 1800 line/mm holographic type that produces a UV (280-380 nm) spectrum in the second order and a visible (560-760 nm) spectrum in the first order. An iris diaphragm (IR1) controls the field of view of the instrument when the ground quartz filter is used. The diffraction grating is mounted on an arm and can be turned by a micrometer driven by a stepper motor to set the dispersed spectrum in the proper place on the focal plane.

A set of lenses controls the beam of light in the fore-optics. First, a plano-convex lens LE2 focuses a parallel beam of light onto the plane of the iris, then another plano-convex lens LE3 collimates light passing through the iris along the optical axis. At the rear of the fore-optics a plano-convex lens LE4 focuses light onto the entrance slit of the monochromator.

The *monochromator* has a vertical entrance slit (ES1). A convex cylindrical-concave spherical lens (LE5) at the entrance slit corrects for coma and astigmatic aberrations inherent in the Ebert design. A spherical mirror (SM1) in the Ebert design is used to both collimate the source beam from the entrance slit side and to image the spectrum on the exit slit side. Inside the monochromator, a blocker is installed to prevent light reflected by the grating surface from getting into the exit slits. There are six exit slits (EX1) and a wavelength-selecting mask (SL1) that determines which slit is in use. The mask, which is driven by a stepper motor, has 8 positions: six positions allow each slit to be open while others are blocked, one position blocks all slits (used for the dark count measurement) and one position has two slits open blocking the remaining four (used in a linearity test).

67

During a measurement operation, the slit mask cyclically opens slits and the photon counts corresponding to the intensities falling on each slit are accumulated in one of seven registers. A cycle of measurements on all slits, including a dark count measurement and the time needed for the mask to move, takes 1.894 sec. with accumulation time for one slit of 0.1147 sec.

Lens LE6 called a Fabry lens and makes radiation which originates at a single point on the grating passing through any of the exit slits fall on the same place on the photomultiplier. The photomultiplier (PM1) is a low-noise EMI 9789QB05 type. The photon pulses are amplified, discriminated and divided by 4, before being transmitted to a counter. Each slit mask position has a separate register associated with it and the microprocessor inside the Brewer spectrophotometer synchronizes the switch of the slit mask position and the active register. Although there are separate registers for each slit position, the same photon counter is used.

The use of stepper motors provides the following accuracies and resolutions. The azimuth drive has a minimum increment (one step) of $0.02°$ and repeatability better than $0.2°$. The resolution of the zenith drive is $0.1°$/step with an accuracy of $0.2°$. The resolution of the drive moving the grating is 0.006 nm/step in the second (UV) order of the produced spectrum with an accuracy of 0.01 nm.

Light from a mercury vapour lamp (ML1) and a quartz halogen lamp (HL1), located just below the zenith prism, are used for wavelength calibration and for monitoring the sensitivity of the spectrometer at different wavelengths. A double-convex lens LE1 directs the light from the lamps along the optical axis.

A microprocessor unit operates all the motors and communicates with a personal computer through an RS-232 link. A power supply provides the necessary voltages for all instrument components [Kipp&Zonen, 1980].

68

4.2   Preparation of Brewer #029 for operation

As one of the first steps in this research, one Brewer spectrophotometer that had not been operational for some time was rebuilt and slightly modified. This work led to a better understanding of the instrumental part of the Brewer ozone spectrophotometer and to identifying areas where improvements are possible. As mentioned above, the Brewer spectrophotometer ozone data is used now for studying ozone trends and for improving atmospheric models. The quality of such research depends on the quality of the ozone data and every attempt should be made to improve the instrument and the data processing.

4.2.1   Hardware refurbishment and modifications

As part of this study, Brewer #029, originally a MKII instrument, was refurbished and then modified to what became known as a MKV or "red" Brewer. Brewer #029 was the primary test instrument for the entire project, however, data collected with other instruments were also used.

Refurbishment

To make Brewer #029 operational, a new photomultiplier and a new micrometer were installed. To ensure that the moving parts were in good shape, overall cleaning and lubricating was performed. Brewer #029 was intended to be installed in high Canadian Arctic so additional heating panels were installed.

Modification

MKV Brewers can take measurements in the visible part of the spectrum in addition to the UV measurements. Visible measurements are taken in the first

order of the Brewer's diffracting grating while the UV measurements are done in the second. To allow the instrument to switch between the two orders a filter wheel with two separate order filters was installed just before the photomultiplier. For the UV part the same filter, UG11, as in the conventional MKII Brewer is used and for the visible an orange glass filter OG550 is used. Figures 4.2 and 4.3 were adopted from the Schott Glass Technologies Inc. on-line catalogue [http://www.us.schott.com] to show the optical characteristics of UG11 and OG550. Since the transmission of UG11 filter has a 'tail' in the visible part (wavelengths 650 nm and longer) of the spectrum, the filter is used in combination with $NiSO_4$ filter that removes the tail.
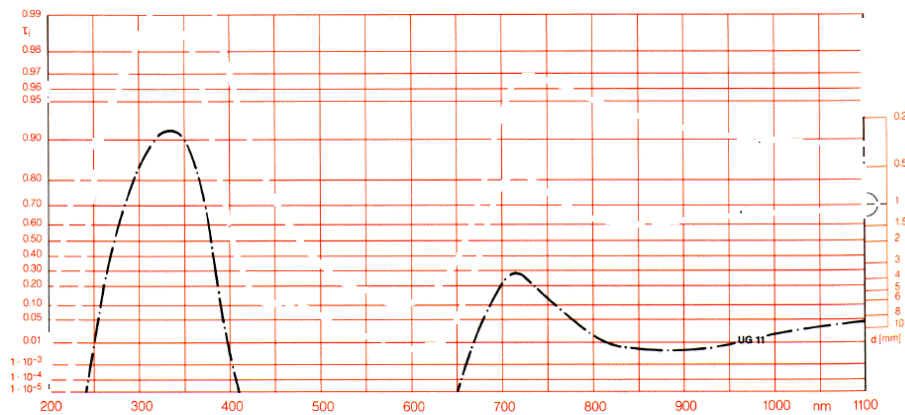
Figure 4.2 Transmittance of UG11 filter, the UV order filter in Brewer spectrophotometers.

It is used in combination with a $NiSO_4$ filter to limit the transmission to the UV only.
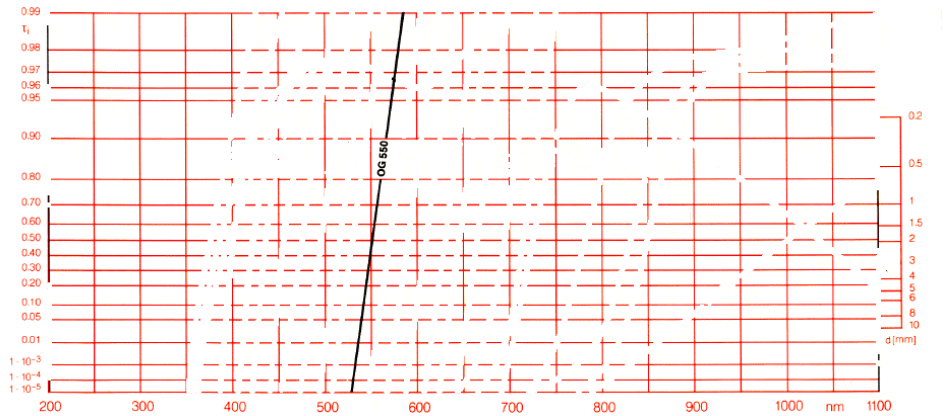
Figure 4.3 Transmittance for the orange glass filter OG550 for the visible part.
It is used in MKV modification of the Brewer spectrophotometer.

This configuration retains the capability of the instrument to take O_3 readings in the UV while adding the visible capability. One big advantage of having the visible part available is that the dispersion test (see below) can be done more easily now since a neon lamp alone can provide enough spectral lines in the visible spectrum to characterize the instrument's optical performance.

4.2.2 Instrument characterization and fine-tuning tests

Several tests have been completed to establish the optical characteristics of the instrument for this study. These tests include the spectral reference test HG, the linearity test to calculate the dead time constant DT, the test to establish the dispersion constants and the slit functions DSP, the sun scan test SC to fine-tune the operating wavelengths, and the temperature test.

Most of the tests used to analyze the optics of the Brewer instrument involve a use of lamps as a light source. Generally, whenever an internal or an external

71

lamp is used, it must be allowed to warm up for a sufficient time so that the lamp's radiance is stable before any tests are conducted. In the following sections, it is assumed that this was done, and so is not mentioned every time this process takes place.

High Voltage (HV) test

Each PMT has its own optimal high voltage setting [Budde, 1983], a setting at which two conditions are met: first, the signal-to-noise ratio is high, and second, a slight change in high voltage only slightly affects the signal.
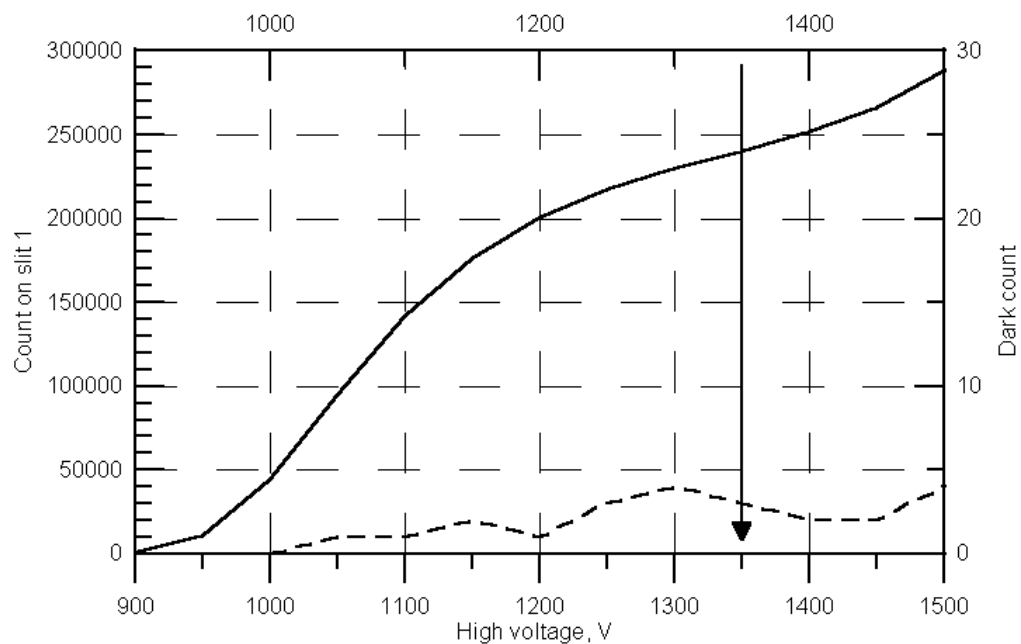
Figure 4.4 The High Voltage test with Brewer #029.

The optimal high voltage setting is 1350 V. Solid line is the counts on slit 1 and the dashed line is the dark count.

In the HV test, the dark current is used as a measure of noise and the signal is measured on slit 1. The manufacturer of the Brewer spectrophotometer suggests a range of high voltage settings between 850 V and 1550 V with an increment of 50 V for the test. Typical values for the photomultiplier model that is used in the Brewers are within these limits. The results of the HV test on Brewer #029 are presented in Figure 4.4. The results suggest that the optimal high voltage, the voltage where $\frac{d^2(counts)}{d^2V}=0$, is 1350 V, a typical value for the PMT in Brewer spectrophotometers.

Spectral reference (HG) test

The Brewer spectrophotometer uses a mercury lamp for its spectral reference. A double line is used, 302.150 nm and 302.347 nm. The line is chosen for its proximity to the operational wavelengths of the Brewer spectrophotometer. Alternatively, the test can be performed using the 296.7 nm line.

The test is performed by taking 12 measurements, 10 steps of the micrometer motor apart, of the intensity from the mercury lamp on slit 0. The resulting scan is compared to a reference scan recorded in the laboratory. The comparison of the scans is done by shifting the two scans against each other and calculating the correlation coefficient between the two after each shift. The interpolated step number resulting in the maximum of the correlation is the reference micrometer position. The micrometer is moved to this position after the HG test and all other micrometer movements are done relative to this reference. If the required adjustment of the micrometer position is more than one and a half steps, the test is repeated. The number of repetitions is limited and the test fails if this limit is reached. The HG test will fail, for example, if the error in the starting micrometer position is greater than 100 steps. In this case, the end sensors are used to set the

micrometer to an approximately correct position and the HG test is performed again.

The spectrometer is temperature compensated, but rapid temperature changes can lead to short-term wavelength errors. Since the temperature inside the instrument changes, the physical dimensions of the instrument's components change, causing the spectrum produced by the grating to shift. To keep an accurate spectral reference, the HG test is performed whenever the internal temperature of the instrument changes by $2°\,C$ as suggested by the manufacturer of the Brewer spectrophotometer.

Dispersion test (DSP)

In this test, the relationship between the step number of the micrometer that moves the grating and the wavelengths seen through each of the exit slits is determined. This is necessary to establish the operating wavelengths of the instrument as well as to be able to perform spectral scans (a UV scan for example). Three discharge lamps with different gases (vapours of Hg, Cd and In) were used to perform this test on Brewer #029. The lamps provide 9 spectral lines in the UV spectral region of the instrument. In addition, a neon lamp was used to provide three spectral lines in the visible part of the spectrum. The lines were scanned with each of the six exit slits and the position of the micrometer at the peak and the spectral width of the scan were established.

A quadratic was used to approximate the dispersion relations for each slit. The maximum fitting error was 0.006 nm in the UV, or about 1 step of the micrometer. Although this method can be improved, the position of the micrometer does not change during direct-sun measurements and thus the actual quality of the dispersion coefficients over a long range of micrometer movements is not impor-

74

tant for the UV ozone measurements. Recently, attempts have been made to improve the dispersion approximation by introducing a more complex formula [Grobner et al., 1998]. It was shown that by using such formula along with processing the data from all 6 slits together, the overall accuracy of wavelength setting is increased. This method has not yet been widely adopted.

For single spectral lines, the shape of the scan represents the slit function of the instrument (Figure 4.5), which, in general, changes with wavelength. It is not recommended to use doublet or triplet lines in this test as it is difficult to determine what wavelength represents the peak of the scan in these cases. The slit function of each exit slit is convolved with the ozone and sulphur dioxide absorption spectra to determine the effective cross-sections.
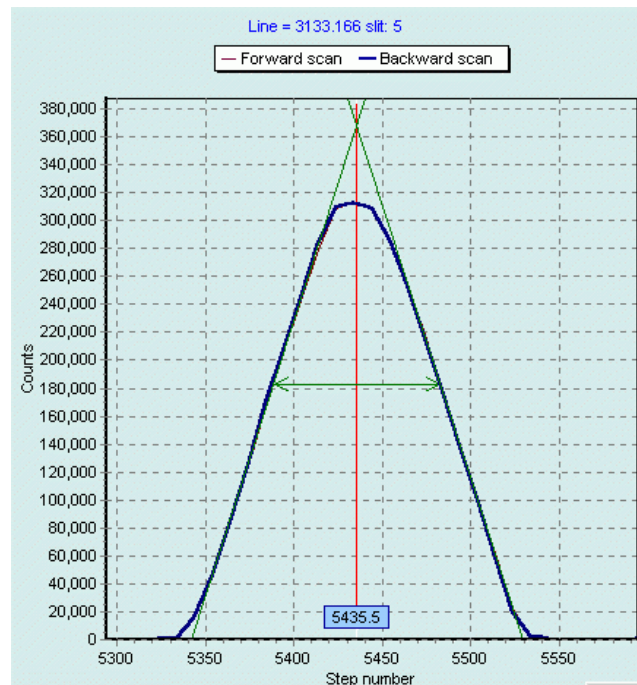
Figure 4.5 A sample of the dispersion test scan.

The graph shows a scan of the 313.32 nm Cd line with slit 5.

75

The dispersion test is usually done at the time of ozone calibration, at least once every two years. Brewer #029 has shown stable dispersion characteristics with a repeatability of the test of 1 micrometer step.

After establishing the dispersion characteristics, a table is prepared with wavelengths at each exit slit and the absorption coefficients for ozone and sulphur dioxide at several positions of the micrometer. The exact operating position is determined with the Sun Scan test.

Sun Scan test (SC)

The design of the slit mask for the Brewer spectrophotometer provides the operating wavelengths near the minima and maxima in the solar spectrum features. The SC test fine-tunes the position of the micrometer that minimizes the sensitivity of the ozone and SO_2 calculations to small changes in the angle of the grating.

To do this, a series of direct-sun measurements were taken at micrometer steps 125 to 153 with a 2-step increment. At each position, the ozone total column was calculated and plotted against the micrometer step number. Then, a quadratic was fitted to the data. One such a plot is presented in Figure 4.6. The position of the micrometer at the maximum of the fitted parabola is the optimal micrometer position where small variations in step number do not result in big changes in ozone calculations.

It is important to note here that the optimal position found this way is specific for the slant ozone column (vertical ozone column times the air mass factor) at the time of the test. In order to find the optimal position of the micrometer for the most of the measurements, a statistical analysis is necessary to establish the median ozone slant column during the year for the site.
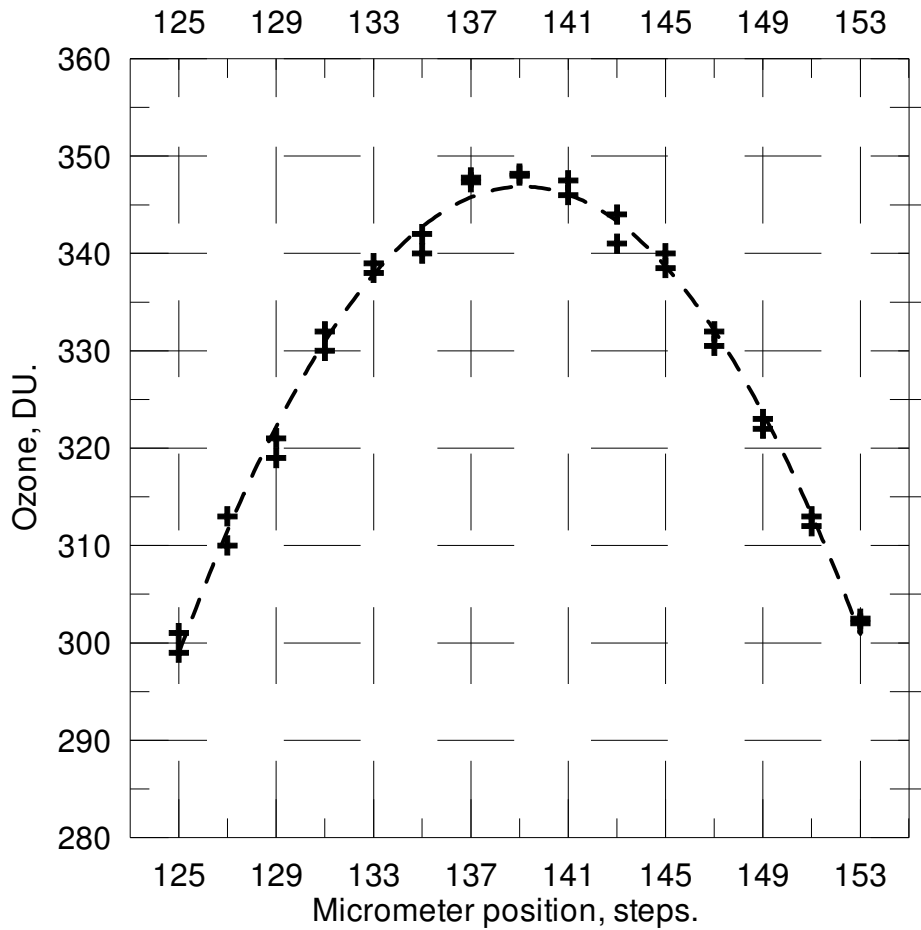
Figure 4.6 A sample of the SC test scan.

Brewer #029. Maximum ozone 348 DU at micrometer step 139.

Then, using Sun Scan test results at different ozone values and different air mass factors, the optimal position corresponding to the median column is interpolated. This is done by plotting the optimal micrometer position as calculated by the test against the slant ozone column and fitting the data with a straight line (Figure 4.7). For Brewer #029 the operating position was set to step 139. This

position of the micrometer translates into the operating wavelength set (302.137, 306.284, 310.023, 313.479, 316.774, 319.966), the wavelengths given in nm.
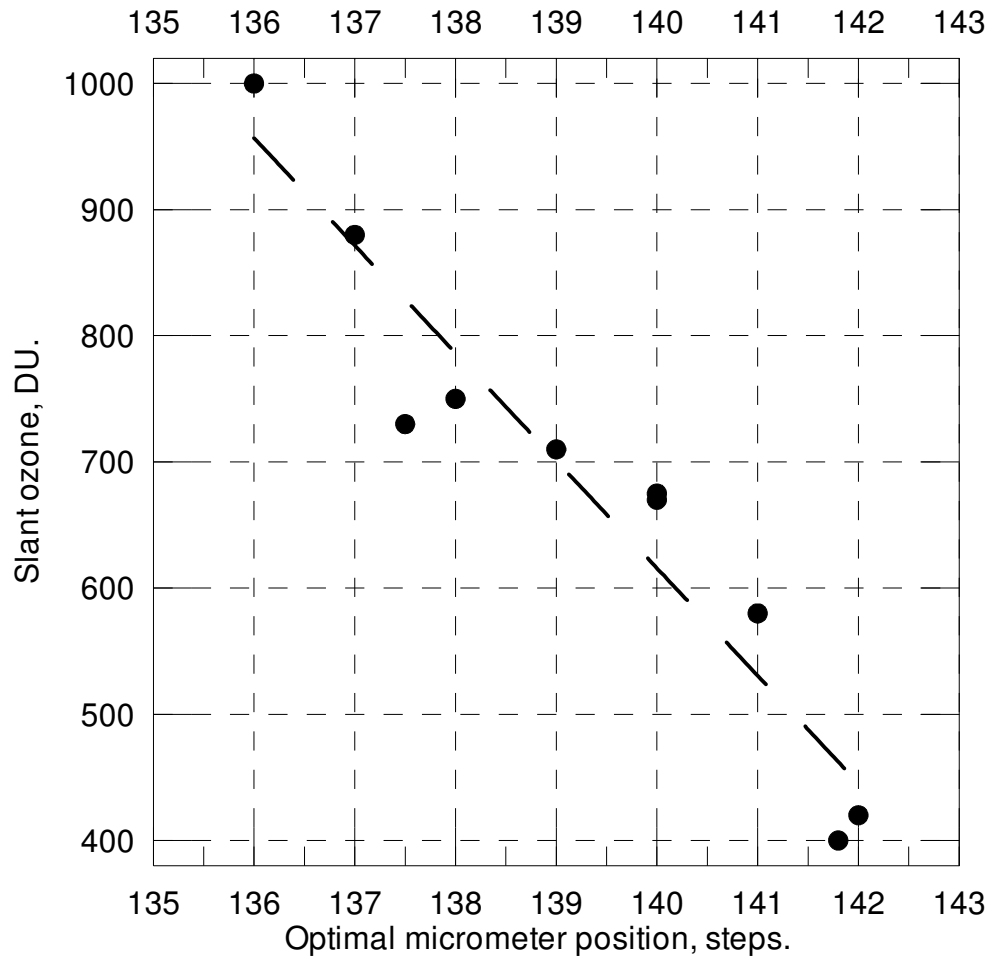
Figure 4.7 Establishing operating micrometer position.

Brewer #029: For Toronto median slant ozone is 680 DU. The operating

position was set to 139 steps.

Dead Time test (DT)

Since the radiance that the detector is exposed to in the Brewer spectrophotometer varies by several orders of magnitude depending on the ozone absorption at a particular wavelength and solar zenith angle, it is very important that the detection system is linear [Ingle, 1972; Lush, 1965]. To ensure the Brewer spectrophotometer's detection system is linear the DT test is used.

During the test the dead time constant DT is calculated using an iterative process. The Poisson formula is used to estimate the number of counts missed by the counting system during the dead time.

Three intensities are measured with a halogen lamp as a source of light. Two of the intensities, F3 and F5, are measured using slits 3 and 5 respectively, the third intensity, F7, is measured with the position of the slit mask where both slit 3 and slit 5 are open at the same time. For each of the intensities the Poisson equation holds:

$$
\begin{aligned}
F3 &= F3_0 \exp(-DT \cdot F3_0) \\
F5 &= F5_0 \exp(-DT \cdot F5_0) \\
F7 &= F7_0 \exp(-DT \cdot F7_0)
\end{aligned}
\tag{4.1}
$$

where F3, F5 and F7 are measured count rates (intensities) and $F3_0$, $F5_0$ and $F7_0$ are actual intensities, as if the dead time is zero.

The goal is to establish the dead time constant DT which, when applied, makes $F7_0=F3_0+F5_0$. This is done iteratively. On first iteration, $F3_0=F3$ and $F5_0=F5$. At each iteration $F7_0$ is set to $F3_0+F5_0$ and the third equation in the system (4.1) is solved for DT and then applied to the first two equations to solve for new estimates of $F3_0$ and $F5_0$. Ten iterations are performed which is enough for the sequence to converge. The standard DT test is repeated with two neutral

density filter positions to make sure the same dead time value can be applied to high and low intensities.

DT test is performed in the laboratory and the value of the dead time is used for correcting all the measured intensities. Also, the test is used for monitoring the detection system and performed at least once a day. The typical value of the dead time for the Brewer spectrophotometer is between 30 and 40 ns. Tests on Brewer #029 suggested the setting for the dead time to be 38 ns.

Run-Stop (RS) test

During normal operation the slit mask moves quickly to cycle from one open slit to another in order to effectively measure the intensities on all slits at same time. To ensure that the intensities measured in this fashion are the same as if they were measured when the slit mask is at rest the RS test is performed. During the test the internal halogen lamp is used as a source of light and the intensities at all slits are measured both in alternating slit mode for a total of approximately 40 seconds of integrating time on each slit, and in the mode when each slit is open for the same integrating time at once before the mask is moved to open the next slit. The ratio of the two intensities at each slit is the indicator of the slit mask performance. The manufacturer recommends the ratio on all slits to be between 0.999 and 1.001. There are ways of tuning the instrument if the ratio is out of range, but those are not in the scope of this dissertation.

Tests on Brewer #029 showed RS values within the recommended range.

Temperature coefficients

In order to measure the effects of internal temperature changes on the instrument response a special test was conducted in the laboratory. The instrument was subjected to a slow warm-up followed by a slow cooling-down; this process was

then repeated. During this process, using the internal halogen lamp as a source of light, the intensities at operating wavelengths were measured regularly to record the instrument response at different temperatures.

As ozone and SO_2 calculations do not depend on the absolute level of intensity, but rather on the relative distribution of radiation among the five operating wavelengths, the temperature coefficients were determined using ratios. The ratios are calculated as described in section 4.3.1. First ratios R were then plotted against the temperature T and a straight line was fitted to the data.

$$R = R_0 + TC \cdot T \qquad (4.2)$$

This linear approximation for the temperature dependence in practice holds with a coefficient of determination greater than 0.9 for all Brewer spectrophotometers.
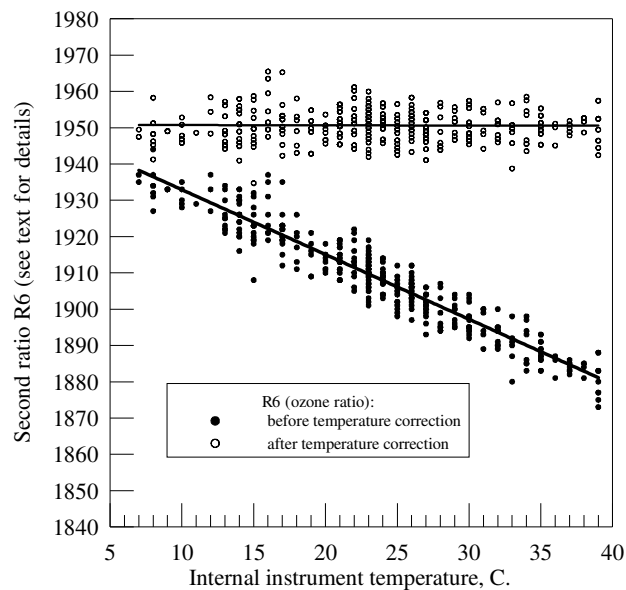
Figure 4.8 The result of temperature correction applied to second ratio R6.

The slope TC of the regression line is the temperature coefficient. Four such coefficients were calculated and used to compensate the results of all intensity measurements at the operating wavelengths. For Brewer #029 these values were set to (-0.4756, -0.8398, -1.5512, -3.0234). Temperature coefficients for second ratios are also calculated. Figure 4.8 shows an example of a temperature correction for second ratio R6 after the temperature test on instrument #029. It is seen in the graph that after the correction the values of R6 have no detectable temperature dependence.

4.3 Brewer operating software

A user of the Brewer spectrophotometer utilizes a computer to send commands to the instrument in the form of character strings. The instrument's microprocessor interprets the commands, executes them and sends a response, also as strings of characters. The low-level command language allows the user to move the motors to any given position, take a reading from a thermistor, take an intensity measurement or read the voltages/currents at designated checkpoints. The high-level commands are written in GWBasic programming language and allow the user to perform measurements and tests. For example, to take a direct-sun ozone measurement the DS command is entered.

The microprocessor's response to the completion of a command depends on the command itself. After completing a command to move a motor to a new position, the instrument's microprocessor returns a confirmation that the command has been completed by sending only a "carriage return" character. In case of other commands, the returned string may contain the requested values and has to be

interpreted by the computer. The temperature and voltage readings require only a simple scale transformation while the intensity readings involve more elaborate calculations to convert them to counts per second and correct for the dark count and the dead time.

4.3.1 Overview of the Standard Brewer algorithm for calculating O_3 and SO_2

A detailed description of the standard Brewer algorithm [Kerr et al. 1985,1988] was developed in early 1980s.

Although the next section is dedicated to the areas of the standard Brewer algorithm where improvements can be made, this section will also mention some issues in the algorithm that require attention. Such comments are underlined for easy identification.

There are additional corrections applied to an intensity reading if the intensity is used for calculating ozone.

Compensating for Rayleigh scattering

For ozone calculations, the intensity at each slit is compensated for Rayleigh scattering using a universal set of coefficients for all Brewer spectrophotometers, which is hard-coded in the software. The values are adjusted according to the instrument location's altitude by the factor of the ratio between the site's normal atmospheric pressure P and the standard atmosphere pressure of 1013 mb

$$F_0^R = F^T{}_0 + Re1\frac{P}{1013} \tag{4.3}$$

With the computers that are now used to run the Brewer software it is possible to easily <u>calculate Rayleigh coefficients individually for each instrument according to its operating wavelength set</u>.

Correcting for the neutral filter attenuation

The standard Brewer software operates under assumption that the neutral density filters used in the Brewer spectrophotometers attenuate all wavelengths equally. Each of the five neutral density filters has an assigned value that is used to compensate for its attenuation. These values are the same for all instruments; they are stored in logarithmic scale and used as follows:

$$F_0^N = F_0^R + ND \tag{4.4}$$

It should be noted here that under the assumption that the filters are wavelength-independent the actual values ND do not affect the ozone calculations since the algorithm for these calculations only works with relative intensities as it is seen below. However, it will be shown later that often <u>these filters are not "neutral" and thus DO affect the ozone calculations</u>.

Calculating ratios

When processing the ozone measurements or the standard lamp test measurements, the ratios of intensities from slits 2 to 6 are calculated. These are called 'ratios' even though they are in the log scale and could be called 'differences'. There are 4 first ratios R1…R4, and 2 second ratios R5 and R6. First ratios are calculated directly from intensity values F2…F6 corrected for the dark current, the dead time, the temperature, and the neutral density filter attenuation, and also for Rayleigh scattering in case of ozone.

84

$$R1 = F5 - F2$$
$$R2 = F5 - F3$$
$$R3 = F5 - F4 \qquad (4.5)$$
$$R4 = F6 - F5$$

The second ratios are derived from the first ratios (thus the name 'second'):

$$R5 = R1 - 3.2R4$$
$$R6 = R2 - 0.5R3 - 1.7R4 \qquad (4.6)$$

Ratios R5 and R6 are also known as SO_2 and O_3 ratios respectively. Combining equations (4.5) and (4.6) second ratios can also be expressed through the values F2…F6

$$R5 = -F2 + 4.2F5 - 3.2F6$$
$$R6 = -F3 + 0.5F4 + 2.2F5 - 1.7F6 \qquad (4.7)$$

The constant factors in the above equations (-1, 4.2, -3.2,….) were derived for a particular Brewer spectrophotometer to make R5 (SO_2 ratio) and R6 (ozone ratio) little dependent on any linear trends in the spectrum while making R6 also independent of SO_2 absorption. These constants are currently used in the standard algorithm for calculating ozone and SO_2 with all Brewer spectrophotometers. Section 4.4 has more details on these constants.

Temperature correction

Each of R1 to R6 are compensated for the instrument's temperature T using temperature coefficients TC (see eq. 4.8)

$$R^T = R + T \cdot TC \qquad (4.9)$$

85

The process of establishing the TC needs to be adjusted for temperature correction of absolute readings. The adjustment is very simple: the TC have to describe the temperature dependence of intensities at each slit rather than the ratios.

Calibration

Calibration of the Brewer spectrophotometer requires establishing its Extra Terrestrial Coefficients (ETC) as noted above. This is done by collecting data throughout the day, preferably at a site with clear air and stable atmospheric conditions. The Canadian Ozone Network uses Mauna Loa observatory (Hawaii, USA) for this process. After collecting the data, a Langley plot is done for the two ratios R5 and R6 to extrapolate the values to zero air mass. During the process only "good" measurements are used, in other words there is a safety procedure that reduces potential errors in establishing the ETC.

Because of the cost and complexity of the above calibration procedure, only a few instruments are regularly taken to Mauna Loa to maintain the absolute calibration. Another method for calibrating the Brewer spectrophotometers is utilized for the rest of the instruments. It involves the transfer of calibration from one instrument to another. This is done by taking ozone measurements with the two instruments working side-by-side and finding the ETC for the instrument being calibrated that give the least discrepancy in the ozone and SO_2 values between the two instruments.

Calculating ozone and sulphur dioxide

In the standard algorithm [see, for example, Kerr et al, 1985, 1988], second ratios R5 and R6 are used to calculate ozone and SO_2. Also, the extraterrestrial coefficients $ETCO_3$ and $ETCSO_2$ established during the calibration process are

involved. The values of the absorption coefficients are obtained from the processing of the dispersion test (section 4.2.2). First, the total ozone column, X_{O3}, is calculated as

$$X_{O3} = \frac{R6 + Re1 - ETCO_3}{\alpha m_{O3}} \qquad (4.10)$$

where Rel is the correction for the Rayleigh scattering, α is the ozone absorption coefficient and m_{O3} is the air mass factor. Then this value is used to calculate SO_2.

$$X_{SO2} = \frac{R5 + Re1 - ETCSO_2 - X_{O3}\alpha'm_{O3}}{\alpha'\beta m_{O3}} \qquad (4.11)$$

where α' is the effect of ozone on SO_2 and β is the SO_2 absorption coefficient.

The spectral response stability of the instrument and the Standard Lamp (SL) test

In order to maintain the quality of ozone and SO_2 calculations achieved by calibration a test of the instrument's stability is performed frequently. During the test, an internal halogen lamp is used as a source of light and measurements are taken in the same way as for direct-sun ozone. Second ratios then are used as indicators of the stability of the instrument and are compared to the values at the time of the last calibration.

4.3.2 Analysis of the standard Brewer algorithm for calculating O_3 and SO_2

In this section several sources of error in calculation of ozone and sulphur dioxide in the Brewer standard algorithm are identified. Addressing all of the

following issues in the proposed improved algorithm (see section 4.4) will increase the quality of the ozone and sulphur dioxide data.

Effect of aerosol presence

Aerosols are always present in the atmosphere and an attempt has to be made to estimate their effect on ozone calculations.

Using b=-1 in Angstrom formula (2.33) the effect on calculated ozone values from the presence of aerosol was estimated for the standard Brewer algorithm for twenty instruments. It worked out to be approximately 1 Dobson unit at aerosol optical depth of 0.3 at 320 nm, a typical value for Toronto. Being proportional to the aerosol optical depth, the effect can be as high as 4 Dobson units, or 1%, on a hazy day. This effect does not depend on aerosol vertical distribution (for the direct-sun observations) and thus will become noticeable also after a volcanic eruption when concentration of aerosols in the stratosphere increases. The quality control built-in to the standard algorithm will reject some such results, but not all.

Effect of high amounts of sulphur dioxide in the path

The standard algorithm suffers also from being sensitive to high values of SO_2 in the atmosphere. The effect varies from instrument to instrument and is in the range of 0.2 Dobson Units in ozone for an SO_2 total column of 1 DU. In urban areas the sulphur dioxide content can jump to 10 DU resulting in an effect on the calculated ozone of 2 DU, or about 0.5%. Being a model inaccuracy, the effect of SO_2 presence is virtually never detected by the safety net of the algorithm.

Effect of high amounts of ozone in the path

Similar to high amounts of SO_2 affecting the ozone calculations, high ozone values will affect the SO_2 calculations as seen in equation (4.11). The effect can

be as high as 0.5 DU in SO$_2$ amount per each 100 DU of ozone. This makes it possible to have 3 DU error in SO$_2$ during ozone maximums at high latitude sites.

Effect of hard-coded Rayleigh coefficients

Because the Rayleigh coefficients are hard-coded in the processing software rather than calculated for each instrument individually, they too contribute to the error in the ozone calculations. The effect can be as high as 1% for some instruments and be negligible for others.

Each of the three sources of errors, aerosol, SO$_2$ and Rayleigh, can produce both positive and negative effects on calculated values of ozone and sometimes compensate each other, but since it is not the case for all instruments, these errors must be minimized where possible.

Effect of the neutral density filters not being neutral

In order to measure the actual attenuation of each of the five neutral density filters at each of the five operating wavelengths a special test was developed. During the test, called F9, the intensity of the internal halogen lamp is measured at all operating wavelengths using no attenuation and then using each of the five neutral density filters. The attenuation of each filter is then calculated separately for each of the wavelengths. To reduce the error associated with a possible instability in the lamp intensity the measurements are done oscillating both filter position and slit number during the entire integration time. Also, the integration time increases for high values of attenuation to keep the same signal-to-noise ratio. Figure 4.9 shows the results of such a test on instrument #029. Since only relative slit-to-slit differences in attenuation are important the graph presents the attenua-

tion in relation to slit 5, i.e. positive values represent larger and negative values represent smaller attenuation than that at slit 5.
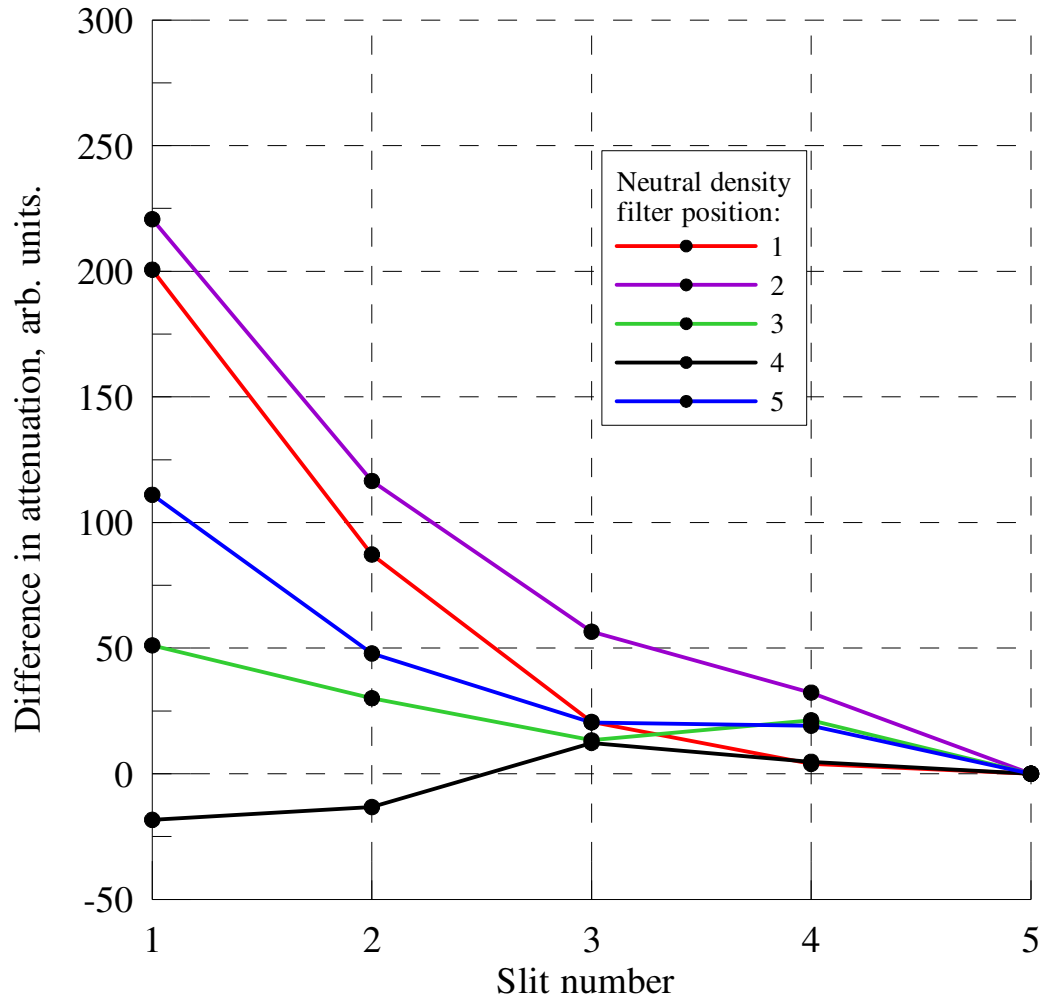
Figure 4.9 Spectral characteristics of a set of neutral density filters. Attenuations are plotted in comparison to those at slit 5.

The resulting values for attenuation can be easily converted into errors in ozone and SO_2 calculations (equations (4.7)). The errors vary from instrument to instrument, can be both positive and negative and they are different at different air-mass factors.   For twenty instruments tested the errors ranged from -20 to 20 Dobson Units for ozone, big enough to be of concern. It should be noted here that the calibration process somewhat compensates for this effect by introducing the extraterrestrial coefficients which absorb most of the effect, but only for the neutral density filter that was used during the calibration and those of similar spectral response. If more than one filter was used, the ETC will have an overall partial compensation for the effect. In other words, the actual effect from spectral difference in attenuation is the difference in the effects between the filter used during the calibration and the rest of the filters in the instrument. In fact, if all the filters in an instrument had exactly the same relative spectral characteristics the ETC would remove the problem altogether. In reality, in all cases tested the filters are spectrally different and have to be dealt with.

Effect of stratospheric temperature change

The use of ozone cross-sections measured at temperature of –45ºC (228K) in the standard Brewer software is based on the assumption of constant stratospheric temperature as well as the lack of accurately measured cross-sections at different temperatures at the time of the software development. Also, the implementation of temperature-dependent ozone cross-sections requires more computational power than was available at the time.

Temperature profiles are measured by a number of methods, including *in-situ* measurements with weather balloons. As noted in section 2.3, it is well established that stratospheric temperature changes during the year at any given location.

This means that the assumption of constant stratospheric temperature introduces a potential error, which now is easily assessable. Using typical values for the Brewer operating wavelengths and a global stratospheric temperature range from 215 K to 245 K the percentage difference in ozone absorption coefficient used in the Brewer algorithm was calculated and presented in Figure 4.10.
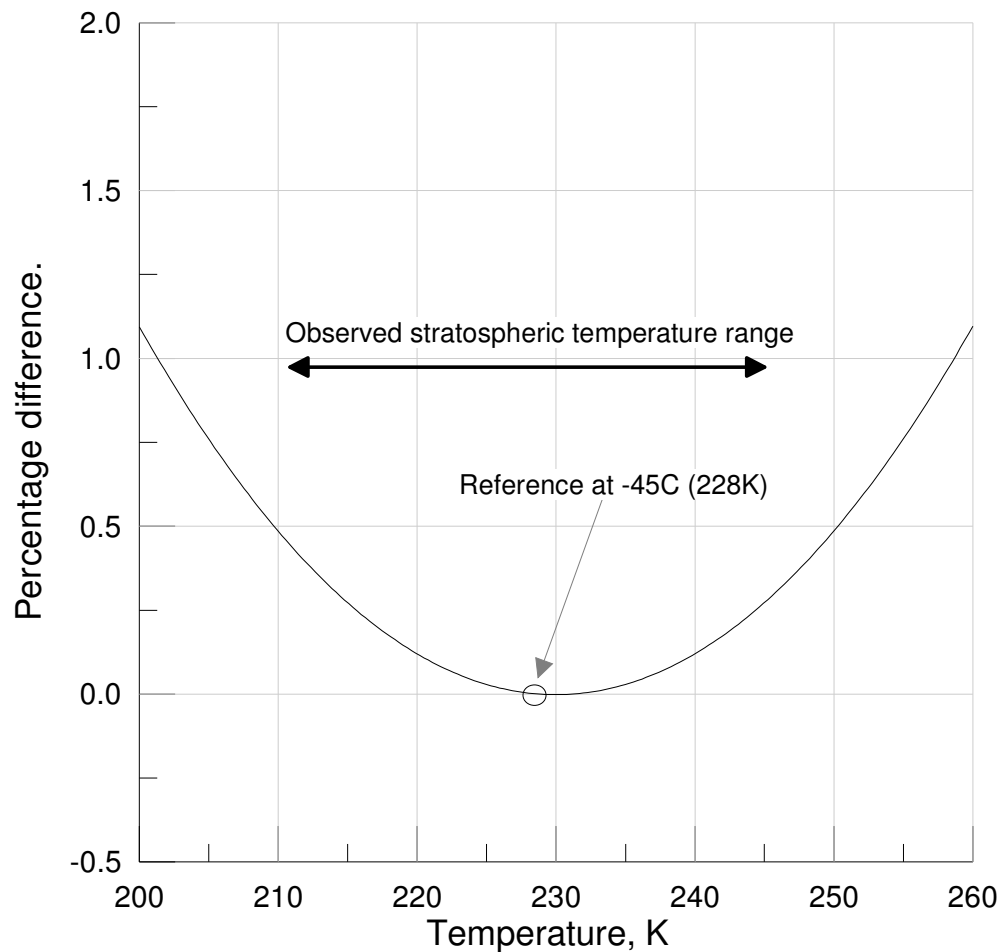
Figure 4.10 Stratospheric temperature change and Brewer calculations. Effect of the change on ozone absorption coefficient as calculated in the Brewer direct-sun method.

The graph shows that the effect should not be more than 0.5%. This result was calculated using the GOME ozone absorption spectra. The result differs slightly from Kerr's [2002] because he used spectra estimated from the direct-sun measurements at 45 wavelengths with one Brewer instead of laboratory measurements. The results of the ozone temperature calculations using the GOME spectra are presented in the next Chapter and they suggest that the GOME spectra are appropriate for use with the Brewer spectrophotometers.

4.4 The improved algorithm for calculating ozone and sulphur dioxide columns with the Brewer spectrophotometer

Here, the general equations developed in section 2.7 (see page 44) will be applied to Brewer-type direct-sun measurements.

The idea behind the improved algorithm developed in this study is solving these equations individually for each instrument, thus using as much information about the optical and mechanical characteristics of the instrument as possible. Also, information about aerosol optical depth and the effective temperature of the ozone layer is derived in addition to the values for ozone and sulphur dioxide.

4.4.1 Near ultraviolet region

In the near-ultraviolet, direct-sun measurements, the Brewer spectrophotometer registers intensities at five wavelengths. These wavelengths are slightly different for each instrument and are approximately 306.3, 310.1, 313.5, 316.8, and 320.0 nm.

Although the spectral resolution of the Brewer instrument is high enough (about 1 nm) for Beer's law to hold for direct-sun measurements [Denney and Sinclair, 1987], absorption cross-sections $\sigma(\lambda)$ do need to be convolved with the slit function $f(\Delta\lambda)$ for each slit to obtain the cross-sections at the instrument resolution $\overline{\sigma}(\lambda)$ as in

$$\overline{\sigma}(\lambda) = \frac{\int \sigma(\lambda')f(\lambda'-\lambda)d\lambda'}{\int f(\lambda'-\lambda)d\lambda'} \tag{4.12}$$

The slit function $f(\Delta\lambda)$ is measured using the dispersion test, which is described in section 4.2.2 (page 74).

To simplify notation, the following equations will use σ to denote cross-sections already convolved with the appropriate slit functions. To further simplify the equations, the equivalent absorption coefficient for standard pressure and temperature is introduced through $k=\sigma N_0$.

Taking into account absorption by ozone (O_3) and sulphur dioxide (SO_2) and scattering by air molecules (R) and aerosol (aer), the total slant optical depth of the atmosphere, $\tau(\lambda)$, can be written as

$$\tau(\lambda) = \tau_{O3}(\lambda) + \tau_{SO2}(\lambda) + \tau_R(\lambda) + \tau_{aer}(\lambda) \tag{4.13}$$

Substituting (2.27), (2.32) and (2.33), write

$$\tau(\lambda) = k_{O3}(\lambda)m_{O3}X_{O3} + k_{SO2}(\lambda)m_{SO2}X_{SO2} + \beta(\lambda)m_R + a\lambda m_{aer} \tag{4.14}$$

The air mass factors for ozone and sulphur dioxide are taken to be the same (layer height at 22 km) with the assumption that there are only a few sites with high level of SO_2 at the ground and most sites will measure stratospheric SO_2 after a volcanic eruption. The error associated with measurements of tropospheric SO_2 using this air mass factor is about 1% at the largest solar zenith angle used by the Brewer spectrophotometer (air mass factor 3.5). This error is much smaller than the achievable accuracy of SO_2 measurements. In the Brewer software the air mass factors are calculated using equation (2.24) with the values R_E=6370 km for the radius of the Earth, h=22 km for ozone and sulphur dioxide, and h=5 km for Rayleigh and aerosol. In the presence of large amounts of stratospheric aerosol, this will lead to an error in aerosol optical depth calculation of up to 1%. Since catastrophic volcanic eruptions do not happen very often, such situations can be dealt with on individual basis.

Recently, a study [Savastiouk, 2004] found that by using h=5.7 km in the Brewer calculations for air mass factors for Rayleigh and aerosol the accuracy of the approximation formula for air mass factor is increased and remains as small as 0.5% at solar zenith angles up to 89 degrees. The study also suggests using a latitude-dependent h for ozone air mass factor based on ozone climatology [e.g. Bowman, 1985].

Using Beer's law the relation between the solar irradiation at wavelength λ and the radiation at the same wavelength reaching the ground, may be written as

$$I_\lambda = I_\lambda^0 e^{-(k_{O3}(\lambda)m_{O3}X_{O3}+k_{SO2}(\lambda)m_{SO}X_{SO2}+\beta_\lambda m_R+a\lambda m_{aer})}$$

(4.15)

where we have used (2.17) and (4.14).

Each Brewer instrument has its own response function, $R(\lambda)$, that describes the instrument's sensitivity at different wavelengths (including any attenuation filters that may be used) and converts radiation units (I_λ) to instrument response units (C_λ) (counts per second in case of the Brewer spectrophotometer). The instrument response function in general depends on the internal temperature of the instrument, but in practice it is easier to correct C_λ for temperature than deal with temperature dependent $R(\lambda)$. In the following equations it will be assumed that the C_λ have been corrected for instrument's temperature, as well as for the dark count and the dead time:

$$C_\lambda = R(\lambda) I_\lambda^0 e^{-(k_{O3}(\lambda) m_{O3} X_{O3} + k_{SO2}(\lambda) m_{SO} X_{SO2} + \beta_\lambda m_R + a\lambda m_{aer})} \qquad (4.16)$$

taking the logarithm of (4.16), gives

$$\ln C_\lambda = \ln R_\lambda + \ln I_\lambda^0 - k_{O3}(\lambda) m_{O3} X_{O3} - k_{SO2}(\lambda) m_{SO2} X_{SO2} - \beta_\lambda m_R - a\lambda m_{aer} \quad (4.17)$$

In order to incorporate the temperature dependence of k_{O3}, equation (2.28) is considered in the vicinity of an estimated temperature T_0:

$$\begin{aligned}
k_{O3}(T) &= (A + BT + CT^2) N_0 \\
&\cong k_{O3}(T_0) + \left.\frac{\partial k_{O3}}{\partial T}\right|_{T=T_0} (T - T_0) \\
&= \left((A + BT_0 + CT_0^2) + (B + 2CT_0)(T - T_0)\right) N_0 \qquad (4.18) \\
&= \left(A - CT_0^2\right) N_0 + \left(B + 2CT_0\right) N_0 T \\
&= A'(T_0) + B'(T_0) T
\end{aligned}$$

where $A'(T_0)=(A-CT_0^2)N_0$ and $B'(T_0)=(B+2CT_0)N_0$. Substituting (4.18) into (4.17) and assigning $ETC_\lambda = \ln R(\lambda) + \ln I^0_\lambda$, write

$$\ln C_\lambda = ETC_\lambda - \left(A'(T_0)+B'(T_0)T\right)m_{O3}X_{O3} - k_{SO2}(\lambda)m_{SO2}X_{SO2} - \beta_\lambda m_R - a\lambda m_{aer} \quad (4.19)$$

The four unknowns in the equation above are X_{O3}, X_{SO2}, parameter 'a' and temperature 'T'. Equation (4.19) is true for each of the five wavelengths measured by the Brewer spectrophotometer. ETC values for each wavelength are found by extrapolating a linear fit to {lnC , m} pairs (also called Langley plot) to zero air-mass, using data from a clear day with little ozone variation. As part of this study an algorithm for processing calibration data collected with different neutral density filters was developed. As mentioned before, actual attenuation values for each filter as a function of wavelength is needed for correct interpretation of the direct-sun measurements. This new algorithm calculates these attenuations from the direct-sun measurements at the same time providing the extraterrestrial spectrum. Section 4.4.5 describes the process and gives an example of such a calculation.

Because all five intensities are measured nearly simultaneously, the five corresponding equations can be solved as a system assuming that the unknowns (ozone column, sulphur dioxide column and aerosol optical depth) stayed constant during the measurement. In order to solve the system, the Singular Value Decomposition (SVD) method is used [see, for example, Stewart 1973]. The algorithm for calculating the SVD of a matrix was taken from Golub [1989].

Two versions of the solution for ozone were realized. The first being the solution of the system of equations (4.17), where temperature of the ozone layer is fixed, and the second being the solution of the system (4.19), where the tempera-

ture of the ozone layer is allowed to vary. The main argument for doing this is to assess the impact of the stray light inside the instrument. Its effect increases as wavelength decreases. This is because the intensity of the solar beam rapidly decreases at shorter wavelengths and a given number of stray light photons will cause a greater effect where the genuine intensity is small. Equations (4.17) and (4.19) can be solved without the data from slit 1, which has the shortest wavelength and the biggest effect from stray light. Equations (4.19) have four unknowns (temperature is additional to those in (4.17)) and solving only four equations (slits 2 through 5) reduces the quality of the solution. Also, the data collected with slit 1 has the most information about the temperature of the ozone layer as the total effect of temperature change is proportional to ozone absorption, which is highest at the wavelength of slit 1. Thus, the temperature-variable solution is obtained by solving all five equations (4.19). To minimize the effect of stray light on slit 1, only data collected at small solar zenith angles is considered. By comparing data from the MKII (single monochromator) and the MKIII (a double monochromator; it has no noticeable stray light effects measuring ozone slant column up to 2000 DU) Brewer versions, the limit was set to ozone slant column to be less than 800 DU, which provided agreement between the two Brewer models to within 1% on slit 1.

The inversion of the system (4.17) can be performed before taking any measurements. The result will be a vector of weighting coefficients w_i that transform the four intensities into ozone values.

$$X_{O3} = \frac{\sum_{i=2}^{6}(\ln C_i - \ln I_{0i} + R_i)w_i}{m_{O3}\sum_{i=2}^{6}\beta(\lambda_i)w_i} \qquad (4.20)$$

The following three tables compare the weighting coefficients for ozone, sulphur dioxide from the original algorithm (see p.85, the same for all Brewers, in bold font) with those calculated by solving system 4.17 individually for four Brewer spectrophotometers. The last of the three tables (Table 4.3) show weighting coefficients for the first iteration in the calculation of ozone temperature.

As one can see, for ozone and sulphur dioxide for some instruments these coefficients are close to the original ones, and for others they are quite different. This shows why there is a need for an individual approach to every instrument. It is also important to note that the individually calculated weighting coefficients do not significantly change the calculated error contributed by the measurements at the 5 operating wavelengths compared to the original weighting coefficients.

Instrument	Slit 1	Slit 2	Slit 3	Slit 4	Slit 5
Original	**0.00**	**-1.00**	**0.50**	**2.20**	**-1.70**
#007	0.00	-1.00	-0.17	3.50	-2.33
#008	0.00	-1.00	-0.43	4.04	-2.61
#042	0.00	-1.00	0.26	2.63	-1.89
#151	0.00	-1.00	0.20	2.75	-1.95

Table 4.1 Weighting coefficients for O_3 calculations for several instruments.

Instrument	Slit 1	Slit 2	Slit 3	Slit 4	Slit 5
Original	**-1.00**	**0.00**	**0.00**	**4.20**	**-3.20**
#007	-1.00	0.00	0.00	4.42	-3.42
#008	-1.00	0.00	0.00	4.44	-3.44
#042	-1.00	0.00	0.00	4.45	-3.45
#151	-1.00	0.00	0.00	4.44	-3.44

Table 4.2 Weighting coefficients for SO_2 calculations for several instruments.

Instrument	Slit 1	Slit 2	Slit 3	Slit 4	Slit 5
#007	-0.28	0.73	0.15	0.76	-1.36
#008	-0.23	0.67	0.09	0.83	-1.36
#042	-0.26	0.68	0.18	0.80	-1.40
#151	-0.25	0.68	0.15	0.81	-1.39

Table 4.3 Weighting coefficients for ozone temperature calculations (for the first iteration) for several instruments.

Calculating these weighting coefficients at the time of an instrument's calibration allows the present Brewer software to be used unchanged with the exception of having these coefficients to be instrument parameters and not hard-coded numbers.

4.4.2 Retrieving the aerosol optical depth in the UV

Once ozone and sulphur dioxide have been retrieved, the only unknown in the system (4.17) is aerosol. Simple arithmetic gives the aerosol optical depth at each operating wavelength. Alternatively, the SVD gives the parameter 'a' for the Angstrom formula. In practice, the two methods gave almost identical results and the former is easier to implement in GWBasic.

4.4.3 Calculating the effective temperature of the ozone layer and "temperature compensated" ozone values

The solution of the temperature dependent system (4.19) is found iteratively, adjusting T_0 at each iteration. The first guess is always $-45°$ C, the temperature assumed by the standard Brewer algorithm. The resulting value of T after each iteration is used as T_0 for the next iteration. The iterative process is continued until it converges. In this study the criterion for the convergence was the absolute value of the difference $T-T_0$. The iterative process stopped when T is within 0.1 degree from T_0, which was usually achieved in 3 or 4 iterations.

4.4.4 The visible region

The interest in developing ozone measurements using the visible part of the solar spectrum is driven by the increasing attention to ground ozone measurements at high latitude stations where ozone has been declining [Fioletov, 1997; Langer, 1999]. As mentioned earlier, ozone measurements in the UV are limited

to relatively small ozone paths due to the very strong ozone absorption in the region. However, the ozone absorption is much less in the visible part of the solar spectrum and this allows the measurements to continue for as long as the sun is above the horizon. This is extremely important at high latitudes where in the winter the sun may not rise high enough for UV measurements.

Before this study, there had been an attempt to use the Brewer spectrophotometer for visible ozone measurements by Kipp&Zonen Inc. (then SCI-TEC Inc.), the manufacturer of the Brewer spectrophotometers. The attempt was unsuccessful for the most part due to inadequate scientific preparation. This included the use of incorrect Rayleigh coefficients as well as a poor choice and insufficient number of operating wavelengths. In addition, the viewing ports (VL1 and VL2 in Figure 4.1) were not covered and allowed visible light scattered from the sky enter the instrument, which was not a problem for the UV operation since the viewing ports block the UV radiation.

Equations

The derivation of the system of linear equations from the previous section (4.4.1) can be repeated for the visible region of the spectrum taking into account that the only strong absorber in the 550-620 nm region is ozone. Other gases that do absorb solar radiation in this region are water vapour (H_2O) and NO_2. These two gases under normal conditions together have optical depth about 0.01 that of ozone and cannot be detected by the Brewer spectrophotometer. Thus, the following equation describes the solar beam for each measured wavelength.

$$\ln C_\lambda = \ln R_\lambda + \ln I_\lambda^0 - k_{O3}(\lambda)m_{O3}X_{O3} - \beta_\lambda m_R - a\lambda m_{aer} \qquad (4.21)$$

Because of relatively small ozone absorption in this region and because the ozone absorption spectrum does not have any high frequency features, more than just five wavelengths are needed. A special program was developed to take measurements in series of five wavelengths covering the region between 550 nm and 620 nm. A total of 25 wavelengths are measured at five different micrometer positions. At each micrometer position the measurements at the five slits are done virtually simultaneously and the five measurements can be treated as contemporaneous. This is not true, however, for all 25 readings and four additional constants are needed to allow for possible changes in absolute intensity between different micrometer positions. This can be easily seen as a change in the response function R by some factor S_i at i^{th} position of the micrometer. Also, the air mass factors will be different for each of the five micrometer positions. Assuming that ozone and aerosol do not change during the course of the measurement the 25 equations can be combined into a system of linear equations

$$
\begin{cases}
\ln C_1 = \ln R_1 + \ln I_1^0 - k_{O3}(\lambda_1)m^1{}_{O3}X_{O3} - \beta_1 m^1{}_R - a\lambda_1 m^1{}_{aer} \\
\vdots \\
\ln C_{25} = \ln R_{25} + \ln S_5 + \ln I_{25}^0 - k_{O3}(\lambda_{25})m^5{}_{O3}X_{O3} - \beta_{25}m^5{}_R - a\lambda_{25}m^5{}_{aer}
\end{cases}
\tag{4.22}
$$

with 6 unknowns: aerosol, ozone and the four constants $S_2 \ldots S_5$. As with UV measurements, extraterrestrials ETC=ln R+ln I are found by a Langley regression for each of the 25 wavelengths. The solution of the system (4.22) is found by Singular Value Decomposition method which essentially finds the least square solution of the system.

4.4.5 Additional tests and calibrations

In addition to the existing tests and calibrations for the Brewer spectropho-
tometer, two more processes are added for all of the above improvements to work.
First, the temperature coefficients (TC) have to be calculated for each operating
wavelength separately (absolute TC), not for ratios as described in section 4.2.2.
This includes obtaining the TC for the operating wavelengths in the visible part of
the spectrum. Second, the attenuation values for each neutral density filter (NDF)
have to be established for each operating wavelength.

Since the internal standard lamp may change its intensity with time, the test
for establishing the absolute TC is best done with an external, more stable lamp.
Alternatively, the test can be performed using the internal lamp when the test is
done during relatively short period of time. After analyzing data from several
instruments, it was concluded that the internal standard lamp could be assumed
stable in terms of absolute intensity within hours, even days, but definitely not
weeks or months. An external lamp should be used where possible.

Two ways were developed for obtaining the NDF attenuations. First, using a
lamp as a source of light and measuring its intensity directly and with each NDF.
Second, analyzing the direct-sun data. In a simplified form, the Beer's law has the
form

$$\ln C_\lambda = ETC_\lambda - ND_i - \Omega_\lambda m \tag{4.23}$$

where the left hand side is the measurement, ETC is the extra-terrestrial constant,
ND represents the NDF attenuation, Ω represents the total effective optical depth
and m is the air mass factor. This equation is valid for each operating wavelength
and on a clear stable day, it is reasonable to assume that Ω for a particular wave-

length is constant, or has very small variations. Then all direct-sun measurements can be combined into one matrix

$$
\begin{cases}
\ln C_{\lambda 1} = ETC_{\lambda 1} - ND_1 - \Omega_{\lambda 1} m_1 \\
\vdots \\
\ln C_{\lambda p} = ETC_{\lambda p} - ND_k - \Omega_{\lambda p} m_n
\end{cases}
\tag{4.24}
$$

with p operating wavelengths, k NDF attenuations and n observations. The system consists of n·p equations and 2p+k unknowns: p extra-terrestrial coefficients, p total effective optical depths and k NDF attenuations. To put it simply, the system gives the results of Langley plots for each wavelength and by assuming the same slope Ω for all NDF, the attenuations of all NDF are retrieved. To further constrain the system, the second ratio ETC (sections 4.3.1 and 4.4.1) are used:

$$
\begin{aligned}
\sum_{l=1}^{5} w_l^{SO2} ETC_l = ETCR5 \\
\sum_{l=1}^{5} w_l^{O3} ETC_l = ETCR6
\end{aligned}
\tag{4.25}
$$

It has been suggested [Kerr, 1985] that the NDF attenuation changes linearly with wavelength. If that were the case, the NDF would not strongly affect the ozone calculation. While it may be true for some instruments, section 5.1 proves this not to be the case in general.
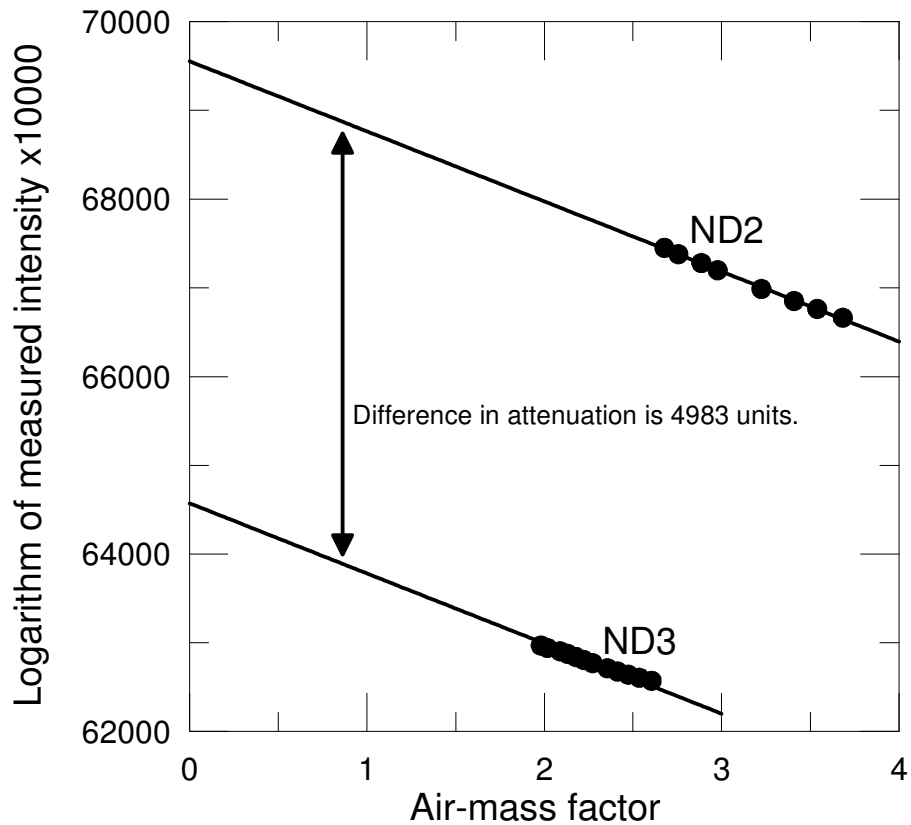
Figure 4.11 Obtaining the NDF attenuations from Langley plots.

Data collected at Mauna Loa observatory with Brewer #017.

Figure 4.11 illustrates how the Langley plots help obtaining the NDF attenua-
tions. The data for the graph was collected with Brewer #017 at Mauna Loa
observatory in 2002. Only data with two NDF are shown for simplicity. The
difference between the attenuation by ND2 and ND3 was estimated at 4983 from
the graph. The hard-coded value in the standard Brewer software difference is
5000 (equivalent to an optical depth of 0.5 base 10).

Usually, on a clear day, there are only a few observations at low attenuation filters and it is often difficult to obtain the NDF values for all 5 NDF in the Brewer spectrophotometer using only direct-sun data. In contrast, using the test with a lamp, it is often hard to collect good data with high attenuation filters as lamps are not bright enough. It was found in this study that the combination of the two methods gives the best results.

4.4.6 Uncertainties and errors

There are a number of sources of uncertainty and error in the direct-sun measurements and their interpretation. These include statistical noise in the photon counting system, changes in the optical characteristics of the atmosphere during the measurement period, inaccuracy in the instrument wavelength settings and changes in the instrument response with time. All of these sources are discussed here.

Reducing the effect of the statistical noise

A longer integration time reduces the effect from random noise. One measurement cycle in the Brewer spectrophotometer is about 1.8 sec; usually the direct-sun measurement consists of 20 such cycles, thus integrating the radiation over a period of about 40 sec. Adjustments of the neutral density filters keep the number of photon counts above $2*10^6$, so that the statistical counting uncertainty is below 0.07%. This corresponds to about 1 DU uncertainty in ozone (regardless of whether the original weighting coefficients are used or the individually calculated).

Dealing with changes in the atmosphere

During the 40-second measurement several changes in the atmosphere can occur. First, the ozone amount can change due to dynamical processes. Second, clouds can partially block the sunlight. The way to deal with this type of uncertainty is to take a number of measurements one after another and compare the results of the retrievals. The Brewer spectrophotometer is programmed to take five 40-second measurements and average the results. The standard deviation of the mean value serves as a measure of precision. The higher the standard deviation, the more likely some of the five measurements are not accurate. The ozone values are rejected if the standard deviation of the mean value is greater than 2.5 DU. This criterion ensures the precision of the ozone measurements to be within 1% under almost all observation conditions.

Minimizing the effect of the uncertainty in wavelength settings

The approximate wavelength positions are chosen with this in mind. To test and fine-tune, the Sun Scan described in section 4.2.2 (page 76) is used. When Sun Scan is done correctly, variations of ±3 micrometer steps from the operating position do not change the ozone values by more than 1 DU when measuring ozone slant amount 600-800 DU. If ozone slant amount is significantly different then the micrometer position must be within 1 step from the calibrated value. To ensure accurate and micrometer setting the HG spectral reference test is performed frequently.

Monitoring the instrument response

The Standard Lamp test (see section 4.3.1) is conducted to monitor the stability of the instrument response. A halogen lamp is used as a source of light in this test. The micrometer is kept in the position where ozone measurements are done.

During the test, intensities at each of the 6 operating wavelengths are collected. The secondary ratios as defined in page 84 are calculated. Because these values do not depend on absolute brightness of the lamp, they can be used to monitor the relative response of the instrument at the various operating wavelengths.

The R6 and R5 values at the time of the instrument's calibration are used as a reference and if the results of the test change between the calibrations, the extraterrestrial coefficients are adjusted to reflect the change. Since R6 and R5 are obtained in the same type of calculations as the secondary ratios for ozone, the adjustment necessary for the extraterrestrial coefficients are simply the difference between the R5 (or R6) at the time of calibration and that after the change in the result of the SL test.

Uncertainties in ozone calculations in the visible spectrum

Measuring ozone at large solar zenith angles requires accurate airmass factor (AMF) calculations both for ozone absorption and for Rayleigh scattering. The improved algorithm described in Savastiouk [2004] provides a 0.5% accuracy of the Rayleigh AMF calculations up to solar zenith angle (SZA) of 87. A bigger uncertainty comes from ozone AMF since it highly depends on ozone vertical distribution, which is not generally known at the time of the measurement. The potential variation in AMF due to global variation in ozone layer height, 18 to 26 km, is 3% at 80 degrees SZA. However, deviation of the ozone layer height from its climatology will translate to a much smaller uncertainty.

Ozone absorption spectra are also a source of uncertainty. Methods like described in Kerr [2002] can proof to be useful for establishing ozone absorption spectra from the atmospheric measurements rather than from the laboratory.

5 Applying the improved algorithm to the direct-sun measurements: Results

There are three major advantages in using the new algorithm for the interpretation of the direct-sun measurements made with the Brewer spectrophotometer in the UV. First, the precision of ozone and sulphur dioxide columns is improved. Second, in addition to ozone and sulphur dioxide columns the new algorithm also yields the aerosol optical depth in the UV and the effective temperature of the ozone layer. Third, the propagation of errors during calibrations is greatly reduced.

Furthermore, the introduction of a working algorithm for measuring the ozone column in the visible part of the spectrum increases the number of days in a year available for direct-sun ozone column measurements by ground-based instruments at high latitude sites. In addition, by calculating the aerosol optical depth in both the UV and the visible region optical characteristics of the aerosol can be assessed.

This section illustrates the effectiveness of the methods developed in the study by providing results of applying the methods to the data collected with the Brewer spectrophotometers in different parts of the globe. The main point here is to show that the improvements are seen in many Brewers and not just one test instrument.

5.1 Improvements in calculating ozone and SO_2

The improved algorithm for deducing ozone and SO_2 was applied to data from a number of the Brewer spectrophotometers. The main step forward in the algo-

rithm is that the model now more accurately describes the physics involved in the Brewer direct-sun measurements individually for each instrument. This makes calculated ozone and SO_2 values less instrument-dependent and reduces the residual.

The comparison of the results of the improved algorithm to those of the standard one showed a change for the better in the standard deviation of the individual results for ozone and SO_2 values in the improved algorithm. The fact that the standard deviation of the ozone values calculated with the improved algorithm is usually smaller then that resulting from the standard algorithm, indicates that the new solution fits the data better. This leads to more observations falling within the 2.5 DU acceptance range for the standard deviation. On average, about 3% more measurements become acceptable.

Since, in the improved algorithm, the aerosol and Rayleigh attenuations are properly taken into account, ozone and SO_2 values are reliable even during periods with a large aerosol optical depth. Figure 5.1 compares the standard and the new algorithm for ozone calculation. The data were collected on July 6, 2002 in Toronto with Brewer #008. As seen in the graph, the difference between the standard ozone values and the values properly compensated for aerosol and Rayleigh is over 1% on this hazy day. The effect on SO_2 is more difficult to present visually as it consists not only of errors from aerosol and Rayleigh but also of those from ozone, which is calculated with these errors.
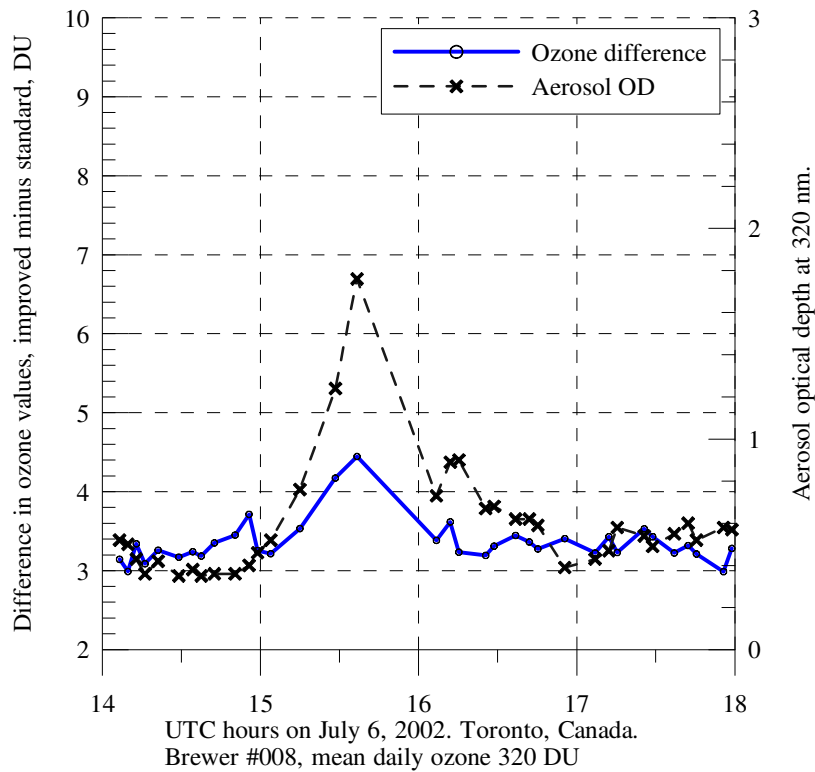
Figure 5.1 Effect of aerosol on ozone calculations.

The solid line shows the difference in ozone between the 'new' and the

standard algorithm.

To show what effect high ozone values can have on sulphur dioxide calcula-
tions, the data from Alert (82.5º N) collected with Brewer #029 on May 10, 2003
were processed with the standard and with the improved algorithm. The results
are in Figure 5.2, where two significant changes can be seen. First, the overall
scatter is reduced in the improved version both for ozone and sulphur dioxide
values. This again confirms that a better model was used in the interpretation for
the measurements.

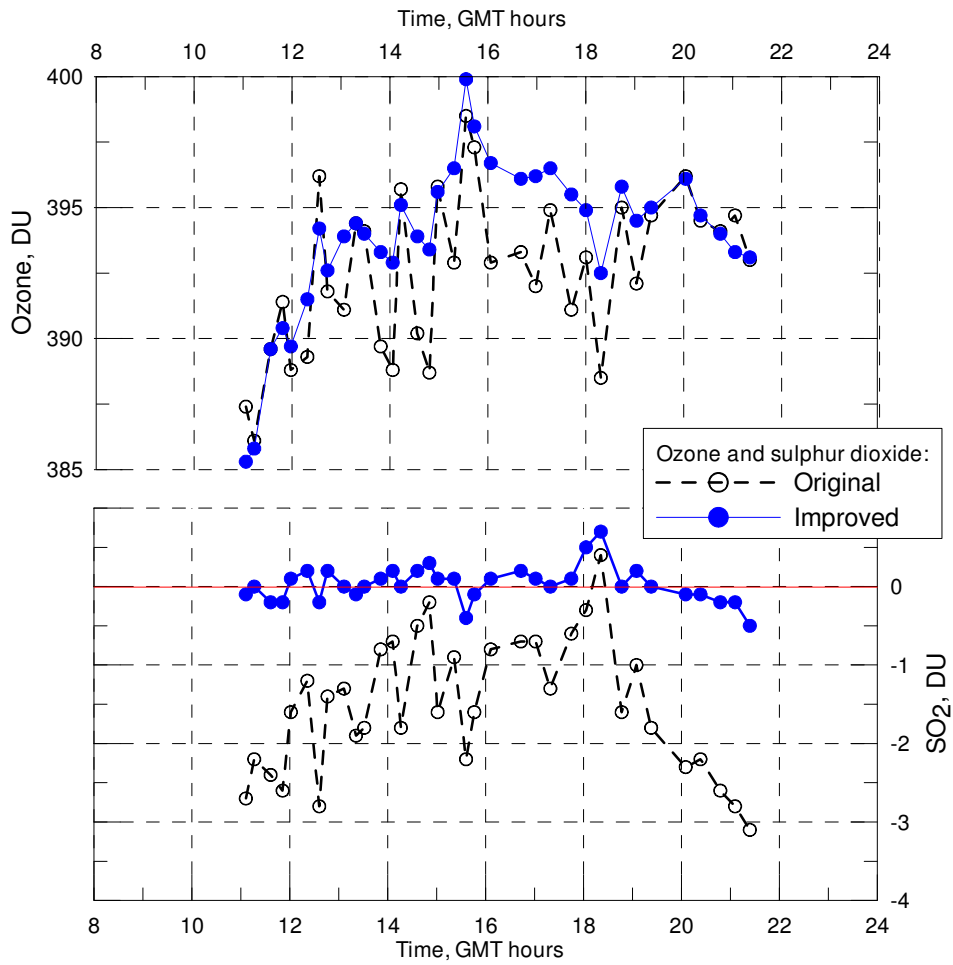Figure 5.2 Eliminating negative SO$_2$ values.

Alert station, Brewer #029, May 10, 2003.

Second, the SO$_2$ values calculated with the improved algorithm are close to 0, where they are expected to be. The standard SO$_2$ values are mostly negative due to impact of high ozone in the path. The range of air mass factors in the data is 2.5 to 3.0, which makes the total slant ozone column in the order of 1100 DU.
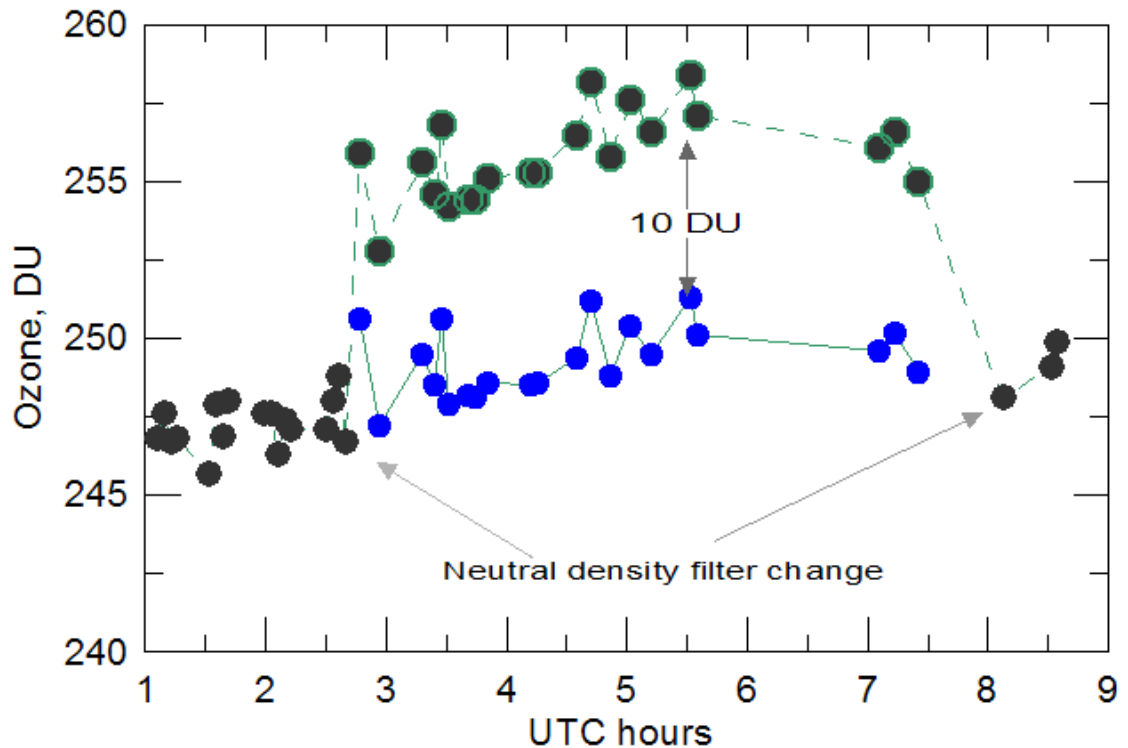
Figure 5.3 Example of a "neutral" filter affecting ozone calculations.
Brewer #090. See text for details.

Using proper characterization of the neutral density filters (NDF) is vital for O_3 and SO_2 retrieval. Figure 5.3 illustrates how large an effect the NDF can have on ozone calculations. The graph presents data from Brewer #090 (Malaysia). In the graph the dashed line shows the standard ozone calculations and the solid line shows the ozone calculated with proper correction for the NDF. In this instrument only the ND3 has a significant impact on ozone, which is about 7 DU, or 3%. The correction for ND3 eliminates the jump in ozone. In this case the jump is so obvious that it is easy to spot. In other cases such jump in ozone can be smaller

and may be interpreted as a real change in ozone. To avoid this it is important to correct all data for the NDF.

5.2   Calculating the aerosol optical depth in UV

First results for aerosol optical depth calculations with the Brewer spectrophotometer were presented in 1995 [Savastiouk, 1995]. This section will focus on results that are more recent and will give examples of the potential that this technique has.

In August of 1998, Brewer spectrophotometer #029 was used as a ground-based ozonometer in the Middle Atmospheric Nitrogen Trend Assessment (MANTRA) Campaign, which took place at Vanscoy, Canada. The data collected with the Brewer #029 was processed using the improved method and the aerosol optical depth was retrieved. The results (Figure 5.4) showed a very good agreement between the aerosol optical depth from the Brewer and the aerosol index calculated from the TOMS data [Savastiouk et al., 2005].
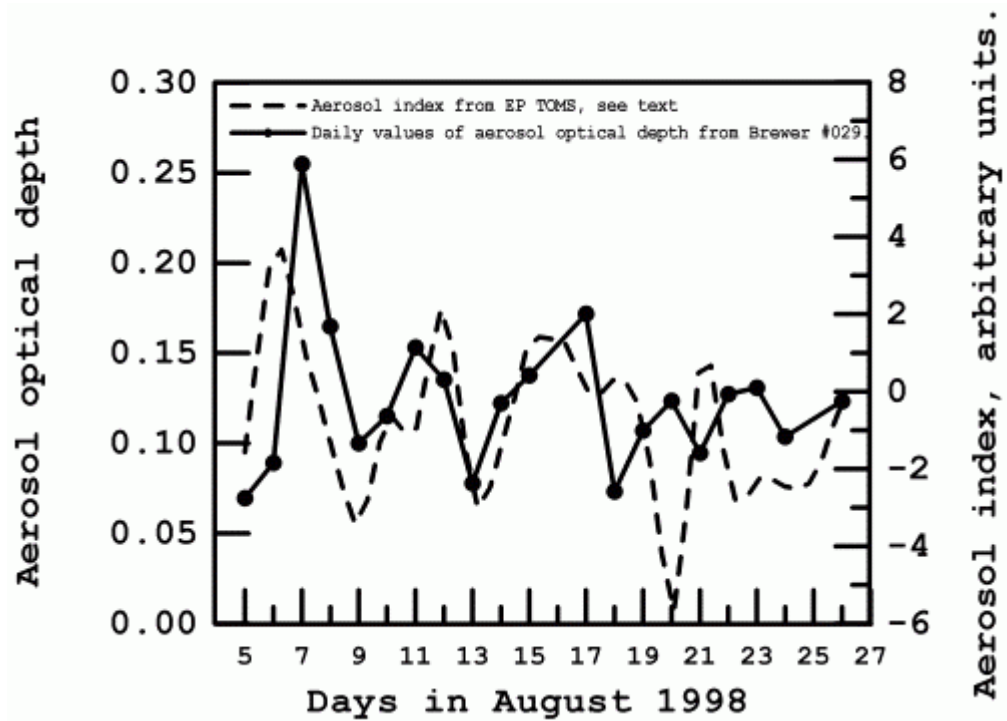
Figure 5.4 AOD from Brewer compared to aerosol index from TOMS.

Adopted from Savastiouk et al. [2005].

In July of 2002 forest fires in Quebec, Canada, sent plumes of smoke to the south. The smoke was detected in Toronto as an increase in aerosol optical depth. The peak of the event in Toronto occurs on July 6. Figure 5.5 presents the results of the aerosol calculations for that day and Figure 5.6 presents a time series of the aerosol optical depth in Toronto. The aerosol index daily summary from TOMS for three days is shown in Figure 5.7. Clearly, the satellite data and the ground based Brewer measurements both detect the maximum increase in the AOD on July 6.

116
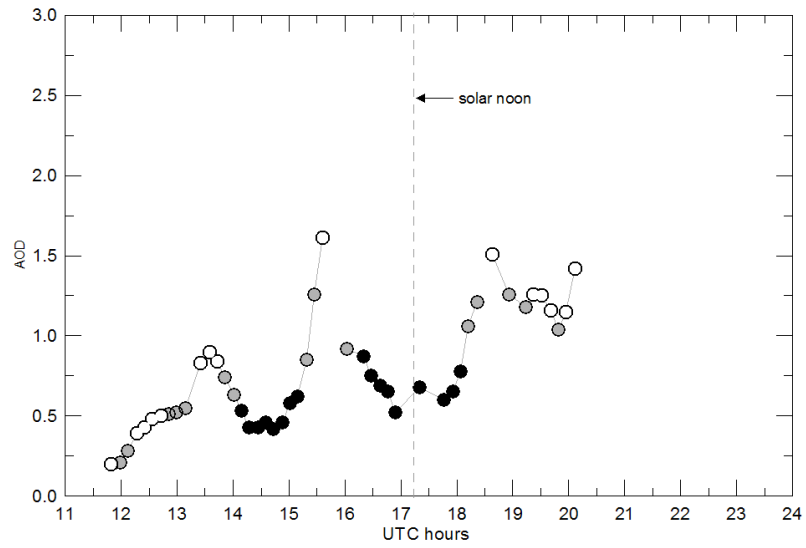
Figure 5.5 Aerosol optical depth at 320 nm on July 6, 2002.
From Brewer #017, Toronto.
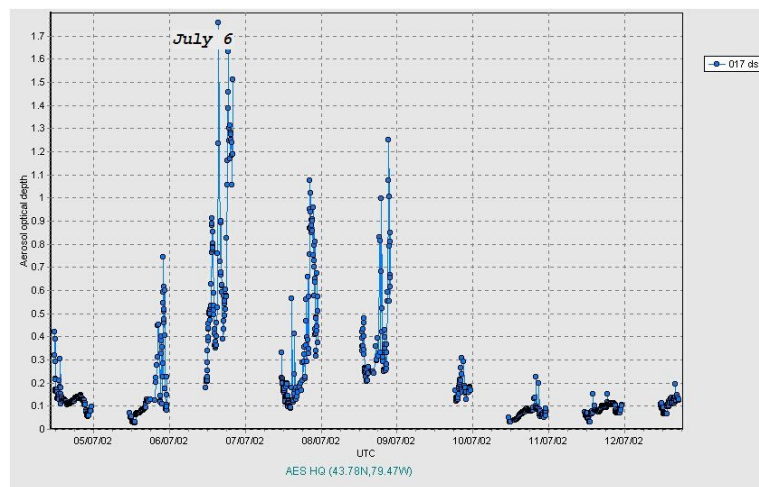
Figure 5.6 Aerosol optical depth at 320 nm.
Derived from the Brewer #017 direct-sun measurements in Toronto.
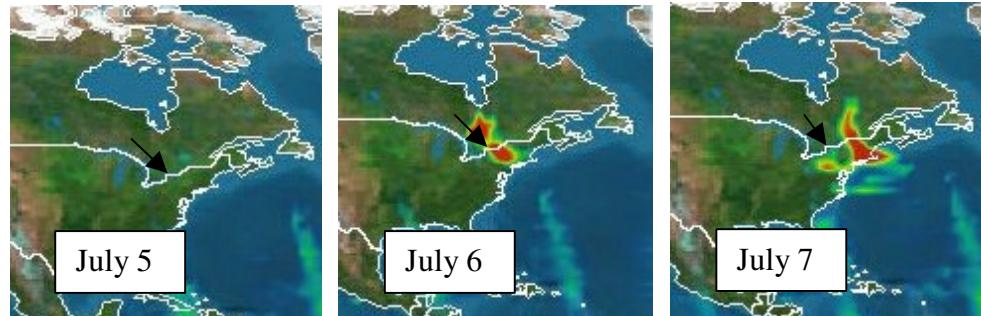
Figure 5.7 Aerosol index daily summary from Satellite Earth Probe. Adopted from TOMS web site. The arrow points to the location of the instrument used for calculation of the AOD in Figures 5.5-5.6.

To illustrate the ability of the algorithm to process previously collected data, the direct-sun measurements from January to May, 2004 made with Brewer #008 in Toronto, Canada were processed and the results are presented in Figure 5.8.
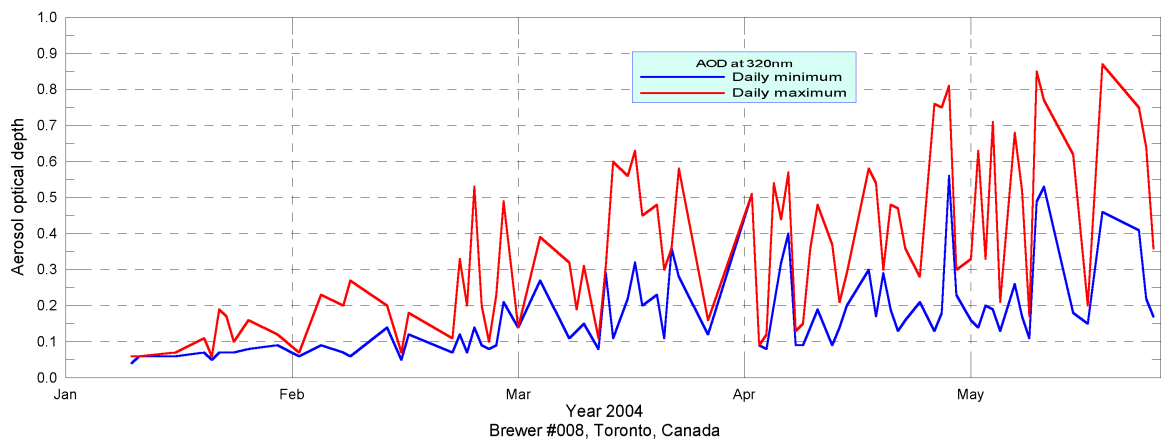
Figure 5.8 Long-term aerosol optical depth calculations.
The daily maximums and minimums only are shown.

Aerosol optical depth values calculated from the Brewer #031 located in the Canadian Arctic in Resolute Bay have been compared to the AERONET spectral radiometer data from the same location. Figure 5.9 shows good agreement between the two sets in the summer of 2004 for a wide range of AOD.
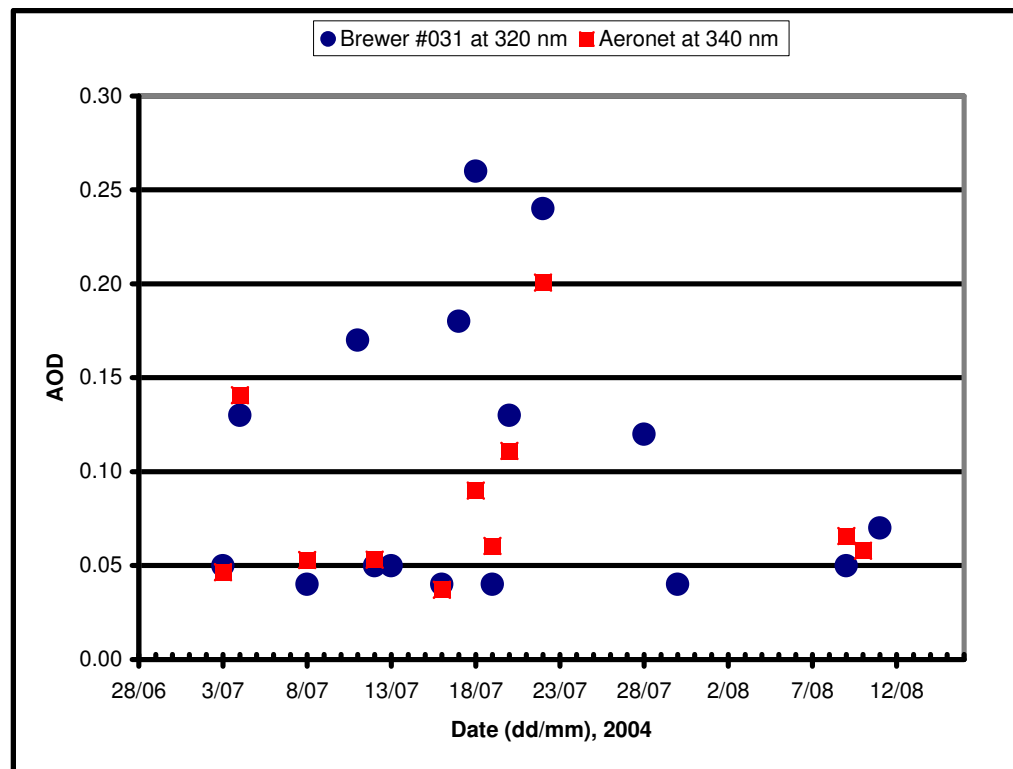
Figure 5.9 A comparison of the aerosol optical depth results from the
Brewer #031 and AERONET spectral radiometer.
Resolute Bay, Canada. Plotted are daily mean values.

5.3   Calculating the effective temperature of the ozone layer

Since the first attempts to extract information about the temperature of the ozone layer from the Brewer data [Savastiouk, 1995], the technique has been improved and more accurate temperature-dependent ozone cross-sections became available. In this section, examples of the implementation of the technique are presented.

To illustrate the technique, data from a two-year period collected with Brewer #078 located in Lindenberg, Germany were processed. The calibration of Brewer #078 was established using the traveling standard Brewer #017 in May of 2002. The data for processing were selected specifically to show how this technique can be used for processing past data. Only the data collected prior to the calibration were used in this processing. Figure 5.10 shows the result of the processing. For comparison purposes the graph also shows individual sonde flight results and 60°N zonal monthly average temperature as measured with sondes at altitude 25 km for 1979-1995.
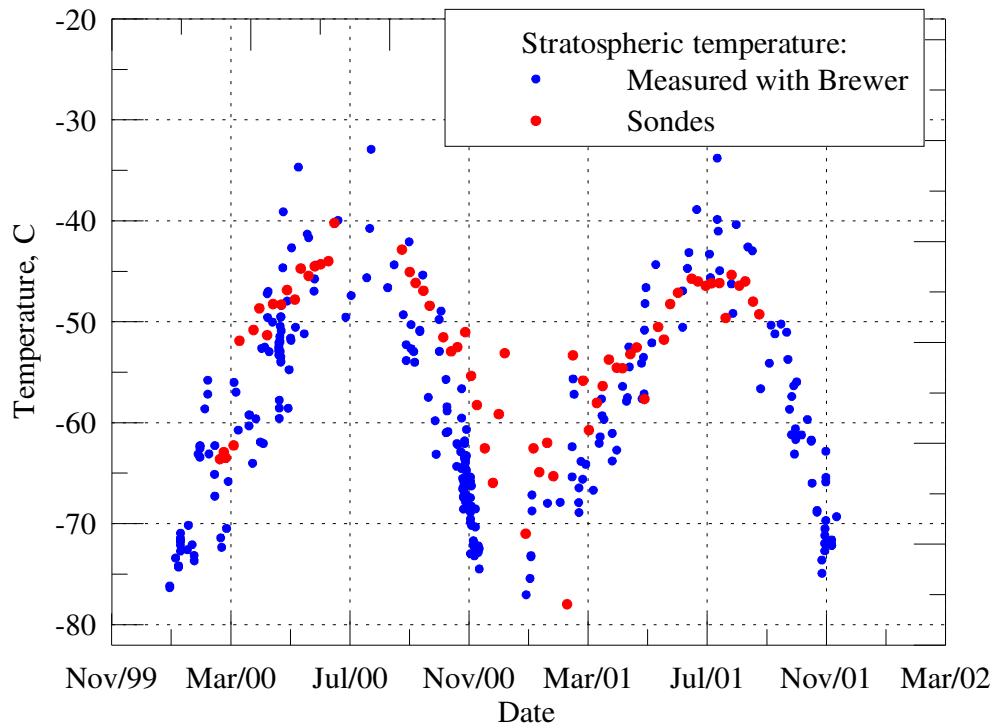
Figure 5.10 The effective temperature of the ozone layer.
Brewer #078, Lindenberg, Germany, 53°N, (data with 2.0<mu<2.5 only). Also shown (in red) are individual sonde flight data for 2000-2001.

The agreement of the Brewer measurements with individual sonde flight temperature results and the scatter of the (blue) points are consistent with calculated error of 2 degrees. Such calculations will be a valuable addition to the daily Brewer measurements.

These calculations can be applied to past data from the entire Brewer network after the appropriate calibration against the traveling standard.

5.4 Reducing the error propagation during calibrations

During the calibration transfer process the instrument that is being calibrated and the reference instrument work side-by-side and take the direct-sun ozone measurements during the day to have as large air mass factor range as possible. This process continues usually for a few days after which the extraterrestrial coefficients are calculated for the instrument being calibrated to have the least deviation in ozone and SO_2 values from the reference instrument. Understandably, if the reference instrument produces ozone and SO_2 values with systematic errors due to the presence of aerosol or non-uniform NDF attenuations, for example, the instrument that is calibrated against it will have some of these errors superimposed with its own. Using the improved algorithm, such propagation of errors is greatly reduced, if not completely eliminated. In addition, the calibration process becomes less dependent on the atmospheric conditions at the time of calibration. High amounts of aerosol, ozone or SO_2 during calibration will not introduce extra errors in the extraterrestrial coefficients. Also, the calibration is no longer dependent on what neutral density filter was used in the process.

5.5 Ozone calculations using the visible part of the solar spectrum

In this section some of the results of calculating ozone from the visible measurements made by these instruments are presented. There are four MKV Brewers in operation now: three are located in the Canadian arctic and one in Oslo, Norway.

The first successful ozone measurements in the visible part of the solar spectrum with the Brewer spectrophotometer were done in 1997 [Donovan et al, 1997] using data from Eureka, Canada.
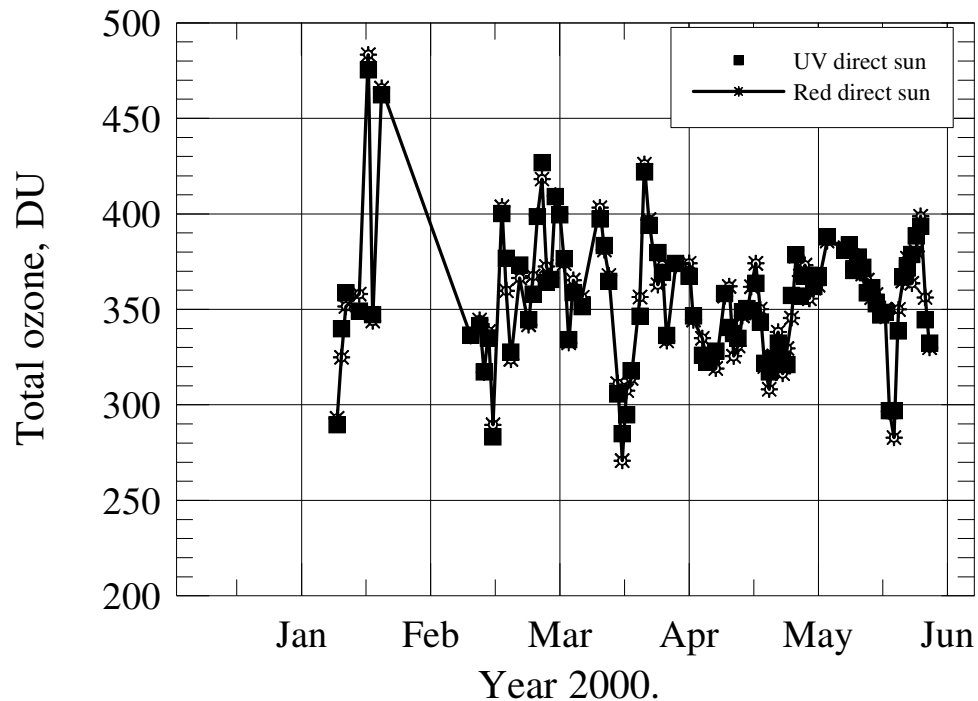
Figure 5.11 Daily mean direct-sun ozone values.
From UV and visible measurements. Brewer #042, Oslo, Norway.

The biggest advantage of the Brewer ozone measurements in the visible part of the spectrum is for high-latitude station, where the UV measurements cannot be performed during the winter season due to large solar zenith angles. Some stations have converted their MKII (UV only) models to MKV models. The only station outside Canada that did the conversion is Oslo University, Norway. After the

conversion of the MKII to MKV, Brewer #042 in Oslo was on a special observation schedule to collect both visible and UV data[2]. The result of data processing is shown in Figure 5.11. The ratio between the two daily averages is plotted in Figure 5.12.
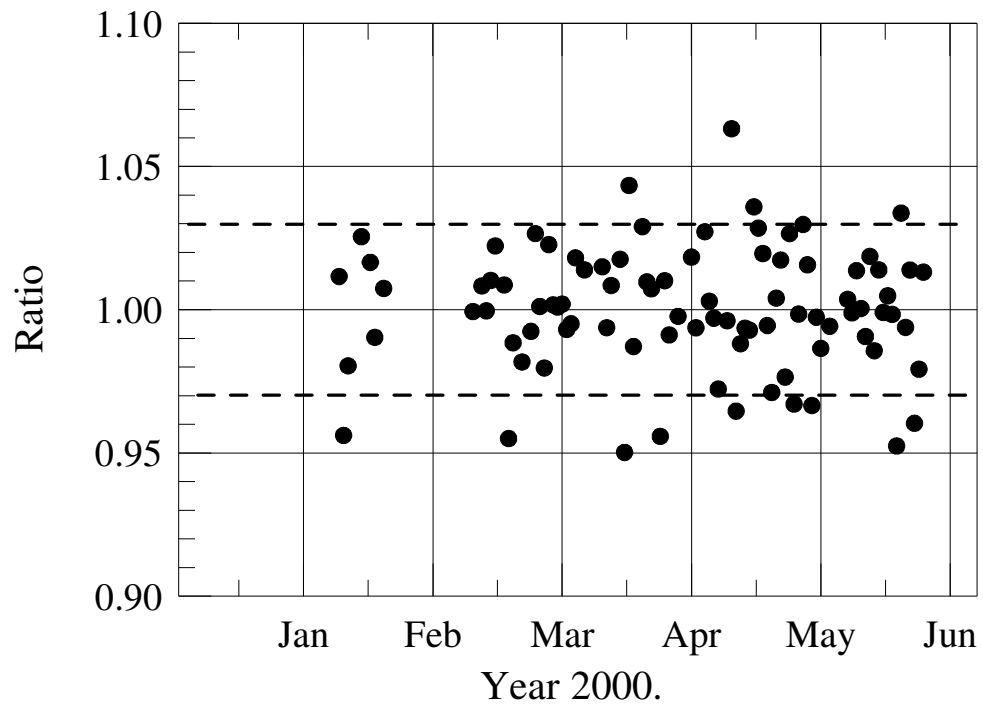
Figure 5.12 Ratio between the daily means from visible and UV direct-sun ozone result.

2 Finn Tonnessen from Oslo University kindly provided data from their MKV Brewer #042.

Figure 5.12 shows that all data from the visible measurements are within 5% from those from UV and most days the ratio is within 3%. If variations during the day, which on some days were as high as 4%, are taken into account, the agreement between the visible and the UV measurements is very good.

6 Conclusions and recommendations

This dissertation has shown the potential of improvements to ozone data quality and accuracy in utilizing data from the Brewer spectrophotometer. A combination of theoretical and instrumentation work along with software programming has been done resulting in better understanding, characterization and utilization of the differences among the Brewer spectrophotometers. As a ground-based instrument, the Brewer spectrophotometer can now provide a reliable means of anchoring standards related to ozone trends calculations.

MKV Brewers now have the means of collecting and processing the data in the visible part of the solar spectrum. This modification of the MKII Brewer spectrophotometer opens possibilities to improving the ground-based ozone measurements at high-latitude sites.

As a general comment, the Brewer spectrophotometer provides a useful tool to study the Earth's atmosphere. With an adequate theoretical basis and data process algorithm the Brewer spectrophotometer can be, and have been used for more than just ozone and sulphur dioxide column observations. And even for ozone and sulphur dioxide, the quality of the results can be improved by incorporating more instrument-specific information into the retrieval algorithm.

It is very important to keep in mind that the improvements described in this work apply to a network of ground-based monitoring stations, not simply to a research instrument in a laboratory. The improvements are mainly in implementation; in making it work.

6.1 Ozone and sulphur dioxide retrieval

It is strongly recommended that the improved algorithm for calculating ozone and SO_2 be adopted. It will contribute to an overall better quality of the column O_3 and SO_2 data around the world. Elimination of errors coming from high O_3, SO_2 or aerosol presence will make global Brewer ozone network more consistent. The satellite community will benefit from a well-established, consistent global ground-based coverage that the Brewer ozone spectrophotometers provide.

The following changes to the existing software are needed in order to implement the recommendations:

- Introduce neutral density filter attenuations for each operating wavelength as instrument parameters
- Introduce the weighting coefficients for calculating the second ratios as instrument parameters
- Calculate the Rayleigh corrections in real-time or make the corrections instrument parameters
- Introduce ozone and sulphur dioxide cross-sections at each operating wavelength as instrument parameters
- Add routine monitoring of the NDF
- Use absolute rather than relative temperature coefficients
- Modify the direct-sun observation routine to include calculations of the aerosol optical depth in the UV

6.2   Aerosol optical depth retrieval

The biggest advantage of this simple method of calculating the aerosol optical depth is that it can be easily applied to all previously collected data. For the future measurements these calculations can be incorporated into the main control program for the Brewer spectrophotometer.

A special measurement can be dedicated to aerosol optical depth by taking readings at two micrometer positions: one at the regular operating wavelengths and the other at longer wavelengths where the effect of ozone is weaker. This will provide more information about spectral behavior of aerosol, which can be used to fine-tune the ozone algorithm for periods of strong aerosol presence.

Also, by exploiting the ability of some Brewer spectrophotometer models (MKIV and MKV) to operate in the visible part of the solar spectrum, aerosol optical depth can be measured in two spectral regions (UV and visible) providing even greater opportunity to retrieve optical characteristics of the aerosol.

6.3   Effective temperature of the ozone layer and temperature-independent ozone retrieval

Although some progress has been made [McLinden, 2002], stray light correction is still an unresolved issue for the Brewer spectrophotometers. Fortunately, this effect decreases as solar zenith angle decreases and reliable measurements of the effective ozone temperature can be made. As with aerosol optical depth, a

dedicated measurement with more than five wavelengths will provide more reliable temperature information.

Any efforts to measure temperature dependence of ozone absorption coefficients should be strongly encouraged. This information will improve present understanding of ozone changes in the atmosphere and will contribute to increased accuracy of ozone measurements.

Implementation of the effective temperature of the ozone layer will most likely happen as an external from the main Brewer software program. Without a very accurate set of temperature dependent ozone cross-sections it will be too big of a step to introduce this measurement as a routine for the Brewer spectrophotometers.

6.4   Measurements in the visible part of the spectrum

MKV Brewers provide an opportunity to have more ozone observations at high-latitude sites. For example, in Fairbanks, Alaska it would be possible to have ground-based ozone measurements all year round.

The advantages of MKV Brewers are not limited to high-latitude stations since aerosol optical depth calculations in the visible part combined with those in the UV will provide information about the optical properties of the aerosols, something that is of increasing interest in the modelling community.

One recommendation is for the manufacturer of the Brewer spectrophotometers to make the instruments so that they can point to the sun at the horizon as it is specified by the design. Right now most instruments can only see the sun above 85 degrees zenith angle.

Since there are no known disadvantages in converting MKII Brewers into MKV, it is recommended to increase the number of MKV Brewer spectrophotometers to further investigate the aerosols. It should be noted that MKIV Brewers (single monochromator, UV and blue visible region) are also capable of providing aerosol optical characteristics, but at wavelengths near 450 nm rather than 600 nm. Together, a MKIV and a MKV can provide very useful aerosol data.

References

Attmannspacher, W., R. Hartmannsgruber, J. Werner, K.W. Rothe, and H. Walther, Intercomparison of ozone profiles obtained by Brewer/Mast sondes and differential absorption laser radar, in *Atmospheric Ozone*, C.S. Zerefos and A. Ghazi, eds., Reidel, Dordrecht, p. 450, 1985.

Barath, F.T., M.C. Chavez, R.E. Cofield, D.A. Flower, M.A. Frerking, M.B. Gram, W.M. Harris, J.R. Holden, R.F. Jarnot, W.G. Kloezeman, G.J. Klose, G.K. Lau, M.S. Loo, B.J. Maddison, R.J. Mattauch, R.P. McKinney, G.E. Peckham, H.M. Pickett, G. Siebes, F.S. Soltis, R.A. Suttie, J.A. Tarsala, J.W. Waters, and W.J. Wilson, The Upper Atmosphere Research Satellite Microwave Limb Sounder Instrument, *J. Geophys. Res.*, **98**, 10751-10762, 1993.

Basher, R.E., Review of the Dobson spectrophotometer and its accuracy, in Atmospheric Ozone, C.S. Zerefos and A. Ghazi, eds., Reidel, Dordrecht, p. 387, 1985.

Bates, D.R., Rayleigh scattering by air, *Planet. Space Sci.*, **32**, 785-790, 1984.

Bhartia, P.K., K.F. Klenk, D. Gordon, and A.J. Fleig, Nimbus-7 total ozone algorithm, in Proceedings of the Fifth Conference on Atmospheric Radiation, American Meteorological Society, Boston, 1983.

Bhartia, P.K., K-F. Klenk, C.K. Wong, D. Gordon, and A.J. Fleig, Intercomparison of the Nimbus 7 SBUV/TOMS total ozone data sets with Dobson and M83 results, *J.Geophys. Res.,* **89**, 5239-5247, 1984.

Bhartia, P.K., A.J. Krueger, S. Taylor, and C. Wellemeyer, Estimation of errors in the TOMS total ozone measurement during the Antarctic ozone campaign of August/September 1987, NASA Conf. Publ. 10014, 1988.

Bojkov, R.D., C.L. Mateer, and A.L. Hansson, Comparison of ground-based and total ozone mapping spectrometer measurements used in assessing the performance of the global ozone observing system, *J. Geophys. Res.,* **93**, 9525-9533, 1988.

Bowman, K-P. and A.J. Krueger, A global climatology of total ozone from the Nimbus 7 total ozone mapping spectrometer, *J. Geophys. Res.,* **90**, 7967-7976, 1985.

Brewer, A.W., Evidence for a world circulation provided by the measurements of helium and water vapor distribution in the stratosphere, *Quart. J.R.Meteor.Soc.*, **75**, 351-363, 1949.

Brewer, A.W. and J.R. Milford, The Oxford-Kew sonde, *Proc. Roy. Soc. A*, **256**, 470-495, 1960.

Brewer, A.W., A replacement for the Dobson Spectrophotometer?, *Pure Appl. Geophys.,* **106-108**, 919-927, 1973.

Brion, T., A. Chakir, B. Coquart, D. Daumont, A. Jenouvrier, J. Malicet and M.F. Merienne, High-resolution measurements of the absorption cross-sections for O3 and NO2, Chemical processes in atmospheric oxidation, Le Bras G. (ed.), Springer Verlag, 157-161, 1997.

Bucholtz, A., Rayleigh-scattering calculations for the terrestrial atmosphere, *Appl. Opt.*, **34**, 2765-2773, 1995.

Budde, W., Physical detectors of optical radiation (Optical radiation measurements; v. 4), Academic Press, New York, USA, 1983.

Burrows, J.P, A. Richter, A. Dehn, B. Deters, S. Himmelmann, S. Voigt and J. Orphal, Atmospheric remote-sensing reference data from GOME-2. Temperature-dependent absorption cross sections of O_3 in the 231-794 nm range, *J. Quant. Spectrosc. Radiat. Transfer,* **61,** 509-517, 1999.

Cebula, R.P., H. Park, and D.F. Heath, Characterization of the Nimbus−7 SBUV Radiometer for the Long-Term Monitoring of Stratospheric Ozone, *J. Atm. Ocean. Tech.,* **5**, 215−227, 1988.

Chapman, S., A theory of upper atmospheric ozone, *Q.J.R. Met. Soc.,* **3**, 103-125, 1930.

Charney, J., and P. Drazin. Propagation of planetary scale disturbances from the lower into the upper atmosphere, *J. Geophys. Res.,* **66,** 83-109, 1961.

Chartrand, D.J., J. de Grandpre and J.C. McConnell, An introduction to stratospheric chemistry, *Atmos-Ocean,* **37**, 309-367, 1999.

Davies, J., D.W. Tarasick, C.T. McElroy, J.B. Kerr, P.F. Fogal and V. Savastiouk, Evaluation of ECC Ozonesonde Preparation Methods from Laboratory Tests and Field Comparisons using MANTRA, *Proc. Quadrennial Ozone Symposium*, Sapporo, Japan, 137-138, 2000.

Deepak, A., Inversion methods in atmospheric remote sounding, 1st International Interactive Workshop on Inversion Methods in Atmospheric Remote Sounding in Williamsburg, VA, Academic Press, New York, USA, 1977.

Deepak, A., Remote sensing of atmospheres and oceans, Academic Press, New York, USA, 1980.

Denney, R.C. and R. Sinclair, Visible and ultraviolet spectroscopy, John Wiley and Sons, Chichester, Great Britain. 1987.

Dobson, G.M.B., A photoelectric spectrophotometer for measuring the amount of atmospheric ozone, *Proc. R. Soc.,* **43**, 324, 1931.

Dobson, G.M.B., Origin and distribution of the polyatomic molecules in the atmosphere, *Proc.R.Soc.London*, **A236**, 187-193, 1956.

Dobson, G.M.B., and C.W.B. Normand, Observers' handbook for the ozone spectrophotometer, *Ann. Int. Geophys. Year,* **5**, 46, 1957.

Dobson, G.M.B. and C.W.B. Normand, Determination of the constants etc., used in the calibration of the amount of ozone from spectrophotometer measurements and the accuracy of the results, *Ann. Int. Geophys. Year*, XVI (Part II), 161, 1962.

Dobson, G.M.B., Annual variation of ozone in Antarctica, *Q. J . R. Meteorol. Soc.,* **92**, 549, 1966.

Dobson, G.M.B., Forty years' research on atmospheric ozone at Oxford: a History, *Appl. Opt.*, **7**, 387-405, 1968.

Donovan, D.P., J.C. Bird, J.A. Whiteway, T.J. Duck, S.R. Pal, A.I. Carswell, J.W. Sandilands, and J.W. Kaminski, Ozone and aerosol observed by lidar in the Canadian Arctic during the winter of 1995/96, *Geophys. Res. Lett.,* **23**, 3317-3320, 1996.

Donovan, D.P., H. Fast, Y. Makino, J.A. Whiteway, J.W. Kaminski, V. Savastiouk, J.C. Bird, A.I. Carswell, J. Davies, T.J. Duck,

C.T. McElroy, R.L. Mittermeier, S.R. Pal, and D. Velkov, Ozone, chlorine oxide, and polar stratospheric clouds observed over the NDSC observatory at Eureka during spring 1997, *Geophys. Res. Lett.,* **24**, 2709-2712, 1997.

Donovan, D.P., A.I. Carswell, T. Shibata, J.C. Bird, T.J. Duck, T.Itabe, T. Nagai, S.R. Pal, O. Uchino, and J.A. Whiteway. Multiwavelength lidar aerosol measurements made at Eureka (80EN, 86EW) during early 1995, *Geophys. Res. Lett.*, **25**, 3139-3142, 1998.

Elanski, N.F., E.A. Kadyshevich, V. Savastiouk, Polarization of the twilight sky: experiment and model calculations, *Izvestia AN*, **29**, 515-524, 1993.

Elanski, N.F., A.Ya. Arabov, A.S. Elokhov, O.V.Makarov, V.Savastiouk, I.A. Senik, Observation of minor atmospheric species content and UV radiation at Mountain Scientific Station Kislovodsk, *Izvestia AN*, **31**, 1995.

Elterman, L., UV, visible and IR attenuation for altitudes to 50 km, AFCRL-68-0153, U.S. Air Force Cambridge Research Laboratory, Redford, Mass., 1968.

Evans, W.F.J., I.A. Asbridge, J.B. Kerr, C.L. Mateer, and R.A. Olafson, The effects of SO_2 on Dobson and Brewer total ozone measurements, Proceedings of the International Ozone Symposium, National Center for Atmospheric Research, Boulder, Colo., p. 48, 1981.

Evans, W.F.J., J.B. Kerr, D.I. Wardle, and A. J. Forester, Monitoring of atmospheric ozone, *Science,* **238**, 1216, 1987.

135

Farman, J.C., B.G. Gardiner and J.D. Shanklin, "Large Losses of Total Ozone in Antarctica Reveal Seasonal ClO/NO Interaction", *Nature,* **315**, 207, 1985.

Fioletov, V.E, J.B. Kerr, D.I. Wardle, J. Davies, E.W. Hare, C.T. McElroy and D.W. Tarasick, Long-term decline of ozone over the Canadian Arctic to early 1997 from ground-based and balloon sonde measurements, *Geophys. Res. Lett.,* **24**, 2705-2708, 1997.

V. E. Fioletov, J. B. Kerr, C. T. McElroy, D. I. Wardle, V. Savastiouk, and T. S. Grajnar, The Brewer Reference Triad, *Geophys. Res. Lett.,* accepted 2005.

Fleig, A.J., P.K. Bhartia, C.G. Wellemeyer, and D.S. Silberstein, Seven years of total ozone from the TOMS instrument - a report on data quality, *Geophys. Res. Lett.,* **13**, 1355-1358, 1986.

Fleig, A.J., R.D. McPeters, P.K. Bhartia, B.M. Schlesinger, R.P. Cebula, K.F. Klenk, S.L. Taylor, and D. F. Heath, Nimbus 7 Solar Backscatter Ultraviolet (SBUV) Ozone Products User's Guide, NASA Reference Publication, 1234, National Aeronautics and Space Administration, Washington, DC, 1990.

Fussen, D., and C. Bingen, A volcanism dependent model for the extinction profile of stratospheric aerosols in the UV-visible range, *Geophys. Res. Lett.,* **26**, 703-706, 1999.

Golub, G.H., and C.F. Van Loan, Matrix Computations. The Johns Hopkins University Press, Baltimore, Md, 1989.

Goody, R.M, and J.C.G. Walker, Atmospheres, Prentice-Hall, Englewood Cliffs, N.J.: 1972.

Goutail, F., J.-P. Pommereau, C. Phillips, C. Deniel, A. Sarkissian, F.Lefevre, E. Kyro, M. Rummukainen, P. Ericksen, S.B Andersen, B.A. Kaastad-Hoiskar, G. Braathen, V. Dorokhov, and V.U. Khattatov, Depletion of column ozone in the Arctic during the winters of 1993-94 and 1994-95, *J.Atmos.Chem.*, **32**, 1-34, 1999.

Grant, W.B., ed., Ozone measuring Instruments for the Stratosphere, Vol. 1 of Collected Works in Optics (Optical Society of America, Washington, D.C., 1989).

Grobner, J., D.I. Wardle, C.T. McElroy and J.B. Kerr, Investigation of the wavelength accuracy of Brewer spectrophotometers, *Appl. Opt.*, **37**, 8352-8360, 1998.

Hare, E.W., V.E. Fioletov, C.T. McElroy, T. Grajnar, V. Savastiouk and E.J. Carty, The Global Brewer Data Management System, Proceedings of the Quadrennial Ozone Symposium, Ed. C. Zerefos, 548-549, 2004.

Hearn, C.H., and J.A. Joens, The near UV absorption spectrum of CS2 and SO2 at 300 K, *J. Quant. Spectrosc. Radiat. Transfer*, **45**, 69-75, 1991.

Herman, J.R., P.K. Bhartia, O. Torres, C. Hsu, C. Seftor, E. Celarier, Global distribution of UV-absorbing aerosols from Nimbus-7/TOMS data, *J. Geophys. Res.*, **102**, 16911-16922, 1997.

Holton, J., An Introduction to Dynamic Meteorology. Academic Press, San Diego. 511 pp. 1992.

Hsu, N.C., J.R. Herman, P.K. Bhartia, C.J. Seftor, O. Torres, A.M. Thompson, J.F. Gleason, T.F. Eck, and B.N. Holben, Detection of Biomass Burning Smoke from TOMS Measurements, *Geophys. Res. Lett.,* **23**, 745-748, 1996

Ingle, J.D., and S.R. Crouch, Pulse overlap effects on linearity and signal-to-noise ratio in photon counting system, *Anal. Chem.*, **44**, 777, 1972.

Iqbal, M., An introduction to solar radiation, Academic Press, New York, USA, 1983.

Kerr, J.B., C.T. McElroy, D.I. Wardle, R.A. Olafson, and W.F.J. Evans, The automated Brewer spectrophotometer, in Atmospheric Ozone, C.S. Zerefos and A. Ghazi, eds., Reidel, Dordrecht, p. 396, 1985.

Kerr, J.B., W.F.J. Evans, and I.A. Asbridge, Recalibration of Dobson field spectrophotometers with a travelling Brewer spectrophotometer standard, in Atmospheric Ozone, C.S. Zerefos and A. Ghazi, eds., Reidel, Dordrecht, p. 38, 1985.

Kerr, J.B., I.A. Asbridge, and W.F.J. Evans, Intercomparison of total ozone measured by the Brewer and Dobson spectrophotometers at Toronto, *J. Geophys. Res.,* **93**, 11129-11133, 1988.

Kerr, J.B., New methodology for deriving total ozone and other atmospheric variables from Brewer spectrophotometer direct sun spectra, *J. Geophys. Res.,* **107**, 4731, 2002.

Kincaid, D.R, W. Cheney, Numerical analysis: mathematics of scientific computing, Brooks/Cole, Pacific Grove, Calif., 1991.

Kipp&Zonen, see SCI-TEC Inc.

Komhyr, W.D., and R.D. Evans, Dobson spectrophotometer total ozone measurement errors caused by interfering absorbing species such as SO_2, NO_2, and photochemically produced O_3 in polluted air, *Geophys. Res. Lett.,* **7**, 157, 1980.

Komhyr, W.D., Dobson spectrophotometer systematic total ozone measurement error, *Geophys. Res. Lett.,* **7**, 161, 1980.

Komhyr, W.D., R.D. Grass, and R. K. Leonard, Dobson spectrophotometer 83: A standard for total ozone measurements, 1962-1987, *J. Geophys. Res.,* **94**, 9847, 1989.

Langer, J., B. Barry, U. Klein, B.-M. Sinnhuber, I. Wohltmann, and K.F. Kunzi, Chemical ozone depletion during Arctic winter 1997/98 derived from ground based millimetre-wave observations, *Geophys. Res. Lett.,* **26**, 599-602, 1999.

Lawson, C.L., and R.J Hanson, Solving least squares problems, Prentice-Hall Inc., Englewood, New Jersey, 1974.

Lenoble, J., Radiative transfer in scattering and absorbing atmospheres: standard computational procedures, A. Deepak, Hampton, VA, USA, 1985.

Lush, H.J., Photomultiplier linearity, *J. Sci. Instrum.*, **42**, 597, 1965.

Malicet, J., D. Daumont, J. Charbonnier, C. Parisse, A. Chakir, and J. Brion., Ozone UV spectroscopy. II. Absorption cross-sections and temperature dependence, *J. Atmos. Chem.*, **21**, 263-273, 1995.

McLinden, C., Stray light and skylight induced errors in a MKII Brewer spectrophotometer, Brewer Workshop, Toronto, 2002.

McPeters, R.D. and G.J. Labow, An Assessment of the Accuracy of 14.5 Years of Nimbus 7 TOMS Version 7 Ozone Data by Comparison with the Dobson Network, *Geophys. Res. Lett.*, **23**, 3695-3698, 1996.

McPeters, R.D., S.M. Hollandsworth, L.E. Flynn, J.R. Herman, and C.J. Seftor, Long-Term Ozone Trends Derived From the 16-Year Combined Nimbus7/Meteor 3 TOMS Version 7 Record, *Geophys. Res. Lett.*, **23**, 3699-3702, 1996.

Mehrtens, H., U. von Zahn, F. Fierli, B. Nardi, and T. Deshler, Type I PSC-particle properties: measurements at ALOMAR 1995 to 1997, *Geophys. Res. Lett.,* **26**, 603-606, 1999.

Molina, L.T., and M.J. Molina, Absolute absorption cross-sections of ozone in the 185- to 350-nm wavelength range, *J. Geophys. Res.*, **91**, 14501-14508, 1986.

Morton, G.A., Photon counting, *Appl. Opt.*, **7**, 1, 1968.

Nicolet, M., On the molecular scattering in the terrestrial atmosphere: an empirical formula for its calculation in the homosphere, *Planet. Space Sci.*, **32**, 1467-1468, 1984.

Paur, R. J., and A. M. Bass, The ultraviolet cross-sections of ozone, II, the results and temperature dependence, in Atmospheric Ozone, C.S. Zerefos and A. Ghazi, eds., Reidel, Dordrecht, p. 611, 1985.

Pendorf, R., Tables of the refractive index for Standard Air and the Rayleigh Scattering Coefficient for the spectral region between 0.2 and 20.0 μ and their application to atmospheric optics, *J. Opt. Soc. Am.*, **47**, 176-180, 1957.

Perliski, L.M., and S. Solomon, On the evaluation of Air mass Factors for atmospheric near-ultraviolet and visible absorption spectroscopy, *J.Geophys. Res.*, **98**, 10363-10374, 1993.

Roscoe, H.K., P.V. Johnston, M.van Roozendael, A. Richter, A. Sarkissian, J. Roscoe, K.E. Preston, J.-C. Lambert, C. Hermans, W. Decuyper, S. Dzienus, T. Winterrath, J. Burrows, F. Goutail, J.-P. Pommereau, E.D.Almeida, J. Hottier, C. Coureul, R. Didier, I. Pundt, L.M. Bartlett, C.T.McElroy, J.E. Kerr, A. Elokhov, G. Giovanelli, F. Ravegnani, M. Premuda, I.Kostadinov, F.Erle, T.Wagner, K. Pfeilsticker, M. Kenntner, L.C. Marquard, M.Gil, O.Puentedura, M.Yela, D.W. Arlander, B.-A. Kaastad-Hoiskar, C.W.Tellefsen, K. K. Tornkvist, B. Heese, R.L. Jones, S.R. Aliwell, and R.A.Freshwater, Slant column measurements of O_3 and NO_2 during NDSC intercomparison of zenith-sky UV-Visible spectrometers in June 1996, *J. Atmos. Chem.*, **32**, 281-314, 1999.

Salby, M.L., Fundamentals of Atmospheric Chemistry, Academic Press, San Diego, 627 pp, 1996.

Savastiouk, V., Procedure of observations of the total ozone content at the network of stations equipped with the Brewer spectrophotometers, in Atmospheric Ozone, Proceedings of the Conference of Young Researchers, Moscow, Russian Academy of Sciences, p. 5-11, 1995.

Savastiouk, V., C.T. McElroy, Brewer Spectrophotometer Total Ozone Measurements Made During the 1998 Middle Atmospheric Nitrogen Trend Assessment (MANTRA) Campaign, *Atmos-Ocean*, accepted for publication, **43** (4), 315–324, 2005.

Savastiouk, V., C.T. McElroy, The ozone and molecular air mass factor calculations for the ground base spectrophotometers, Proceedings of the Quadrennial Ozone Symposium, Ed. C. Zerefos, 498-499, 2004.

Savastiouk, V., C.T. McElroy and K. Lamb, Calibrating the Brewer spectrophotometers with the traveling standard Brewer #017, Proceedings of the Quadrennial Ozone Symposium, Ed. C. Zerefos, 577-578, 2004.

Savastiouk, V., C.T. McElroy, An algorithm for real-time calculations of the aerosol optical depth with the Brewer Spectrophotometer, Proceedings of the Quadrennial Ozone Symposium, Ed. C. Zerefos, 500-501, 2004.

Savastiouk, V., On the real-time measurements of the aerosol optical depth in UV with the Brewer spectrophotometers, a report for Meteorological Service of Canada, 2004.

SCI-TEC Inc. (now Kipp&Zonen), BREWER MKII Spectrophotometer Operator's Manual, 1980.

Solomon, S., A. L. Schmeltekopf, and R.W. Sanders, On the interpretation of zenith-sky absorption measurements, *J. Geophys. Res.,* **92**, 8311-8319, 1987.

Stewart, G., Introduction to Matrix Computations, Academic Press, New York, N. Y., 1973.

Stolarski, R.S., The Antarctic ozone hole, *Sci. Am.,* **258**, 30, 1988.

Stolarski, R.S., A.J. Krueger, M.R. Schoeberl, R.D. McPeters, P.A. Newman, and J.C. Alpert, Nimbus 7 satellite measurements of the springtime Antarctic ozone decrease, *Nature,* **322**, 808, 1986.

Teillet, P.M., Rayleigh optical depth comparisons from various sources, *Appl. Opt.*, **29**, 1897-1900, 1990.

Toon, G.C., J.-F. Blavier, B. Sen, R.J. Salawitch, G.B. Osterman, J. Notholt, M. Rex, C.T. McElroy, and J.M. Russell III, Ground-based observations of Arctic O3 loss during spring and summer 1997, *J. Geophys. Res.*, **104,** 26497-26510, 1999.

Torres, O., J.R. Herman, P.K. Bhartia, and Z. Ahmad, 1995, Properties of Mount Pinatubo Aerosols as Derived From Nimbus−7 Total Ozone Mapping Spectrometer Measurements, *J. Geophys. Res.*, **100**, 14043−14055, 1995.

Torres, O., P.K. Bhartia, J.R. Herman and Z. Ahmad, Derivation of aerosol properties from satellite measurements of backscattered ultraviolet radiation, *J. Geophys. Res.*, 103: 17099-17110, 1998.

Torres, O., P.K. Bhartia, J.R. Herman, A. Sinyuk and B. Holben, A long term record of aerosol optical thickness from TOMS observations and comparison to AERONET measurements, *J. Atm. Sci.*, **59**, 398-413, 2002.

Vigroux, E., Contribution a l′etude experimentale de l′absorption de l′ozone, *Ann. Phys.*, **8**, 709, 1953.

Wardle, D.I., C.D. Walshaw, and T.W. Wormell, A new instrument for atmospheric ozone, *Nature,* **199**, 1177, 1963.

Wayne, R.P., Chemistry of Atmospheres. Oxford Press, New York. 404 pp. 1991.

World Meteorological Organization, Scientific Assessment of Ozone Depletion: 2002, WMO Global Ozone Research and Monitoring Project - Report, Geneva, 2002.

Yue, G.K., L.R. Poole, M.P. McCormick, R.E. Veiga, P.H. Wang, V. Rizi, F. Masc, A. D'Altorio, and G. Visconti, Comparing Simultaneous Stratospheric Aerosol And Ozone Lidar Measurements With SAGE II Data After The Mount Pinatubo Eruption, *Geophys. Res. Lett.*, **22**, 1881-1884, 1995.

Zerefos, C.S., K. Tourpali, B.R. Bojkov, D.S. Balis, B. Rognerund, and I.S.A. Isaksen. Solar activity total column ozone relationships: Observations and model studies with heterogeneous chemistry, *J. Geophys. Res.,* **102,** 1561-1569, 1997.

Appendix A. Summary of Brewer #029 instrument's constants

	Slit 0	Slit 1	Slit 2	Slit 3	Slit 4	Slit 5
DC 1, nm	281.789	286.162	290.130	293.803	297.403	300.782
DC 2 x10^3 nm/step	5.73283	5.69173	5.63995	5.57652	5.45635	541566
DC 3 x10^8 nm/step^2	-2.82852	-3.24225	-3.54938	-3.62957	-2.61613	-2.88793
Operating wavelength, nm	302.137	306.284	310.023	313.479	316.774	319.966
Slit width, nm	0.7720	1.142	1.113	1.113	1.096	1.074
O_3 absorption, cm^{-1}		1.783	1.006	0.6774	0.3747	0.2961

Table A.1 Dispersion characteristics of Brewer #029.

Established during the dispersion test.

	Slit 1	Slit 2	Slit 3	Slit 4	Slit 5
TC, ºC^{-1}	-0.42349	-1.1035	-1.5324	-2.2273	-3.7743

Table A.2 Temperature coefficients for Brewer #029.